



MESENCHYMAL STEM CELL PRE-TREATMENT WITH CYTOKINES AND
HYDROGEN PEROXIDE MODIFIES THEIR ADHESION TO CARDIAC
ENDOTHELIUM AND MURINE HEART SECTIONS

AND

A PRELIMINARY STUDY OF THE MOLECULAR REGULATION OF PLACENTAL
GROWTH FACTOR AND VASCULAR ENDOTHELIAL GROWTH FACTOR IN
MURINE
PREADIPOCYTES

by

MARY FRANCES O'LEARY

This thesis is submitted in partial fulfilment of the requirements for the award of the
degree of MRes

College of Medical and Dental Sciences
University of Birmingham
May 2014

UNIVERSITY OF
BIRMINGHAM

University of Birmingham Research Archive

e-theses repository

This unpublished thesis/dissertation is copyright of the author and/or third parties. The intellectual property rights of the author or third parties in respect of this work are as defined by The Copyright Designs and Patents Act 1988 or as modified by any successor legislation.

Any use made of information contained in this thesis/dissertation must be in accordance with that legislation and must be properly acknowledged. Further distribution or reproduction in any format is prohibited without the permission of the copyright holder.

MESENCHYMAL STEM CELL PRE-TREATMENT WITH CYTOKINES AND
HYDROGEN PEROXIDE MODIFIES THEIR ADHESION TO CARDIAC
ENDOTHELIUM AND MURINE HEART SECTIONS

by

MARY FRANCES O'LEARY

This project is submitted in partial fulfilment of the requirements for the award of the
degree of MRes

College of Medical and Dental Sciences

University of Birmingham

May 2014

Abstract

Introduction: Mesenchymal stem cells (MSCs) have therapeutic potential for myocardial infarctions, yet their recruitment to injured myocardium is poor. Optimising their endothelial adhesion may improve their recruitment to such myocardium.

Pretreating haematopoietic stem cells with inflammatory cytokines or hydrogen peroxide (H_2O_2) improves their endothelial adhesion. I therefore tested whether such pretreatment of MSCs enhances their adhesion to cardiovascular endothelium.

Methods: Primary murine (mMSCs) or human (hMSCs) MSCs were incubated with cytokines or H_2O_2 and their adhesion to murine cardiac endothelial cells (MuCEC), human coronary artery endothelial cells (HCAECs) and murine heart sections determined. **Results:** Pre-treating mMSCs (passage 7-9) with H_2O_2 and IFN γ significantly increased their adhesion to MuCEC. However, the effect of H_2O_2 was lost when higher passage mMSCs (passage 10) were used. hMSC adhesion to HCAEC significantly increased with SDF-1 α and IL-8 pre-treatment. Adhesion of mMSCs to healthy heart sections was significantly decreased by mMSC pretreatment with H_2O_2 , murine IL-8 and SDF-1 α . **Conclusion:** This study indicates that cytokine/ H_2O_2 pretreatment of MSCs can improve their cardiac endothelial adhesion, but not their adhesion to naïve cardiac sections. Interestingly, the species of MSC origin, cell passage number and the adhesive surface used influenced the manner in which adhesion was altered.

Acknowledgements

I am grateful to Dr. Neena Kalia for her excellent supervision of this project. Special thanks also to Dr. Dean Kavanagh for his support of this work. I thank Dean, along with Joseph Robinson and Adam Boulton for their help and advice, as well as the endless supply of tea. I also express my gratitude to the Wellcome Trust, for the provision of a studentship which has allowed this work to be carried out.

Table of Contents		Page
1.	Literature Review	1
1.1	Introduction/Overview	1
1.2	MSC Characterisation	1
1.3	Myocardial Infarction and Chronic Disease Burden	2
1.4	MSC Homing to Sites of Tissue Injury	3
1.5	Mechanisms of MSC homing to injured Myocardium	4
1.6	Clinical Studies of MSC Treatment in Cardiac Disease	7
1.7	MSC-Mediated Healing in Cardiac Disease	9
1.8	Improving MSC Homing	10
1.9	Hypothesis and Aims	12
2.	Methods	14
2.1	Cell Culture	14
2.1.1	Murine Cardiac Endothelial Cells	14
2.1.2	Murine Mesenchymal Stem Cells	14
2.1.3	Human Coronary Artery Endothelial Cells	15
2.1.4	Human Mesenchymal Stem Cells	15
2.2	Static Adhesion Assays	16
2.2.1	Static Adhesion Assay – Murine Mesenchymal Stem Cells and Murine Cardiac Endothelial Cells	16
2.2.2	Static Adhesion Assay – Human Mesenchymal Stem Cells and Human Coronary Artery Endothelial Cells	17
2.3	Stamper-Woodruff Assay	18
2.4	Statistical Analysis	19
3.	Results	20
3.1	Murine Static Adhesion Assay – Cytokine and H ₂ O ₂ treatments	20

3.2	Murine Static Adhesion Assay – Various H ₂ O ₂ Concentrations	24
3.3	Human Static Adhesion Assay	28
3.4	Stamper-Woodruff Assay	32
4.	Discussion	36
4.1	Enhancing MSC Adhesion to Murine Cardiac Endothelium	36
4.2	Enhancing MSC Adhesion to Human Coronary Artery Endothelium	38
4.3	MSC Adhesion to Murine Cardiac Sections	40
4.4	Concluding Remarks	43
5.	References	44

List of Figures	Page
Figure 1.1. Mechanism of MSC homing along a chemokine gradient.	5
Figure 1.2. MSC chemokine receptors and their ligands.	6
Figure 3.1. Static adhesion of pretreated murine mesenchymal stem cells (mMSCs) to murine cardiac endothelium (MuCEC).	22
Figure 3.2. Effect of pretreatment on the static adhesion of murine mesenchymal stem cells (mMSCs) to murine cardiac endothelium (MuCEC).	22
Figure 3.3. Effect of H ₂ O ₂ pretreatment on murine mesenchymal stem cell (mMSC) static adhesion to a confluent murine cardiac endothelial (MuCEC) monolayer – representative images.	23
Figure 3.4. Static adhesion of H ₂ O ₂ pretreated murine mesenchymal stem cells (mMSCs) to murine cardiac endothelium (MuCEC).	27
Figure 3.5. Effect of H ₂ O ₂ pretreatment on the static adhesion of murine mesenchymal stem cells (mMSCs) to murine cardiac endothelium (MuCEC).	27
Figure 3.6. Static adhesion of pretreated human mesenchymal stem cells (hMSCs) to human cardiac endothelium (HCAEC).	30
Figure 3.7. Effect of pretreatment on the static adhesion of human mesenchymal stem cells (hMSCs) to human cardiac endothelium (HCAEC).	30
Figure 3.8. Effect of SDF-1 α pretreatment on human mesenchymal stem cell (hMSC) static adhesion to a confluent human cardiac endothelial (HCAEC) monolayer – representative images.	31
Figure 3.9. Adhesion of pretreated murine mesenchymal stem cells (mMSCs) to murine cardiac sections.	34
Figure 3.10. Effect of pretreatment on the static adhesion of murine mesenchymal stem cells (mMSCs) to murine cardiac sections.	34

Figure 3.11. Representative fluorescence images of murine mesenchymal stem cell (mMSC) adhesion to murine cardiac sections. 35

Figure 4.1. Distribution of cardiac VCAM-1 expression in murine heart. 42

List of Tables	Page
Table 3.1. Descriptive statistics for the static adhesion of pretreated murine mesenchymal stem cells (mMSCs) to murine cardiac endothelium (MuCEC).	21
Table 3.2. Shapiro-Wilk test of normality for observations of pretreated murine mesenchymal stem cell (mMSC) adhesion to murine cardiac endothelium (MuCEC).	21
Table 3.3. Descriptive statistics for the static adhesion of H ₂ O ₂ -treated murine mesenchymal stem cells (mMSCs) to murine cardiac endothelium (MuCEC).	25
Table 3.4. Shapiro-Wilk test of normality for observations of pretreated murine mesenchymal stem cell (mMSC) adhesion to murine cardiac endothelium (MuCEC).	25
Table 3.5. Murine mesenchymal stem cell (mMSC) viability after H ₂ O ₂ treatment.	26
Table 3.6. Descriptive statistics for the static adhesion of pretreated human mesenchymal stem cells (hMSCs) to human cardiac endothelium (HCAEC).	29
Table 3.7. Shapiro-Wilk test of normality for observations of pretreated human mesenchymal stem cell (hMSC) adhesion to human coronary artery endothelium (HCAEC).	29
Table 3.8. Descriptive statistics for the adhesion of pretreated murine mesenchymal stem cells (mMSCs) to murine cardiac sections.	33
Table 3.9. Shapiro-Wilk test on observations of pretreated murine mesenchymal stem cell (mMSC) adhesion to murine cardiac sections.	33

1. Literature Review

1.1 Introduction/Overview

Cardiovascular disease (CVD), the chronic burden of which is increasing, has significant societal and personal costs. Inadequate healing of myocardial infarctions (MIs) and the subsequent development of chronic CVD is a major contributor to this burden. Mesenchymal stem cells (MSCs) are nonhaematopoietic stromal cells possessing multilineage potential. They are capable of differentiating into osteoblasts, chondrocytes, adipocytes and myoblasts (1). MSCs have the potential to augment post-MI myocardial repair via their cytoprotective, proangiogenic, proarteriogenic, inotropic and immunomodulatory properties. Clinical studies have shown MSCs to have therapeutic merit for cardiac disease. However, the recruitment of systemically-delivered MSCs to sites of ischaemic injury is poor. Optimising MSC adhesion to endothelium may improve their homing to such injured tissues, thus potentially enhancing their therapeutic benefits. Our lab has previously increased haematopoietic stem cell (HSC) adhesion to injured gut and kidney (*in vitro* and *in vivo*), by pre-treating HSCs with inflammatory cytokines or hydrogen peroxide (H₂O₂). We therefore tested whether such strategies could improve MSC adhesion to cardiac endothelium and murine heart sections.

1.2 MSC Characterisation

The minimal criteria for the definition of human MSCs (hMSCs) are: adherence to plastic in culture, a phenotype which is positive for the surface antigens CD105, CD73, CD90 and negative for CD45, CD34, CD14/CD11b, CD79α/CD19 and HLA-DR. They must also be capable of *in vitro* differentiation into osteoblasts, adipocytes and chondroblasts (2). This is thought to represent the best current definition of a

hMSC. Murine MSCs express different surface epitopes to hMSCs. A recent study characterised the surface markers of conditionally immortalised mMSCs by flow cytometry, identifying CD9, CD24, CD29, CD44, CD47, CD49e, CD98 CD81, VCAM-1, CD138, CD147, Cr11 and Sca1 as highly expressed on the cell surface (3). However, expression of surface markers has been found to differ between various mouse strains (4).

1.3 Myocardial Infarction and Chronic Disease Burden

Myocardial necrosis that is consistent with myocardial ischaemia constitutes an MI. An MI is most often caused by underlying coronary atherosclerosis (5). 7 % of US adults have coronary heart disease (CHD), with an MI prevalence of 4.3 % for men and 2.2 % for women (6). Despite this considerable MI disease burden, community surveillance studies of MI outcomes show a recent decline in the severity of MI and in its fatality rate, particularly among younger individuals (6,7). However, the incidence of heart failure — one complication of MI — is increasing (8). This phenomenon has been attributed to an ageing population and the falling MI fatality rate (9). Consequently, the optimisation of post-infarct myocardial healing is desirable, in order to prevent or ameliorate complications of an infarcted myocardium.

The long-term repair of a myocardial infarct is both adaptive (e.g. weakened necrotic tissue, which predisposes the myocardium to rupture is eventually replaced by scar tissue) and maladaptive (e.g. ventricular dilation and distortion, impaired cardiac performance) (10). The post-infarct inflammatory milieu is an important driver of myocardial repair and has many interconnected elements. These include the initiation of a cytokine cascade, complement activation, reactive oxygen species (ROS)

production and neutrophils migration to the site of injury (11). Within the healing heart there exists a balance between pro-inflammatory and anti-inflammatory elements. Myocardial mast cell numbers increase during MI healing. Mast cell-derived histamine, tryptase, TGF- β , bFGF and VEGF promote fibroblast proliferation, type 1 collagen production and angiogenesis – all essential components of myocardial repair (11). Optimising these responses presents a considerable challenge. However, as the following discussion demonstrates, MSCs have the potential to augment myocardial repair via their cytoprotective, proangiogenic, proarteriogenic, inotropic and immunomodulatory properties.

1.4 MSC Homing to Sites of Tissue Injury

In vitro evidence suggests that MSCs preferentially adhere to injured tissue. Aldridge *et al.* showed significantly increased adhesion of hMSCs to sections of diseased and healthy human liver. This adhesion appears to be CD29 and CD44 dependent (12).

In vivo evidence points to widespread MSC homing to and engraftment in injured tissues. Lung engraftment of bleomycin-resistant MSCs is increased 23-fold in bleomycin-induced lung injury (13). Human adipose-derived MSCs implant into the intestine of in rats with radiation induced intestinal injury – no homing of hAd-MSCs is observed in normal intestine (14). Focused irradiation (abdominal and hind limb) considerably increases MSC engraftment at the irradiated site (15).

There is substantial evidence that these observations of MSC homing to injured tissue are replicated in heart. Interpretation of some studies is complicated by the use of bone marrow mononuclear cell (BMMC)/bone marrow derived stem cell (BMDSC) populations, which are likely to contain haematopoietic and mesenchymal subpopulations. Strong evidence exists that such mixed populations home to and are

retained by IR injured hearts (16,17). However, these studies do not reflect the homing capacity of MSCs alone. Several studies have described homing of MSC populations to injured heart. In one such study, canine MSCs were administered intravenously 72 hours post-MI. Initial MSC uptake was primarily to the lung, in a perfusion-dependent manner. At 24 hours post-MSC injection, MSC redistribution to the heart was increased in infarcted hearts compared to controls (18). Despite this, the MSCs that engrafted in the injured heart represented a small proportion of those which had been injected. Freyman *et al.* administered MSCs to pigs 15 minutes post-MI, via intravenous (IV), endocardial (EC), intracoronary (IC) routes. No sham surgery or MSC placebo controls were used. At 14 days IV MSCs were not detectable within the infarcts. For the IC and EC routes, retention was 6 % and 3 % respectively (19). Several studies have shown cardiac uptake of IV-administered (20) and intraventricularly-administered (21) MSCs to be significantly greater in infarcted hearts compared to sham-operated controls. Furthermore, intraventricular administration of MSCs significantly decreases lung uptake compared to IV administration and increases myocardial uptake of the cells (21). Others have presented compelling visual evidence for MSC engraftment in MI zones (although no quantification of this observation is provided) (22).

In summary, there is strong evidence for preferential uptake of MSCs to infarcted heart, although this uptake is small in absolute terms, particularly if MSCs are administered IV.

1.5 Mechanisms of MSC Homing to Injured Myocardium

In order to enhance the homing of MSCs to injured myocardium, the mechanisms underlying this homing must be established. It is conceptually useful to divide the

mediators of MSC homing into: (1) the cytokines/chemokines which attract MSCs bearing corresponding receptors to the site of injury and (2) the adhesion molecules which allow this chemotactic attraction to manifest as MSC rolling, adhesion and transmigration.

The act of haematopoietic stem cell (HSC) homing is well described as a sequence of selectin-mediated rolling, integrin-mediated adhesion and transmigration (23). MSCs appear to home in a similar manner. *In vitro* and *in vivo* assays of MSC behaviour have demonstrated extension of podia as well as rolling and firm adhesion behaviour (23). Rolling can be induced on immobilised P-selectin and inhibited by anti P-selectin antibodies. Additionally, endothelial anti-VCAM-1 and MSC anti-VLA-4 treatment impair MSC binding to human umbilical vein endothelial cells (HUVEC) (23). Thus MSCs undergo a series of homing steps similar to those observed in HSCs (26) (Fig. 1.1).

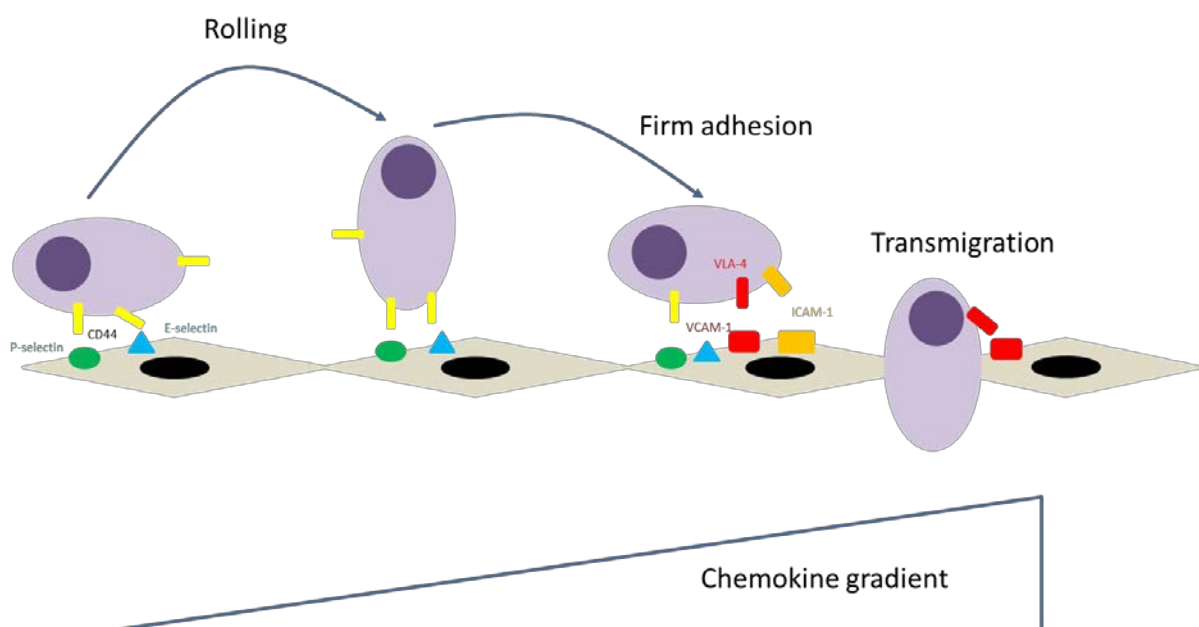


Figure 1.1. Mechanism of MSC homing along a chemokine gradient. MSC rolling is selectin-mediated, with CD44 implicated as the principal ligand (MSC expression of PSGL-1 and ESL-1 is low). Firm endothelial adhesion of MSCs is mediated by the integrins and selectins. VCAM-1-VLA-4 interactions allow transendothelial MSC migration. Adapted from: Salem HK. Stem Cells 2010;28:585–596.

There exist many chemokine receptor-ligand pairs which might play a role in MSC chemotaxis to injured myocardium. Such relationships have been comprehensively characterised by microarray profiling of ischaemically injured mouse hearts, combined with FACS/RT-PCR analysis of MSCs (25). These findings are well summarised in a review by Wu *et al.* (Fig. 1.2) (26). Although some differences exist between mMSCs and hMSCs, their receptor profile is largely similar (26).

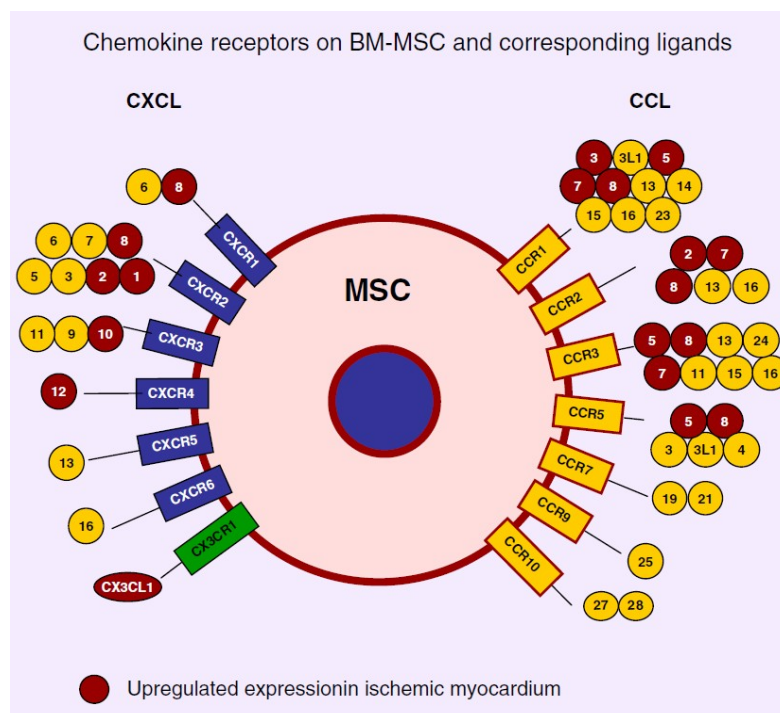


Figure 1.2. MSC chemokine receptors and their ligands. Ligands whose expression has been shown to be upregulated in ischaemic myocardium are shown in red. Expression of those in yellow has not been investigated. Adapted from Wu Y, Zhao RCH. *Stem Cell Rev and Rep* 2012;8:243–250.

It is evident from Fig. 1.2 that considerable scope remains for investigating the expression of chemokine receptors and ligands in MI. The relative importance of each chemokine/ligand pair in MSC homing is also of interest but has not been fully characterised. This information could allow focused enhancement of MSC homing. *In*

vitro, hMSCs migrate most prominently in response to PDGF-AB and IGF-1. CCL5, SDF-1 and CCL22 (formerly MDC) have a minor effect, although this is enhanced by pre-incubation of MSCs with TNF α which increases MSC CCR2, CCR3 and CCR4 expression. (27). Integrin β 1 but not CXCR4 blockade causes a significant reduction in MSC recruitment to a myocardial infarct (26). However, the MSCs in this particular study were used at passages 4-5, at which stage CXCR4 expression is known to decline (26). Schenk *et al.* merged measurements of post-MI myocardial chemokine expression and MSC chemokine receptor expression. CCL3 (Formerly MCP-3), a CCR1/CCR2 ligand, was implicated as an important MSC homing agent. When CCL3 was overexpressed 1 month post-infarct, MSC homing to the heart was restored (28). In murine IR-injured hearts, CCL2 (MCP-1)-CCR2 interactions have also been implicated as important for the significant increase in MSC homing to infarct border zones (29).

1.6 Clinical Studies of MSC Treatment in Cardiac Disease

Given the considerable evidence that MSCs home to IR injured heart, it is important to establish whether they are capable of producing a therapeutic benefit. In pigs, transepicardial injection of MSCs into IR-injured myocardium prevents a further decline in left ventricular ejection fraction (LVEF) (30,31) and improves blood flow in infarct and border zones (31). Such improvements have also been observed in sheep (32). Transendocardial injection of MSCs has been similarly successful. MSC injection in pigs 3 days post-MI has been shown to limit the surface area and depth of myocardial scar formation (33). Furthermore, at 8 weeks following treatment, cardiac function improved in the pigs receiving MSCs whereas the systolic and diastolic function of the control group declined (33). Other animal studies of transendocardial MSC injection have confirmed these findings and have also demonstrated an MSC-

induced improvement in myocardial blood flow, capillary density and ischaemic area (34,35).

IV administration of MSCs is complicated by their lung entrapment and low engraftment in the heart. Some clinical benefit has been described. In one study IV injection of MSCs 15 minutes post cardiac reperfusion in pigs improved the end systolic pressure-volume and preload-stroke work relationships at 12 weeks – without an improvement in LVEF (36). No improvements in scar thickness/size, vessel density, left ventricular end diastolic pressure (LVEDP), left ventricular systolic pressure (LVSP) were been observed (36), although a study in rats has described significant improvements in these outcomes (22). These are parameters which are consistently improve with intramyocardial MSC injection (see above). Another study in pigs has described IV-MSC induced improvements in LVEF and wall thickening at 12 weeks post MI (37). However, the magnitude of this LVEF improvement was not large, and may not represent a clinically meaningful increase.

MSC treatment has been trialled clinically in post-MI patients and in those with ischaemic cardiomyopathy/LV dysfunction. One study showed that IC injection of autologous MSCs within 12 hours of MI increased ventricular wall movement velocity at the site of infarction at 3 months, decreased perfusion defects and improved LVEF (38). Another recent study reported no change in LVEF with transendocardial autologous MSC treatment, although these patients had ischaemic cardiomyopathy, rather than a recent MI. Interestingly, their performance on a 6-minute walk test improved with MSC treatment (40). The recently published POSEIDON trial examined allogeneic and autologous transendocardial MSC injection in those with LV dysfunction. MSCs reduced mean end diastolic elastance, but there was no increase in EF. Despite this, autologous MSCS produced a significant improvement in the 6-

minute walk test and quality of life. Neither MSC treatment improved exercise VO_{2max} (40). One major trial has examined IV administration of (allogeneic) MSCs. The treatment improved subjective symptom scores, but not the 6-minute walk test. Baseline LVEF was similar in both groups. There was a modest MSC-mediated increase in LVEF at 6 months compared to post-MI baseline. Animal and human studies consistently demonstrate a therapeutic benefit with post-MI MSC therapy, however the optimal mode and timing of administration remain to be clarified.

1.7 MSC-Mediated Healing in Cardiac Disease

Evidence suggests that MSCs differentiate into cardiac cells, albeit in low numbers. Even with intramyocardial injection, only ~0.44 % of MSCs remain within healthy myocardium at 4 days (41). However, MSCs that remain in healthy and infarcted myocardium beyond 1 week assume a cardiomyocyte morphology; immunohistochemistry reveals *de novo* expression of desmin, β -myosin heavy chain, α actinin, cardiac troponin T and phospholamban (41,42). MSC participation in coronary angiogenesis has been shown in a swine and canine models of ischaemic cardiomyopathy (34,43).

Given that MSC retention within the heart is poor, other mechanisms are likely to contribute to their clinical benefit. MSCs release a wide range of cytokines, growth factors and chemokines which may promote adaptive cardiac remodelling. These include adrenomedullin, angiogenin, angiopoietin-1, fibroblast growth factors (FGFs), insulin-like growth factor-1 (IGF-1), matrix metalloproteinases and VEGF (44). Injecting conditioned medium from MSCs overexpressing Akt into post-MI rat hearts reduces infarct size and improves LV function (45,46). Genes expressing VEGF, IGF-1 and FGF-2 are upregulated in these MSCs. Bone marrow mononuclear cell supernatants contain VEGF, IL-1 β , PDGF, and IGF-1. Intramyocardial injection of these su-

pernatants significantly improves post-infarct microvessel density, decreases fibrotic area and improves cardiac function (47). In summary, MSCs release factors which promote extracellular matrix growth, and which have cytoprotective, proangiogenic, proarteriogenic and inotropic properties (44,48).

MSCs also have immunomodulatory potential. The importance of the post-MI inflammatory response to adaptive and maladaptive cardiac remodelling is outlined in section 1.3. In traumatic brain injury models, MSC administration reduces macrophage and leukocyte infiltration to the injured tissue, levels of pro-inflammatory cytokines are also reduced and levels of anti-inflammatory cytokines increased (49). MSC prostaglandin E2 release in sepsis promotes anti-inflammatory IL-10 release from macrophages and confers a survival benefit (50). Intramyocardial bone marrow-derived progenitor cell (BM-MNC) injection into infarcted myocardium induces IL-10 dependent improvements in cardiac function; improvements have not been observed with IL-10 knockout BM-MNCs (51). It is likely that MSCs exert some of their therapeutic effect in an immunomodulatory fashion.

1.8 Improving MSC Homing

Given the strong evidence that MSCs improve myocardial healing and the evidence for their poor retention in the heart, developing strategies to enhance MSC recruitment to injured myocardium is vital. Furthermore, IV injection of MSCs is desirable; intramyocardial injection is invasive. In order for such injections to be clinically viable, MSC recruitment to injured heart must be improved. The paracrine as well as transdifferentiation actions of MSCs are likely to be enhanced by MSC localisation at the site of injury. Chemical/cytokine pretreatment of MSCs is one

avenue of exploration. Others, such as genetic modification of MSCs to increase their expression of adhesion molecules are beyond the scope of this discussion.

The chemokine receptor-ligand pairs which appear to be most important in chemotactic MSC homing to IR injured heart are discussed in section 1.5, along with the mediators of endothelial MSC rolling and transmigration. This physiological response to injury may be exploited in order to enhance MSC recruitment. Our lab has successfully increased *in vitro* and *in vivo* HSC adherence to IR injured kidney and intestine by pretreating the cells with SDF-1 α , keratinocyte chemokine (KC) and H₂O₂ (52–54). The underlying mechanism appears to be increased cell surface clustering of integrins, resulting in enhanced integrin-ligand affinity and avidity (52–54). MSCs appear to respond to such priming in a similar fashion. Pretreating MSCs with a cytokine cocktail (Flt-3 ligand, stem cell factor [SCF], IL-6, hepatocyte growth factor [HGF] and IL-3) has been shown to increase cell surface expression of CXCR4. Functionally, this resulted in increased MSC homing to SDF-1 and the bone marrow of sub-lethally irradiated mice (55). Prenatal transplantation of SDF-1 α -pretreated fetal blood MSCs increases CXCR4 cell surface expression and promotes bone MSC engraftment (56). *In vitro*, TNF α pretreatment of MSCs can improve their homing towards chemokines; this is accompanied by increased cell surface expression of CCR2, CCR3 and CCR4, but not CXCR4 (27). Pretreating MSCs with IL-1 β may promote their intestinal homing in a murine colitis model, via increased cell surface expression of CXCR4. Murine colitis treatment with such MSCs improved survival, attenuated weight-loss and reduced the histopathological severity of the disease compared with untreated MSCs (57). It is clear that priming MSCs with cytokines has the potential to improve their homing to IR injured hearts, but evidence is as yet limited. Segers *et al.* pretreated cardiac microvascular endothelium (CMVE)

and aortic endothelium (AE) with cytokines, demonstrating the well-described increase in MSC adherence to TNF α -activated endothelium (58). However, when both endothelium and MSCs were treated with TNF α , there was no additive effect. The authors also report treating MSCs with other cytokines (e.g. IL-1 β , SDF-1 α , IL-3), but their observations of the resulting endothelial MSC adhesion are not reported. Segers *et al.* also showed that intraventricular injection of TNF α -pretreated MSCs increases their retention in uninjured heart 3-fold. Although abundant MSC accumulation in infarcted tissue is reported, the effect of TNF α pretreatment on MSC accumulation in these injured tissues is not stated (58). Furthermore, the potential therapeutic benefit of administering cytokine-pretreated MSCs to IR injured hearts is not addressed in this study.

In summary, it is clear that MSCs can augment post-MI myocardial repair. However, their homing to injured myocardium is sub-optimal. Our lab has demonstrated increased HSC adhesion to injured gut and kidney, by pre-treating HSCs with inflammatory cytokines or hydrogen peroxide (H₂O₂). Others have presented evidence that cytokine treatment of MSCs increases their chemokine receptor expression and homing towards chemokines. No study has adequately examined whether cytokine/H₂O₂ pretreatment of MSCs enhances their adhesion to cardiovascular endothelium, their homing to IR-injured heart or their therapeutic benefit in MI. The work described in this thesis explores whether cytokine pretreatment of MSCs improves their *in vitro* adhesion to cardiac endothelium and murine cardiac sections.

1.9 Hypothesis and Aims

The evidence outlined above clearly demonstrates the therapeutic potential of MSCs

in MI. It also shows that cytokine pretreatment of MSCs has the potential to improve their homing to injury sites and their endothelial adhesion. No study has adequately examined the effects of such pretreatment on MSC adhesion to cardiovascular endothelium. Furthermore, H₂O₂ pretreatment of HSCs promotes increased integrin clustering at the cell surface, thus improving HSC endothelial adhesion and retention in ischaemically-injured organs. We therefore hypothesised that:

1. Cytokine and H₂O₂ pretreatment of murine and human MSCs would improve their static adhesion to cardiac endothelium.
2. Cytokine and H₂O₂ pretreatment of murine MSCs would improve their static adhesion to murine cardiac sections.

This work aimed to:

1. Determine whether pretreatment of murine MSCs with cytokines/H₂O₂ alters their adhesion to murine cardiac endothelium.
2. Investigate whether pretreatment of human MSCs with cytokines/H₂O₂ alters their adhesion to human coronary artery endothelium.
3. Establish whether pretreatment of murine MSCs with cytokines/H₂O₂ alters their adhesion to murine cardiac sections.

2. Methods

All materials were obtained from Sigma-Aldrich, St. Louis, MO, USA unless otherwise stated.

2.1 Cell Culture

2.1.1 Murine Cardiac Endothelial Cells

Immortalised mouse cardiac endothelial cells (MuCEC, obtained from Dr. Elaine Lidington, Imperial College School of Medicine, UK), were cultured in T75 cell culture flasks, each containing 15mL Dulbecco's Modified Eagle Medium supplemented with 10 % fetal bovine serum (FBS), 100µg/mL penicillin/streptomycin (PS), 2mM L-glutamine, 10 ng/mL murine epidermal growth factor (mEGF). The cells were incubated at 37 °C, 5 % CO₂. Cells were fed every 2-3 days and subcultured (1:4) when 90 % confluent.

Subcultivation was carried out under sterile conditions in a class II safety cabinet. The spent culture media was aspirated and the vessel washed once with PBS. The cells were enzymatically dissociated using 7 mL of 3x trypsin. 7 mL of serum- containing medium was added to the flask. The contents of the flask were centrifuged at 300 g, 21 °C for 10 minutes. The supernatant was removed and the pellet resuspended in media. The cell suspension was split into culture flasks containing 14 mL of prewarmed (37 °C) media. The flasks were incubated at 37 °C, 5 % CO₂.

2.1.2 Murine Mesenchymal Stem Cells

Cells were isolated from mouse bone marrow according to the procedure described by Houlihan et. al. (20). Briefly, the cells were isolated from the tibia and femora of

C57Bl/6 mice. These bones were isolated, crushed with a pestle and mortar and incubated with collagenase-containing DMEM. The cell suspension was filtered and the erythrocytes lysed. The suspension was then incubated with allophycocyanin (APC)-conjugated PDGFR- α , FITC-conjugated Sca-1, phycoerythrin (PE)-conjugated CD45 and Ter119. The MSC (PDGFR- α^+ Sca-1 $^+$ CD45 $^-$ Ter119 $^-$) population was isolated by flow cytometry. The MSCs were transferred to a cell culture plate containing 2mL Minimum Essential Medium Eagle (MEM) supplemented with 10 % FBS, 100 μ g/mL penicillin/streptomycin (PS), 2mM L-glutamine, 10 ng/mL transforming growth factor β (complete MEM) and incubated at 37 °C, 5 % CO₂. They were subcultured at 90 % confluence.

Subsequent passages were grown in T75 culture flasks, each containing 15 mL complete MEM and were incubated at 37°C, 5 % CO₂. They were fed every 2-3 days and subcultured (1:3), according to the protocol described in section 2.1.1. The MSCs were used between passages 7 and 10 (inclusive).

2.1.3 Human Coronary Artery Endothelial Cells

Human coronary artery endothelial cells (HCAECs, PromoCell, Heidelberg, Germany) were cultured at at 37 °C, 5 % CO₂ in T75 flasks containing 14 mL growth medium (Endothelial Cell Growth Medium, Promocell, Heidelberg, Germany). The HCAECs were fed every 2-3 days and subcultured (1:3) at 90 % confluence (see Section 2.1.1).

2.1.4 Human Mesenchymal Stem Cells

hMSCs (Lonza, MD, USA) cultured at at 37 °C, 5 % CO₂ in T75 flasks containing 14 mL Mesenchymal Stem Cell Basal Medium (MSCBM), (Lonza, MD, USA),

supplemented with Mesenchymal Stem Cell Growth Supplement (MCGS) (Lonza, MD, USA). The hMSCs were fed every 2-3 days and subcultured (see Section 2.1.3) when 90 % confluent.

2.2 Static Adhesion Assays

2.2.1 Static Adhesion Assay – Murine Mesenchymal Stem Cells and Murine Cardiac Endothelial Cells.

Static adhesion assays were repeated in triplicate. Initially, MSCs (passages 7-9) were pretreated with variety of cytokine/chemical solutions (TNF α , IL-1 β , IFN γ , KC and SDF-1 α , at 100 ng/mL, 100 μ M H₂O₂, MEM control). Additional assays used MSC (passage 10) pretreatment with a range of H₂O₂ concentrations (MEM control, 1 μ M, 10 μ M, 100 μ M, 500 μ M, 1 mM). H₂O₂ treatment solutions were freshly prepared for each experiment, to mitigate the effect of H₂O₂ decomposition.

200 μ L of sterile 2 % gelatin was pipetted into each well of a 24-well plate and incubated at 37 °C, 5% CO₂ for 30 minutes. MuCECs were dissociated from their culture flask (see Section 2.1.1) and the pellet resuspended in DMEM. Gelatin which had not adhered to the plate was aspirated from the wells. 500 μ L of cell suspension was added to each well. The plate was incubated at 37 °C, 5 % CO₂.

Once the MuCECs had grown to confluence, the medium was removed and each well washed twice with PBS. 500 μ L of complete MEM, containing TNF α at 100 ng/mL was added to each well and incubated for 4 hours at 37 °C, 5 % CO₂. One well was not treated with TNF α – 500 μ L of complete MEM was added to this well. MSC treatment solutions were prepared (see above). MSCs were dissociated from their culture flask and centrifuged as described in section 2.1.2. They were resuspended in

1 μL CFSE/1 mL PBS and incubated at 37 °C, 5 % CO_2 for 15 minutes. 1 mL of complete MEM was added and the cells centrifuged at 300 g 21 °C for 10 minutes. The MSCs were resuspended in 2 mL of PBS. 20 μL of the suspension was retained for cell counting and the remaining sample was centrifuged as before. The resulting pellet was resuspended in MEM. 1×10^5 cells were added to each of 8 eppendorfs. The cells were centrifuged as before and each pellet resuspended in 1 mL of treatment solution. Each eppendorf was then incubated for 1 hour at 37 °C. The cell suspensions were again centrifuged and the pellet resuspended in PBS. MEM was aspirated from the 24-well plate and it was washed 3 times with PBS. 500 μL of treated cell suspension (5×10^4 cells) was added to each well and the plate incubated at 37 °C for 20 minutes. The wells were washed gently with PBS twice and then 350 μL of formalin was added to each. The plate was incubated for 15 minutes at room temperature. The wells were washed once with PBS and if not imaged immediately, stored at 4 °C in the dark, with 500 μL of PBS in each well.

The plate was imaged at 10x magnification on a digital inverted fluorescence microscope (EVOS fl, Fischer Scientific, Waltham, MA, USA). 5 views of each well were obtained. The first field of view was taken at the centre of each well, with subsequent fields obtained by moving just beyond the limit of the last field, in a predefined pattern. The cells in each field were counted using a blinded cell counting program.

2.2.2 Static Adhesion Assay – Human Mesenchymal Stem Cells and Human Coronary Artery Endothelial Cells.

Again, static adhesion assays were repeated in triplicate. hMSCs (passages 2-3) were pretreated with variety of cytokine/chemical solutions ($\text{TNF}\alpha$, $\text{IFN}\gamma$, $\text{SDF}\alpha$, IL-8,

IL-6 at 100 ng/mL, 100 μ M H_2O_2 and an MSCBM control) and their adhesion to a confluent HCAEC monolayer quantified. Endothelial Cell Growth Medium was used during the endothelial activation step. MSCBM medium was used for hMSC incubations. The procedure was otherwise as described in section 2.2.1.

2.3 Stamper-Woodruff Assay

Stamper-Woodruff assays were carried out to examine the adherence of mMSCs (passage 10), pretreated with variety of cytokine/chemical solutions to murine heart sections. The treatments were $TNF\alpha$, $IL-1\beta$, $IFN\gamma$, KC, $SDF\alpha$ at 100ng/mL, 100 μ M H_2O_2 and an MEM control. Sham hearts were excised, placed in liquid nitrogen and stored at -80 °C. The hearts were cryosectioned, the sections transferred to glass slides, fixed in acetone for 20 minutes, allowed to air-dry and then stored at -20 °C.

MSCs were CFSE labelled and treated as described in section 2.2.1. Slides were brought to room temperature and re-fixed in acetone for 5 minutes. Once dry, each section was washed gently three times. A hydrophobic pen (ImmEdge, Vector Laboratories, Peterborough, UK) was used to draw a barrier around each section. 5×10^4 MSCs in 100 μ L MEM were added to each section and incubated at room temperature, in the dark, for 20 minutes. The sections were washed three times as before, fixed in acetone for 5 minutes and washed again. A water based mounting medium (Hydromount, National Diagnostics, Atlanta, GA, USA) was dropped onto each section and a coverslip applied. Slides were left to dry in the dark overnight at room temperature), then stored at 4 °C.

The sections were imaged at 10x magnification on a digital inverted fluorescence microscope. 5 views of each section (placed on the stage with its long axis horizontal, apex of the heart on the right) were obtained. The first field of view was

taken at the lower leftmost point of the section with subsequent fields obtained by moving just beyond the limit of the last field, in a predefined pattern. The cells in each field were counted using a blinded cell counting program.

2.4 Statistical Analysis

Shapiro-Wilk tests of normality were carried out on all data groups. Transformation of non-normal data was considered inappropriate, given the small sample sizes. Data was analysed by Kruskal Wallis tests, with post-hoc Mann-Whitney U analysis (IBM SPSS Statistics 21).

3. Results

3.1 Murine Static Adhesion Assay – Cytokine and H₂O₂ Treatments

The median values for each group are presented along with maximum, minimum and interquartile range (IQR) values (Table 3.1). The Shapiro-Wilk test demonstrated significant deviation from normality in 6 of the 8 treatment groups (i.e. $p < 0.05$) (Table 3.2). As the data is largely non-parametric, it is presented in the box and whisker plot format, to allow the reader to appreciate its spread (Fig. 3.1).

Considerable inter-group and intra-group variation in cell counts per field of view can be seen. The data is also presented in the more conventional bar chart format (Fig. 3.2). A significant increase in MSC adhesion to cardiac endothelium was observed with H₂O₂ ($p < 0.0001$) and IFN γ ($p = 0.04$) pretreatment of the MSCs (Fig. 3.2).

Representative fluorescent microscopy images demonstrate the H₂O₂-induced increase in MSC adhesion to a confluent cardiac endothelial monolayer (Fig. 3.3).

Table 3.1. Descriptive statistics for the static adhesion of pretreated murine mesenchymal stem cells (mMSCs) to murine cardiac endothelium (MuCEC). mMSCs (passage 7-9) were CFSE labelled, then pretreated for 1 hour with a cytokine (100 ng/mL), H₂O₂ (100 μM) or medium alone (control). Treated mMSCs were incubated for 20 minutes with TNFα-activated confluent MuCEC monolayers on a 24-well plate (5x10⁴ cells/well). mMSC adhesion was systematically assessed at 10x magnification using a fluorescence microscope. NEA = no endothelial activation with TNFα, KC = keratinocyte chemokine, IQR = interquartile range. n=3, 5 observations per experiment.

	Minimum	Median	IQR	Maximum
	(cells/field of view)			
Control	0	25	19	49
NEA	4	19	77	574
TNFα	3	47	77	389
IL-1β	2	8	26	62
IFNγ	6	36	34	65
KC	0	23	139	226
SDF-1α	8	29	112	185
H₂O₂	14	69	100	254

Table 3.2. Shapiro-Wilk test of normality for observations of pretreated murine mesenchymal stem cell (mMSC) adhesion to murine cardiac endothelium (MuCEC). mMSCs (passage 7-9) were CFSE labelled, then pretreated for 1 hour with a cytokine (100 ng/mL), H₂O₂ (100 μM) or medium alone (control). Treated mMSCs were incubated for 20 minutes with TNFα-activated confluent MuCEC monolayers on a 24-well plate (5x10⁴ cells/well). mMSC adhesion was systematically assessed at 10x magnification using a fluorescence microscope. n=3, 5 observations per experiment.

	Statistic	N	Sig.*
Control	.950	15	.517
NEA	.597	15	.000
TNFα	.673	15	.000
IL-1β	.796	15	.003
IFNγ	.941	15	.389
KC	.784	15	.002
SDF-1α	.779	15	.002
H₂O₂	.874	15	.039

*p<0.05

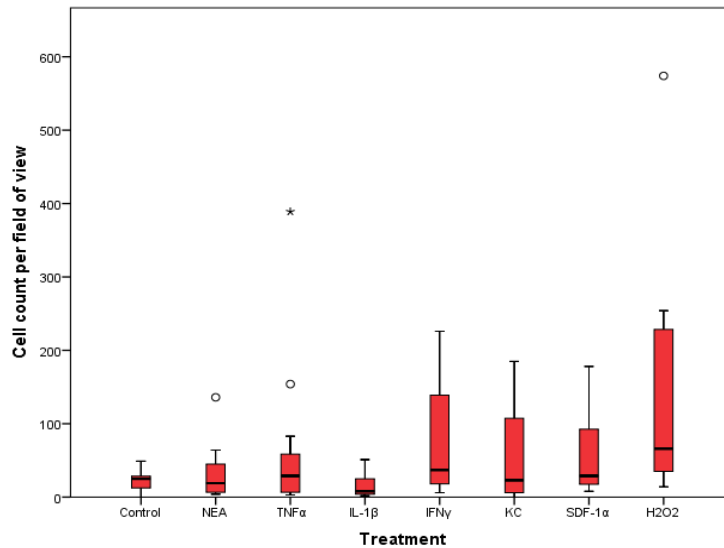


Figure 3.1. Static adhesion of pretreated murine mesenchymal stem cells (mMSCs) to murine cardiac endothelium (MuCEC). mMSCs (passage 7-9) were CFSE labelled, then pretreated for 1 hour with a cytokine (100 ng/mL), H₂O₂ (100 μM) or medium alone (control). Treated mMSCs were incubated for 20 minutes with TNFα-activated confluent MuCEC monolayers on a 24-well plate (5x10⁴ cells/well). mMSC adhesion was systematically assessed at 10x magnification using a fluorescence microscope. n=3, 5 observations per experiment. NEA = no endothelial activation, KC = keratinocyte chemokine. Black line denotes median value. Boxes = interquartile range (IQR). Bars = highest/lowest datum within 1.5IQR of upper/lower quartile. ° = outlier >1.5IQR of upper/lower quartile but < 3 box lengths from upper end of box. * = extreme outlier > 3 box lengths from upper end of box.

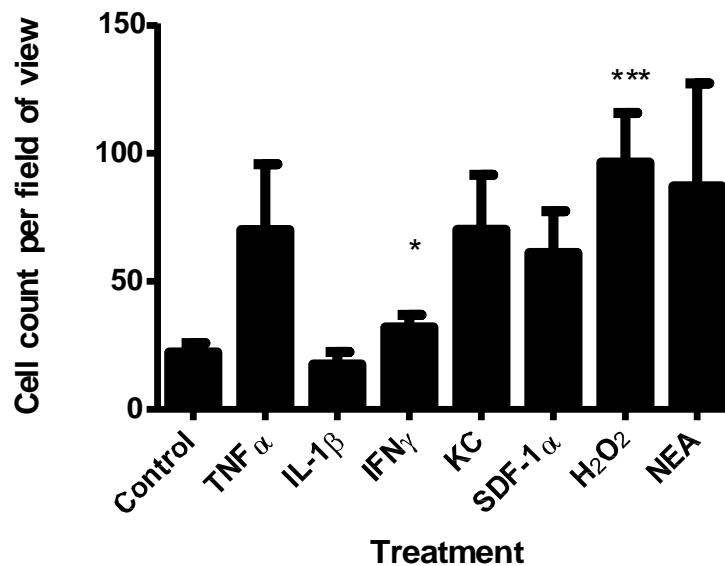


Figure 3.2. Effect of pretreatment on the static adhesion of murine mesenchymal stem cells (mMSCs) to murine cardiac endothelium (MuCEC). mMSCs (passage 7-9) were CFSE labelled, then pretreated for 1 hour with a cytokine (100 ng/mL), H₂O₂ (100 μM) or medium alone (control). Treated mMSCs were incubated for 20 minutes with TNFα-activated confluent MuCEC monolayers on a 24-well plate (5x10⁴ cells/well). mMSC adhesion was systematically assessed at 10x magnification using a fluorescence microscope. Data presented as mean ± SEM. n=3, 5 observations per experiment. NEA = no endothelial activation, KC = keratinocyte chemokine. * = p < 0.05, *** = p < 0.001 vs. control.

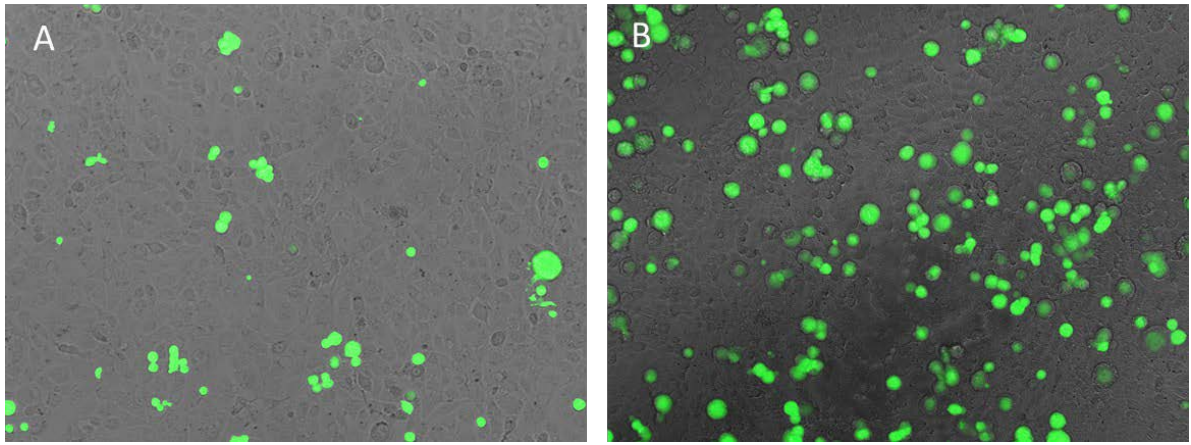


Figure 3.3. Effect of H₂O₂ pretreatment on murine mesenchymal stem cell (mMSC) static adhesion to a confluent murine cardiac endothelial (MuCEC) monolayer – representative images. mMSCs (passage 7-9) were CFSE labelled, then pretreated for 1 hour with 100 μM H₂O₂ or medium alone (control). Treated MSCs were incubated for 20 minutes with confluent MuCEC monolayers on a 24-well plate (5x10⁴ cells/well). MSC adhesion was systematically assessed at 10x magnification using a fluorescence microscope. (A) control; (B) 100 μM H₂O₂.

3.2 Murine Static Adhesion Assay – Various H₂O₂ Concentrations

The median cell count per field of view values for each group are detailed, along with the maximum value, minimum value and the IQR (Table 3.3). Shapiro-Wilk tests demonstrated a deviation from normality in 4 of the 6 treatment groups (table 3.4). Again, considerable within-group variation in cell count per field of view values can be appreciated; for this reason the data is presented in the box and whisker plot as well as the bar chart format (Fig. 3.4, Fig. 3.5). No significant difference was detected between the groups (Fig. 3.5). 100 µM H₂O₂ pretreatment of MSCs (Fig. 3.5) did not increase their endothelial adhesion, despite our earlier observations to the contrary (Fig. 3.2). We had hoped to perform Annexin V/Propidium iodide flow cytometry to determine MSC viability with H₂O₂ treatment. This was not possible in the time available. Haemocytometer counts of live/dead cells by trypan blue staining did not reveal any obvious increase in cell death with H₂O₂ treatments up to 1 mM (Table 3.5).

Table 3.3. Descriptive statistics for the static adhesion of H₂O₂-treated murine mesenchymal stem cells (mMSCs) to murine cardiac endothelium (MuCEC).

mMSCs (passage 10) were CFSE labelled, then pretreated for 1 hour with H₂O₂ or medium alone (control). Treated mMSCs were incubated for 20 minutes with TNF α -activated confluent MuCEC monolayers on a 24-well plate (5x10⁴ cells/well). MSC adhesion was systematically assessed at 10x magnification using a fluorescence microscope. n=3, 5 observations per experiment. IQR = interquartile range

	Minimum	Median	IQR	Maximum
	Cell count/field of view			
Control	6	28	74	110
1μM	14	30	23	69
10μM	12	36	58	95
100μM	17	42	62	157
500μM	5	46	51	118
1mM	18	40	89	137

Table 3.4. Shapiro-Wilk test of normality for observations of pretreated murine mesenchymal stem cell (mMSC) adhesion to murine cardiac endothelium (MuCEC).

mMSCs (passage 10) were CFSE labelled, then pretreated for 1 hour with H₂O₂ or medium alone (control). Treated mMSCs were incubated for 20 minutes with TNF α -activated confluent MuCEC monolayers on a 24-well plate (5x10⁴ cells/well). mMSC adhesion was systematically assessed at 10x magnification using a fluorescence microscope. n=3, 5 observations per experiment.

	Statistic	N	Sig.*
Control	.845	15	.015
1μM	.915	15	.162
10μM	.869	15	.033
100μM	.837	15	.011
500μM	.945	15	.444
1mM	.792	15	.003

*p<0.05

Table 3.5. Murine mesenchymal stem cell (mMSC) viability after H₂O₂ treatment.
 mMSCs were treated with H₂O₂ or medium alone (control) for 1 hour. The cells were centrifuged and the pellet resuspended in medium (100,000 cells/mL medium). 20 μ L of cell suspension was diluted 1:1 with trypan blue. The total number of live and dead cells in 4 haemocytometer corner squares was counted. n=3, data presented is mean of the three experiments performed.

	Live (cells)	Dead (cells)	% Dead
Control	16.0	6.8	42.5
1 μM	9.0	3.3	27.0
10 μM	9.3	5.0	34.9
100 μM	15.7	4.3	21.7
500 μM	14.7	10.7	42.1
1 mM	20.0	9.7	32.6

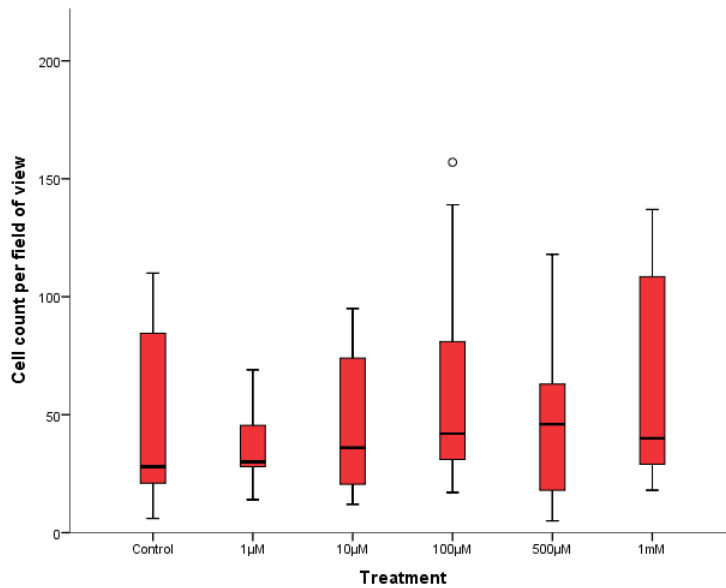


Figure 3.4. Static adhesion of H₂O₂ pretreated murine mesenchymal stem cells (mMSCs) to murine cardiac endothelium (MuCEC). mMSCs (passage 10) were CFSE labelled, then pretreated for 1 hour with H₂O₂ or medium alone (control). Treated mMSCs were incubated for 20 minutes with confluent MuCEC monolayers on a 24-well plate (5x10⁴ cells/well). mMSC adhesion was systematically assessed at 10x magnification using a fluorescence microscope. n=3, 5 observations per experiment. Black line denotes median value. Boxes = interquartile range (IQR). Bars = highest/lowest datum within 1.5IQR of upper/lower quartile. ° = outlier >1.5IQR of upper/lower quartile but < 3 box lengths from upper end of box.

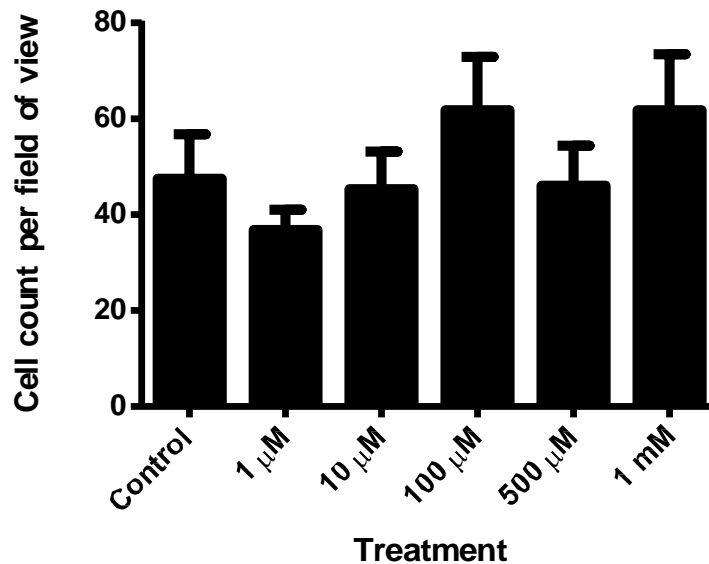


Figure 3.5. Effect of H₂O₂ pretreatment on the static adhesion of murine mesenchymal stem cells (mMSCs) to murine cardiac endothelium (MuCEC). mMSCs (passage 10) were CFSE labelled, then pretreated for 1 hour with H₂O₂ or medium alone (control). Treated mMSCs were incubated for 20 minutes with TNF α -activated confluent MuCEC monolayers on a 24-well plate (5x10⁴ cells/well). mMSC adhesion was systematically assessed at 10x magnification using a fluorescence microscope. Data presented as mean \pm SEM. n=3, 5 observations per experiment.

3.3 Human Static Adhesion Assay

The median cell count per field of view values for each group are detailed, along with the maximum value, minimum value and the IQR (Table 3.6). The data was normally distributed in 6 of 8 groups (Table 3.7). Given this, use of parametric statistical tests was considered. However, the variances between groups were not equal (Levene's test significance < 0.0001), thus violating another assumption of ANOVA. Non-parametric statistical analysis was retained.

Prominent intra and inter-group differences in cell counts are evident when the data is visualised on a box and whisker plot (Fig 3.6). Pretreating MSCs with SDF-1 α and IL-8 significantly increased their adhesion to HCAECs ($p = 0.034$, $p = 0.029$ respectively). Representative fluorescent microscopy images demonstrate the SDF-1 α -induced increase in MSC adhesion to HCAECs (Fig. 3.8). Cells within a confluent HCAEC monolayer were observed to be less densely packed than those in a MuCEC monolayer (Fig.3.3, Fig. 3.8).

Table 3.6. Descriptive statistics for the static adhesion of pretreated human mesenchymal stem cells (hMSCs) to human cardiac endothelium (HCAEC). hMSCs (passage 2-3) were CFSE labelled, then pretreated for 1 hour with a cytokine (100 ng/mL), H₂O₂ (100 μM) or medium alone (control). Treated hMSCs were incubated for 20 minutes with confluent TNFα-activated HCAEC monolayers on a 24-well plate (5x10⁴ cells/well). hMSC adhesion was systematically assessed at 10x magnification using a fluorescence microscope. IQR = interquartile range, NEA = no endothelial activation. n=3, 5 observations per experiment.

	Minimum	Median	IQR	Maximum
Control	5	12	22	42
NEA	5	26	26	65
TNFα	8	30	25	50
SDF-1α	8	32	37	81
IL-8	10	21	36	83
IL-6	7	17	15	31
IFNγ	3	13	13	41
H₂O₂	2	9	13	24

Table 3.7. Shapiro-Wilk test of normality for observations of pretreated human mesenchymal stem cell (hMSC) adhesion to human coronary artery endothelium (HCAEC). hMSCs (passage 2-3) were CFSE labelled, then pretreated for 1 hour with a cytokine (100 ng/mL), H₂O₂ (100 μM) or medium alone (control). Treated hMSCs were incubated for 20 minutes with TNFα-activated confluent HCAEC monolayers on a 24-well plate (5x10⁴ cells/well). hMSC adhesion was systematically assessed at 10x magnification using a fluorescence microscope. NEA = no endothelial activation n=3, 5 observations per experiment.

	Statistic	N	Sig.*
Control	.870	15	.034
NEA	.917	15	.172
TNFα	.946	15	.465
SDF-1α	.894	15	.076
IL-8	.860	15	.024
IL-6	.932	15	.297
IFNγ	.917	15	.176
H₂O₂	.918	15	.179

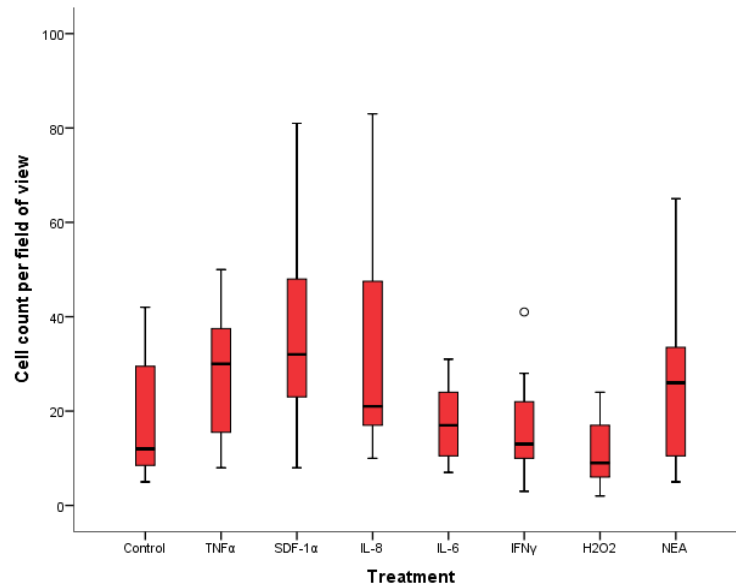


Figure 3.6. Static adhesion of pretreated human mesenchymal stem cells (hMSCs) to human cardiac endothelium (HCAEC). hMSCs (passage 2-3) were CFSE labelled, then pretreated for 1 hour with a cytokine (100 ng/mL), H₂O₂ (100 μM) or medium alone (control). Treated hMSCs were incubated for 20 minutes with TNFα-activated, confluent HCAEC monolayers on a 24-well plate (5x10⁴ cells/well). hMSC adhesion was systematically assessed at 10x magnification using a fluorescence microscope. NEA = no endothelial activation. n=3, 5 observations per experiment. Black line denotes median value. Boxes = interquartile range (IQR). Bars = highest/lowest datum within 1.5IQR of upper/lower quartile. ° = outlier >1.5IQR of upper/lower quartile but < 3 box lengths from upper end of box.

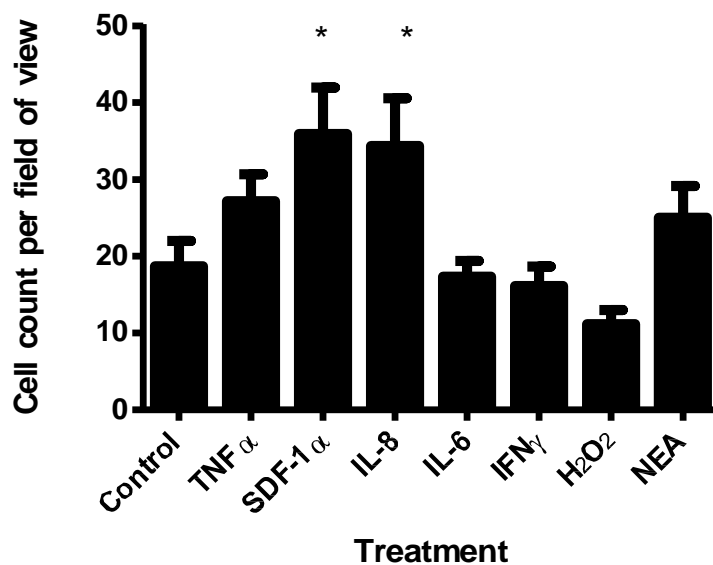


Figure 3.7. Effect of pretreatment on the static adhesion of human mesenchymal stem cells (hMSCs) to human cardiac endothelium (HCAEC). hMSCs (passage 2-3) were CFSE labelled, then pretreated for 1 hour with a cytokine (100 ng/mL), H₂O₂ (100 μM) or medium alone (control). Treated hMSCs were incubated for 20 minutes with TNFα-activated, confluent HCAEC monolayers on a 24-well plate (5x10⁴ cells/well). hMSC adhesion was systematically assessed at 10x magnification using a fluorescence microscope. NEA = no endothelial activation. Data presented as mean ± SEM. n=3, 5 observations per experiment. chemokine. * = p<0.05 vs. control.

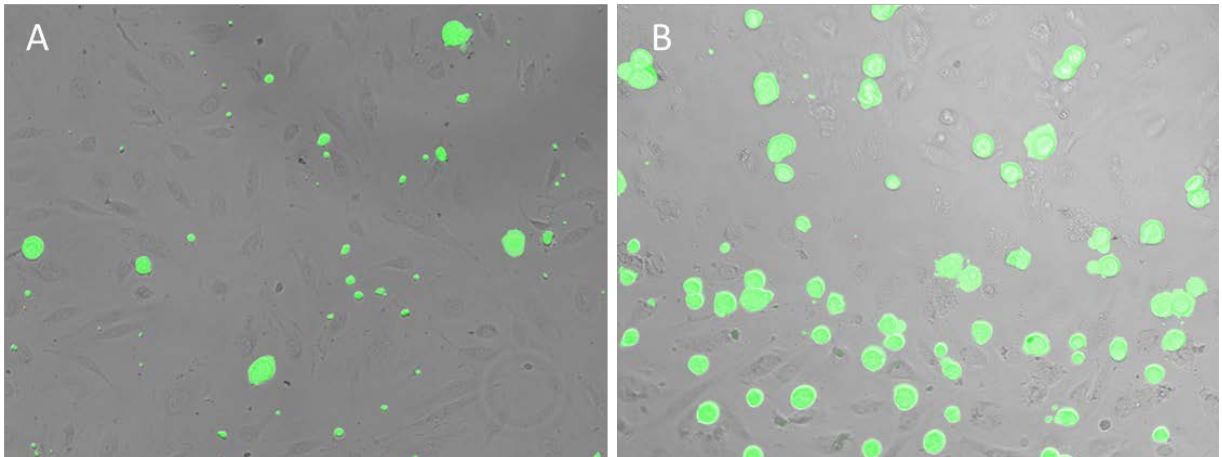


Figure 3.8. Effect of SDF-1 α pretreatment on human mesenchymal stem cell (hMSC) static adhesion to a confluent human cardiac endothelial (HCAEC) monolayer – representative images. hMSCs (passage 2-3) were CFSE labelled, then pretreated for 1 hour with SDF-1 α (100 ng/mL) or medium alone (control). Treated hMSCs were incubated for 20 minutes with confluent HCAEC monolayers on a 24-well plate (5×10^4 cells/well). hMSC adhesion was systematically assessed at 10x magnification using a fluorescence microscope. (A) control; (B) SDF-1 α .

3.4 Stamper-Woodruff Assay.

As in previous sections, the median cell count per field of view values for each group are detailed, along with the maximum value, minimum value and the IQR (Table 3.8). The data was non-parametric in all groups (Table 3.9). The non-normal spread of data is evident on a box and whisker plot, with outlying data points featuring prominently (Fig. 3.9). Representative fluorescence microscopy images illustrate the considerable variation in numbers of adherent mMSCs in the TNF α -treated group (Fig. 3.11, panels A-C). Fewer MSCs adhered to murine heart sections per field of view (mean 10.2 cells) compared to a MuCEC monolayer (mean 51 cells) (Fig. 3.1, 3.2, 3.4, 3.5 3.9, 3.10). MSC adherence to murine cardiac sections was significantly decreased by H₂O₂ ($p = 0.001$), KC ($p = 0.026$) and SDF-1 α ($p = 0.046$) (Fig. 3.10). Notably, in some fields of view, across all treatment conditions, MSCs were observed to cluster at the intraventricular endothelial/endocardial surfaces (Fig. 3.11, panels D-F).

Table 3.8. Descriptive statistics for the adhesion of pretreated murine mesenchymal stem cells (mMSCs) to murine cardiac sections. mMSCs (passage 10) were CFSE labelled, then pretreated for 1 hour with a cytokine (100 ng/mL), H₂O₂ (100 µM) or medium alone (control). Treated mMSCs were incubated for 20 minutes with acetone-fixed murine cardiac sections (5x10⁴ cells/section). mMSC adhesion was systematically assessed at 10x magnification using a fluorescence microscope. n=4, 5 observations per experiment. IQR = interquartile range.

	Minimum	Median	IQR	Maximum
Control	2	9	14	117
TNFα	0	9	6.5	120
IL-1β	1	6	8	25
IFNγ	1	5.5	11	51
KC	0	4.5	13.75	35
SDF-1α	0	6.5	9.5	60
H2O2 (100µM)	0	5	4.75	38

Table 3.9. Shapiro-Wilk test on observations of pretreated murine mesenchymal stem cell (mMSC) adhesion to murine cardiac sections. mMSCs (passage 10) were CFSE labelled, then pretreated for 1 hour with a cytokine (100 ng/mL), H₂O₂ (100 µM) or medium alone (control). Treated mMSCs were incubated for 20 minutes with acetone-fixed murine cardiac sections (5x10⁴ cells/section). hMSC adhesion was systematically assessed at 10x magnification using a fluorescence microscope. n=3, 5 observations per experiment.

	Statistic	N	Sig.*
Control	.575	40	.000
TNFα	.463	40	.000
IL-1β	.905	40	.003
IFNγ	.715	40	.000
KC	.835	40	.000
SDF-1α	.703	40	.000
H₂O₂	.692	40	.000

*p<0.05

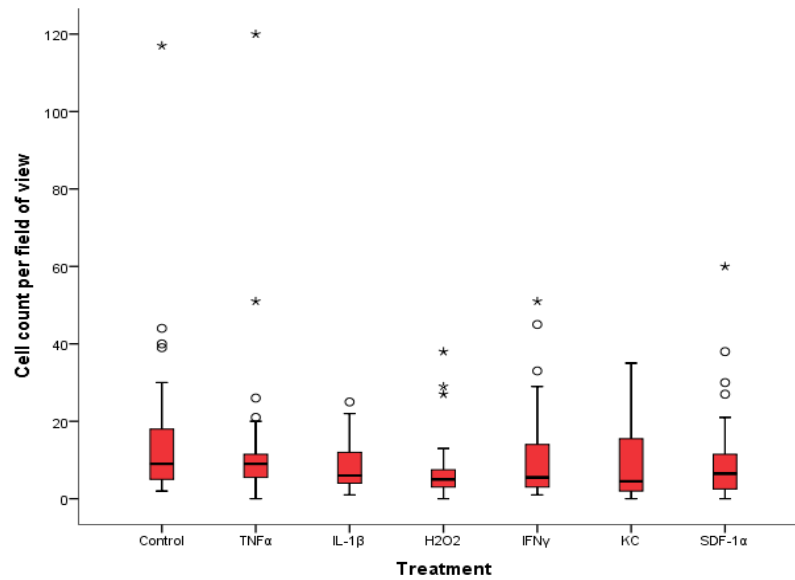


Figure 3.9. Adhesion of pretreated murine mesenchymal stem cells (mMSCs) to murine cardiac sections. mMSCs (passage 10) were CFSE labelled, then pretreated for 1 hour with a cytokine (100 ng/mL), H₂O₂ (100 μ M) or medium alone (control). Treated mMSCs were incubated for 20 minutes with acetone-fixed murine cardiac sections (5x10⁴ cells/section). mMSC adhesion was systematically assessed at 10x magnification using a fluorescence microscope. n=4, 5 observations per experiment. KC = keratinocyte chemokine. Black line denotes median value. Boxes = interquartile range (IQR). Bars = highest/lowest datum within 1.5IQR of upper/lower quartile. \circ = outlier >1.5IQR of upper/lower quartile but < 3 box lengths from upper end of box. * = extreme outlier > 3 box lengths from upper end of box.

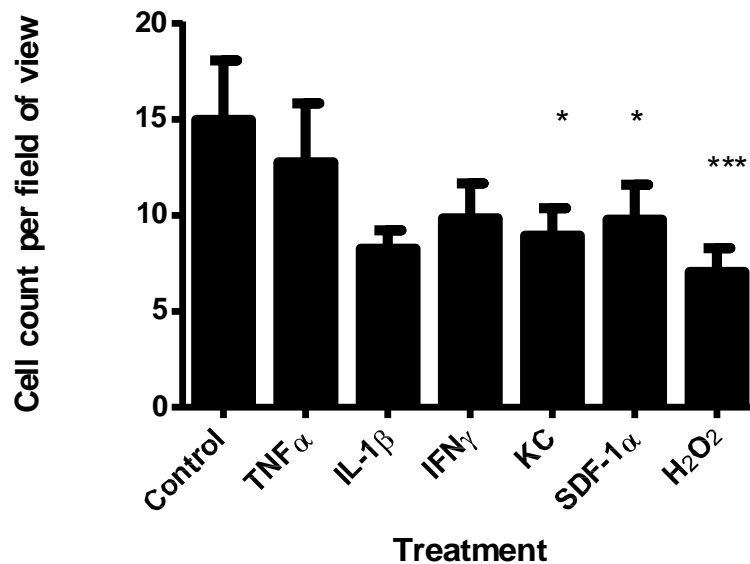


Figure 3.10. Effect of pretreatment on the static adhesion of murine mesenchymal stem cells (mMSCs) to murine cardiac sections. mMSCs (passage 10) were CFSE labelled, then pretreated for 1 hour with a cytokine (100 ng/mL), H₂O₂ (100 μ M) or medium alone (control). Treated mMSCs were incubated for 20 minutes with acetone-fixed murine cardiac sections (5x10⁴ cells/section). mMSC adhesion was systematically assessed at 10x magnification using a fluorescence microscope. n=4, 5 observations per experiment. KC = keratinocyte chemokine. * = p<0.05, *** = p<0.001 vs. control.

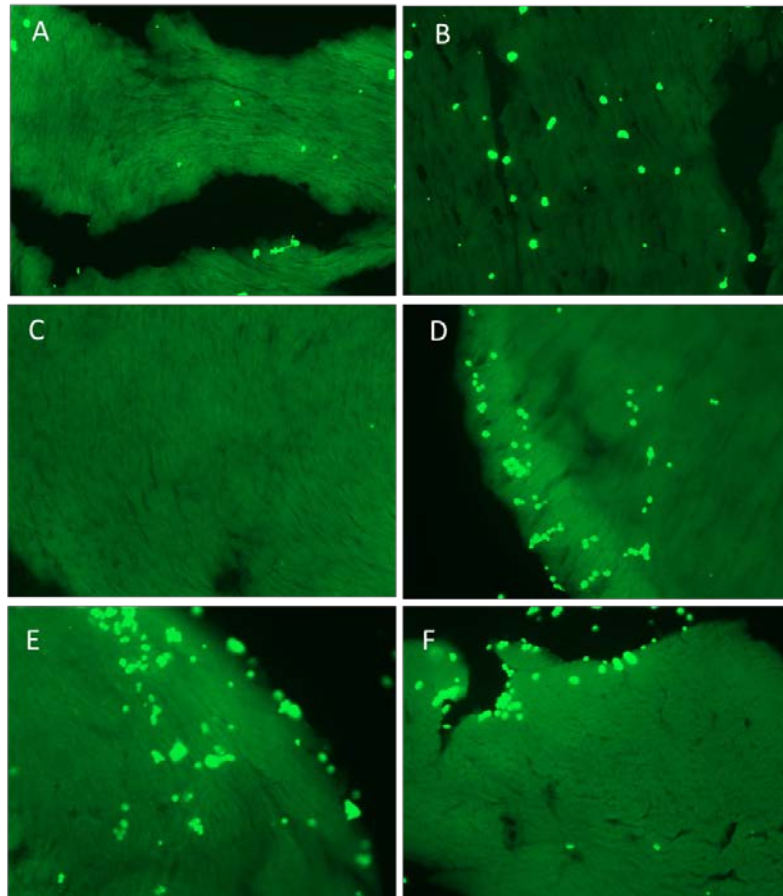


Figure 3.11. Representative fluorescence images of murine mesenchymal stem cell (mMSC) adhesion to murine cardiac sections. mMSCs (passage 10) were CFSE-labelled, then pretreated for 1 hour with cytokines/ H_2O_2 or medium alone (control). Treated mMSCs were incubated for 20 minutes with acetone-fixed murine cardiac sections (5×10^4 cells/section). mMSC adhesion was visualised at 10x magnification using a fluorescence microscope. (A,B,C) = images illustrating the variability in $TNF-\alpha$ -treated mMSC adherence to cardiac sections. (D,E,F) Endothelial/endocardial clustering of MSCs.

4. Discussion

4.1 Enhancing MSC Adhesion to Murine Cardiac Endothelium.

Pretreatment of mMSCs with H₂O₂ and IFN γ significantly increased their adhesion to a confluent MuCEC monolayer, with H₂O₂ producing a 4.3-fold increase in MSC adhesion (Fig. 3.2). Previous evidence from our lab has shown H₂O₂ to increase HSC adhesion to IR injured kidney and intestine. Furthermore, a H₂O₂-mediated increase in cell surface integrin clustering has been shown to mediate this enhanced adhesion (52–54). Such clustering is known to enhance integrin binding avidity (59). This is the first time H₂O₂ has been shown to promote MSC adhesion to endothelium. Further study is required to determine whether the mechanisms responsible for this enhanced adhesion are similar in MSCs and HSCs. IFN γ increased MSC adhesion to MuCEC 1.4-fold. Treatment of MSCs with IFN γ has previously been shown to increase their cell surface expression of ICAM-1 and VCAM-1 (60), possibly explaining the increase in adhesion to MuCEC observed here. Furthermore, expression of these adhesion molecules is important for MSC-mediated immunoregulation (60), raising the possibility that IFN γ pretreatment of MSCs may enhance their immunomodulatory potential in the heart. As outlined in section 1, MSC pretreatment with SDF-1 α , TNF α and IL-1 β has previously shown chemotactic promise (27,56,57), yet no significant increase in MSC adhesion to MuCEC was found here. This may appear surprising, given the considerably greater mean cell count values obtained for SDF-1 α , TNF α and IL-1 β , compared to IFN γ (Fig. 3.2). However, it must be remembered that the Kruskal-Wallis one-way analysis of variance is based on ranked data. That the changes in cell count induced by SDF-1 α , TNF α and IL-1 β were statistically insignificant can be better appreciated by examining the data spread (Fig. 3.1). The number of assays completed was limited

by time constraints and the number of MSCs which were available. Given the large standard error which appears inherent to the assay (Fig. 3.1, Fig 3.2) a greater number of assays may demonstrate a significant effect of KC, SDF-1 α and TNF α . I suggest that the standard deviation values derived from this data will be useful in designing future experiments with sufficient numbers to detect a meaningful change in adhesion.

Given the pronounced effect of H₂O₂ discussed above, a range of H₂O₂ concentrations were then used for MSC pretreatment, to establish whether there was a dose-response effect on adhesion to MuCEC. Contrary to expectations, the 100 μ M H₂O₂-mediated increase in MSC adherence to MuCEC was not reproduced, and none of the additional concentrations had a significant effect (Fig. 3.5). In the earlier experiments discussed above, MSCs were used between passages 7-9. It was necessary to use the MSCs in subsequent experiments at passage 10. A passage-related decline in MSC surface receptor expression is well described. CXCR4 expression declines beyond passages 4-5 (26). Honczarenko *et al.* demonstrated a marked decline in MSC cell surface chemokine expression at passages 12-16, with an accompanying decrease in the expression of adhesion molecules such as ICAM-1, ICAM-2 and VCAM-1. As a result, passage 16 MSCs did not display chemotactic responses *in vitro* (61). It is possible that such alterations in surface protein expression underlie the failure of H₂O₂ to alter MSC adhesion to MuCEC at passage 10. Further work should aim to characterise passage-related alterations in such expression, in parallel with alterations in MSC adhesion. This is of vital clinical relevance. To date, IV-administered MSCs have been used before passage 5 in human clinical trials, largely due to concerns about their tumorigenic potential at later passages (62–64). It may be that MSCs are also clinically less effective at later

passages. I suggest that their passage-related adhesive properties be fully characterised and that future work be carried out at clinically relevant passages.

It is possible that H₂O₂ treatment of MSCs alters cell viability. Only adherent, viable cells are of therapeutic relevance. A FACS Annexin V/Propidium Iodide apoptosis assay was planned. However, the limited availability of MSCs within the time-frame of this project prevented its completion. Trypan blue staining counts of live/ dead cells are presented in section 3.2. It appears that H₂O₂ pretreatment of MSCs up to 1 mM does not enhance cell death.

4.2 Enhancing MSC Adhesion to Human Coronary Artery Endothelium.

Pretreatment of passage 2 and 3 hMSCs (clinically relevant passages; see above) with SDF-1 α and IL-8 significantly increased their adhesion to confluent HCAEC monolayers. TNF α , IL-6, IFN γ , and H₂O₂ did not modify MSC adhesion to HCAEC. There is an apparent trend towards TNF α increasing hMSC adhesion to HCAEC (Fig. 3.7), but this did not reach significance ($p = 0.059$). As with the experiments described in section 4.1, the number assays was limited by the quantity of MSCs which could be generated in the time available. Again, this work would benefit from additional assays being completed, and from this data being used to design experiments with sufficient numbers to detect relevant changes in MSC adhesion.

SDF-1 α is known to enhance hMSC chemotactic homing *in vitro* and *in vivo*, apparently via inducing increased MSC surface expression of CXCR4 (27,56). The effect of SDF-1 α and IL-8 on hMSC integrin activation (critical for endothelial adhesion and transmigration of MSCs) is less well characterised. SDF-1 α and IL-8 may increase adhesion of hMSCs to VCAM-1 in a parallel plate flow chamber, although the underlying mechanism has not been characterised (65). It is possible

that increased hMSC expression and/or clustering of $\alpha 4\beta 1$ integrin underlies this increase in adhesion. Importantly, Ciuculescu *et al.* highlighted considerable inter-donor variability in hMSC response to chemokine stimulation. SDF-1 α increased hMSC adhesion to VCAM-1 in 2/5 MSC donors, IL-8 significantly enhanced such adhesion in 1/5 donors (65). Thus, it may be that a broad chemokine cocktail would provide the best opportunity for enhancing endothelial adhesion of autologous MSCs in a clinical context. Alternatively, a reliable method of *in vitro* MSC screening may allow individualised pretreatment of MSCs. We used a commercially available primary hMSC product. Our results are therefore representative of the MSC donors used to generate that product. In order to generate an accurate picture of the aggregate response of hMSCs to cytokine/ H₂O₂ priming, it may be necessary to assess such treatments in MSCs from multiple, defined donors.

Although TNF α pretreated MSCs did not display significantly increased adherence to HCAEC, a trend was evident. It is plausible that further investigation might reveal a significant effect. *In vitro* and *in vivo* homing of rat MSCs is enhanced by preincubation with TNF α (66,67). The underlying mechanisms are unclear. Some describe an increase in MSC VCAM-1 expression, without alterations in ICAM-1, VLA-4 and L-selectin expression (66). Others have shown a TNF α -induced increase in MSC ICAM-1 expression, with no alteration in VCAM-1 expression (67). Segers *et al.* showed that TNF α pretreatment of rodent MSCs significantly increases their adhesion to coronary microvascular endothelium (CMVE). Furthermore, this adhesion was dependent on VCAM-1 induction (but not induction of ICAM-1 or VLA-4) in both CMVE and MSCs (58). MSC VLA4 interactions with endothelial VCAM-1 are traditionally described. However, this work suggests that MSC VCAM-1, not just VLA4, mediates their adhesion to endothelium. Although studies of TNF α pretreated

hMSCs are lacking, this evidence from rat MSCs indicates that TNF α does have the potential to enhance MSC endothelial adherence. Characterisation of the effects of TNF α pretreatment on hMSCs and their adhesion to endothelium is therefore warranted.

100 μ M H₂O₂ did not alter hMSC HCAEC adhesion. In the absence of mechanistic data, it is difficult to explain the difference between the mMSC and hMSC responses to H₂O₂. It may be that H₂O₂ pretreatment of hMSCs does not induce the increase in cell surface integrin clustering (seen in HSCs), which may occur in H₂O₂-responsive mMSCs. Future research must characterise these mechanisms.

4.3 MSC Adhesion to Murine Cardiac Sections

MSC adherence to murine cardiac sections was considerably less than that to MuCEC. MSC adherence to murine cardiac sections was significantly decreased by H₂O₂, KC, and SDF-1 α (0.58, 0.47 and 0.62-fold respectively). MSCs clustered at the intraventricular endothelial/endocardial surfaces in some fields of view, although this was not a universal phenomenon.

The reduced overall adhesion of MSCs to cardiac sections, compared to a confluent endothelial monolayer may be explained by recent work that has shown no VCAM-1 expression in adult cardiomyocytes; adult cardiac expression of VCAM-1 is restricted to the endocardium, heart valves and vascular endothelium (68) (Fig. 4.1). Given the majority of cardiac section area consists of cardiomyocytes, poor MSC adhesion (likely due to limited VLA-4-VCAM-1 interaction) is unsurprising. This poor adhesion may also be explained by passage-related changes in MSC adhesion capacity which are discussed above. The MSCs used in the Stamper-Woodruff assays were at passage 10, those used in the static adhesion assays were between passage 7 and

passage 9. The persistence of VCAM-1 within the endocardium and vascular endothelium (Fig. 4.1), may explain the (unquantified) phenomenon of MSC clustering at intraventricular endothelial/endocardial surfaces in some sections (Fig. 3.11). I propose that future Stamper-Woodruff assay sections should be chosen so that a comparable ventricular/endocardial area is represented on the sections used for each treatment condition. The sections could be counterstained to allow ventricular and vascular endothelium to be identified. The relative cardiomyocyte and endothelial distribution of adherent MSCs may then be quantified. Sectioning of murine heart to expose the ventricular endothelial surface area may better allow measurement of MSC adhesion potential to this surface. It is unclear whether poor MSC adherence to cardiomyocytes is of clinical concern. Endothelial VCAM-1-mediated adhesion and transmigration may be of principal concern for improving the myocardial uptake of IV-administered MSCs. It is however possible that poor MSC adhesion to myocardial sections indicates a propensity for poor intra-myocardial retention. This would be of concern in the intramyocardial and intracoronary injection of MSCs, as well as in their IV administration. Given the considerable retention of IV-administered MSCs in the lungs (18), exploration of the mechanisms underlying both cardiac MSC uptake and their intramyocardial retention is essential.

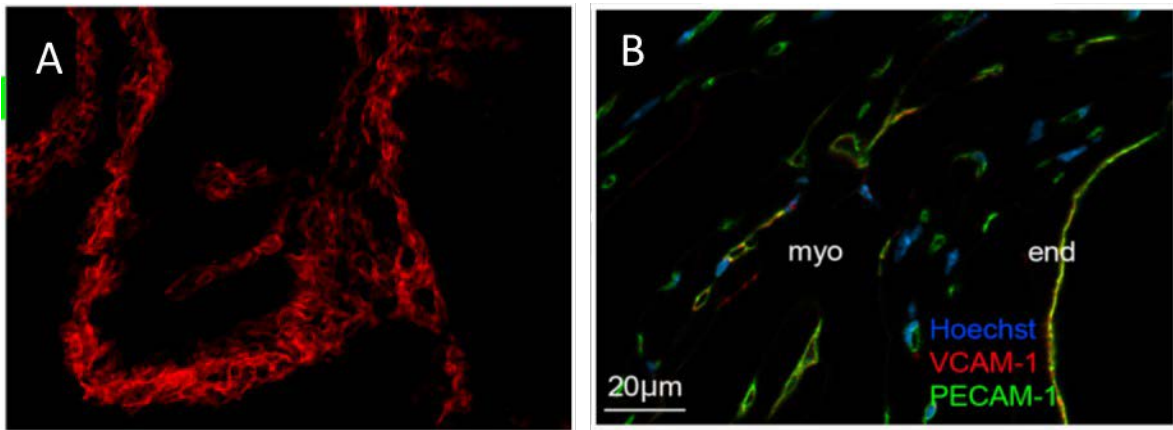


Figure 4.1. Distribution of cardiac VCAM-1 expression in murine heart. (A) Embryonic myocardium (B) Adult myocardium. From: Ponten A, et al. PLoS ONE 2013;8(12): e82403.

It is surprising that H_2O_2 , KC and SDF-1 α reduced MSC adhesion to murine cardiac sections. This is difficult to explain when coupled with a significant increase in H_2O_2 -pretreated MSC adhesion to MuCEC, along with accompanying trends towards an increase in KC and SDF-1 α adhesion (Fig. 3.2). Explanation of this result is further complicated by the absence of accompanying mechanistic data. mMSCs should respond in a similar manner to the identical treatments across the two experiments. Two plausible explanations for this exist. Firstly, the adhesive capabilities of the MSCs used in the Stamper-Woodruff assays may be impaired due to their late passage (passage 10, see discussion above) in comparison to those used in the equivalent static adhesion assay (passage 7-9). Secondly, the dominant mechanism mediating their adhesion to VCAM-1 deficient cardiac sections may differ from that mediating their adhesion to MuCEC. If this is the case, MSC pretreatment may have a different effect on their adhesion to cardiac sections. In any case, VCAM-1 is upregulated in adult heart following ischaemia-reperfusion injury (69), raising the possibility that MSC adhesion would be enhanced by cytokine/MSC pretreatment in such sections. This work was planned, but time constraints did not allow its completion. It is clear

that considerable further work is required to answer the questions raised here. Again, this data can inform this additional work, allowing robust study design with sufficient numbers to detect meaningful results.

4.4 Concluding Remarks

The pretreatment of MSCs with cytokines or H₂O₂ has the potential to improve their homing to injured myocardium. This work has provided a number of important insights into that potential. Firstly, there may exist an inter-species difference in the effectiveness of cytokines and H₂O₂ to improve MSC endothelial adherence; H₂O₂ may not be an effective primer of hMSC adhesion. Secondly, the use of mMSCs at later, and therefore clinically irrelevant passages, may impair the ability of pretreatment to alter their adhesive properties. Caution should therefore be exercised in the interpretation of murine data and data derived from late-passage MSCs. Furthermore, the inter-donor differences in MSC response to individual cytokines must be borne in mind. A more complete examination of the response of hMSCs from clearly defined donors to cytokine priming is desirable. It is unclear whether the poor adhesion of mMSCs to cardiac sections is of clinical relevance. It may be that their endothelial adhesive properties are of greater importance for their uptake into injured myocardium. This should be explored further. This work is limited by the small sample sizes, but this data may be used to design powerful future experiments with adequate numbers to detect clinically meaningful changes in MSC adhesion. Discussion of this work is limited by our lack of knowledge of underlying mechanisms explaining the changes observed. Such mechanisms must be characterised. Finally, this *in vitro* work must be accompanied by *in vivo* studies of MSC homing to IR-injured myocardium and exploration of the functional consequences of improving such homing.

5. References

1. Chamberlain G, Fox J, Ashton B, Middleton J. Concise review: mesenchymal stem cells: their phenotype, differentiation capacity, immunological features, and potential for homing. *Stem Cells Dayt Ohio*. 2007 Nov;25(11):2739–49.
2. Dominici M, Le Blanc K, Mueller I, Slaper-Cortenbach I, Marini F, Krause D, et al. Minimal criteria for defining multipotent mesenchymal stromal cells. The International Society for Cellular Therapy position statement. *Cytotherapy*. 2006;8(4):315–7.
3. Rostovskaya M, Anastassiadis K. Differential expression of surface markers in mouse bone marrow mesenchymal stromal cell subpopulations with distinct lineage commitment. *PLoS One*. 2012;7(12):e51221.
4. Peister A, Mellad JA, Larson BL, Hall BM, Gibson LF, Prockop DJ. Adult stem cells from bone marrow (MSCs) isolated from different strains of inbred mice vary in surface epitopes, rates of proliferation, and differentiation potential. *Blood*. 2004 Mar 1;103(5):1662–8.
5. Thygesen K, Alpert JS, White HD, Jaffe AS, Apple FS, Galvani M, et al. Universal definition of myocardial infarction Kristian Thygesen, Joseph S. Alpert and Harvey D. White on behalf of the Joint ESC/ACCF/AHA/WHF Task Force for the Redefinition of Myocardial Infarction. *Eur Heart J*. 2007 Oct 1;28(20):2525–38.
6. Roger VL, Go AS, Lloyd-Jones DM, Benjamin EJ, Berry JD, Borden WB, et al. Heart disease and stroke statistics--2012 update: a report from the American Heart Association. *Circulation*. 2012 Jan 3;125(1):e2–e220.
7. Roger VL. Epidemiology of myocardial infarction. *Med Clin North Am*. 2007 Jul;91(4):537–ix.
8. McMurray JJV, Stewart S. The burden of heart failure. *Eur Heart J Suppl*. 2002 Apr 1;4(suppl D):D50–D58.
9. Stewart S, MacIntyre K, Capewell S, McMurray JJV. Heart failure and the aging population: an increasing burden in the 21st century? *Heart*. 2003 Jan 1;89(1):49–53.
10. Sutton MGSJ, Sharpe N. Left Ventricular Remodeling After Myocardial Infarction Pathophysiology and Therapy. *Circulation*. 2000 Jun 27;101(25):2981–8.
11. Frangogiannis NG, Smith CW, Entman ML. The inflammatory response in myocardial infarction. *Cardiovasc Res*. 2002 Jan;53(1):31–47.
12. Aldridge V, Garg A, Davies N, Bartlett DC, Youster J, Beard H, et al. Human mesenchymal stem cells are recruited to injured liver in a β 1-integrin and CD44 dependent manner. *Hepatology*. 2012 Sep;56(3):1063–73.
13. Ortiz LA, Gambelli F, McBride C, Gaupp D, Baddoo M, Kaminski N, et al.

Mesenchymal stem cell engraftment in lung is enhanced in response to bleomycin exposure and ameliorates its fibrotic effects. *Proc Natl Acad Sci U S A*. 2003 Jul 8;100(14):8407–11.

14. Chang P, Qu Y, Liu Y, Cui S, Zhu D, Wang H, et al. Multi-therapeutic effects of human adipose-derived mesenchymal stem cells on radiation-induced intestinal injury. *Cell Death Dis*. 2013;4:e685.
15. François S, Bensidhoum M, Mouiseddine M, Mazurier C, Allenet B, Semont A, et al. Local irradiation not only induces homing of human mesenchymal stem cells at exposed sites but promotes their widespread engraftment to multiple organs: a study of their quantitative distribution after irradiation damage. *Stem Cells Dayt Ohio*. 2006 Apr;24(4):1020–9.
16. Sheikh AY, Lin S-A, Cao F, Cao Y, van der Bogt KEA, Chu P, et al. Molecular imaging of bone marrow mononuclear cell homing and engraftment in ischemic myocardium. *Stem Cells Dayt Ohio*. 2007 Oct;25(10):2677–84.
17. Mouquet F, Pfister O, Jain M, Oikonomopoulos A, Ngoy S, Summer R, et al. Restoration of cardiac progenitor cells after myocardial infarction by self-proliferation and selective homing of bone marrow-derived stem cells. *Circ Res*. 2005 Nov 25;97(11):1090–2.
18. Kraitchman DL, Tatsumi M, Gilson WD, Ishimori T, Kedziorek D, Walczak P, et al. Dynamic Imaging of Allogeneic Mesenchymal Stem Cells Trafficking to Myocardial Infarction. *Circulation*. 2005 Sep 6;112(10):1451–61.
19. Freyman T, Polin G, Osman H, Crary J, Lu M, Cheng L, et al. A quantitative, randomized study evaluating three methods of mesenchymal stem cell delivery following myocardial infarction. *Eur Heart J*. 2006 May;27(9):1114–22.
20. Assis ACM, Carvalho JL, Jacoby BA, Ferreira RLB, Castanheira P, Diniz SOF, et al. Time-dependent migration of systemically delivered bone marrow mesenchymal stem cells to the infarcted heart. *Cell Transplant*. 2010;19(2):219–30.
21. Barbash IM, Chouraqui P, Baron J, Feinberg MS, Etzion S, Tessone A, et al. Systemic Delivery of Bone Marrow–Derived Mesenchymal Stem Cells to the Infarcted Myocardium Feasibility, Cell Migration, and Body Distribution. *Circulation*. 2003 Aug 19;108(7):863–8.
22. Nagaya N, Fujii T, Iwase T, Ohgushi H, Itoh T, Uematsu M, et al. Intravenous administration of mesenchymal stem cells improves cardiac function in rats with acute myocardial infarction through angiogenesis and myogenesis. *Am J Physiol Heart Circ Physiol*. 2004 Dec;287(6):H2670–2676.
23. Rüster B, Göttig S, Ludwig RJ, Bistrrian R, Müller S, Seifried E, et al. Mesenchymal stem cells display coordinated rolling and adhesion behavior on endothelial cells. *Blood*. 2006 Dec 1;108(12):3938–44.
24. Salem HK, Thiemermann C. Mesenchymal stromal cells: current understanding and clinical status. *Stem Cells Dayt Ohio*. 2010 Mar 31;28(3):585–96.

25. Ip JE, Wu Y, Huang J, Zhang L, Pratt RE, Dzau VJ. Mesenchymal stem cells use integrin beta1 not CXC chemokine receptor 4 for myocardial migration and engraftment. *Mol Biol Cell*. 2007 Aug;18(8):2873–82.
26. Wu Y, Zhao RCH. The role of chemokines in mesenchymal stem cell homing to myocardium. *Stem Cell Rev*. 2012 Mar;8(1):243–50.
27. Ponte AL, Marais E, Gallay N, Langonné A, Delorme B, Héroult O, et al. The in vitro migration capacity of human bone marrow mesenchymal stem cells: comparison of chemokine and growth factor chemotactic activities. *Stem Cells Dayt Ohio*. 2007 Jul;25(7):1737–45.
28. Schenk S, Mal N, Finan A, Zhang M, Kiedrowski M, Popovic Z, et al. Monocyte chemotactic protein-3 is a myocardial mesenchymal stem cell homing factor. *Stem Cells Dayt Ohio*. 2007 Jan;25(1):245–51.
29. Belema-Bedada F, Uchida S, Martire A, Kostin S, Braun T. Efficient homing of multipotent adult mesenchymal stem cells depends on FROUNT-mediated clustering of CCR2. *Cell Stem Cell*. 2008 Jun 5;2(6):566–75.
30. Makkar RR, Price MJ, Lill M, Frantzen M, Takizawa K, Kleisli T, et al. Intramyocardial injection of allogeneic bone marrow-derived mesenchymal stem cells without immunosuppression preserves cardiac function in a porcine model of myocardial infarction. *J Cardiovasc Pharmacol Ther*. 2005 Dec;10(4):225–33.
31. Schuleri KH, Feigenbaum GS, Centola M, Weiss ES, Zimmet JM, Turney J, et al. Autologous mesenchymal stem cells produce reverse remodeling in chronic ischaemic cardiomyopathy. *Eur Heart J*. 2009 Nov;30(22):2722–32.
32. Hamamoto H, Gorman JH 3rd, Ryan LP, Hinmon R, Martens TP, Schuster MD, et al. Allogeneic mesenchymal precursor cell therapy to limit remodeling after myocardial infarction: the effect of cell dosage. *Ann Thorac Surg*. 2009 Mar;87(3):794–801.
33. Amado LC, Saliaris AP, Schuleri KH, St John M, Xie J-S, Cattaneo S, et al. Cardiac repair with intramyocardial injection of allogeneic mesenchymal stem cells after myocardial infarction. *Proc Natl Acad Sci U S A*. 2005 Aug 9;102(32):11474–9.
34. Quevedo HC, Hatzistergos KE, Oskouei BN, Feigenbaum GS, Rodriguez JE, Valdes D, et al. Allogeneic mesenchymal stem cells restore cardiac function in chronic ischemic cardiomyopathy via trilineage differentiating capacity. *Proc Natl Acad Sci U S A*. 2009 Aug 18;106(33):14022–7.
35. Perin EC, Silva GV, Assad JAR, Vela D, Buja LM, Sousa ALS, et al. Comparison of intracoronary and transendocardial delivery of allogeneic mesenchymal cells in a canine model of acute myocardial infarction. *J Mol Cell Cardiol*. 2008 Mar;44(3):486–95.
36. Halkos ME, Zhao Z-Q, Kerendi F, Wang N-P, Jiang R, Schmarkey LS, et al. Intravenous infusion of mesenchymal stem cells enhances regional perfusion and improves ventricular function in a porcine model of myocardial infarction.

Basic Res Cardiol. 2008 Nov;103(6):525–36.

37. Price MJ, Chou C-C, Frantzen M, Miyamoto T, Kar S, Lee S, et al. Intravenous mesenchymal stem cell therapy early after reperfused acute myocardial infarction improves left ventricular function and alters electrophysiologic properties. *Int J Cardiol.* 2006 Aug 10;111(2):231–9.
38. Chen S, Fang W, Ye F, Liu Y-H, Qian J, Shan S, et al. Effect on left ventricular function of intracoronary transplantation of autologous bone marrow mesenchymal stem cell in patients with acute myocardial infarction. *Am J Cardiol.* 2004 Jul 1;94(1):92–5.
39. Heldman AW, DiFede DL, Fishman JE, Zambrano JP, Trachtenberg BH, Karantalis V, et al. Transendocardial mesenchymal stem cells and mononuclear bone marrow cells for ischemic cardiomyopathy: the TAC-HFT randomized trial. *JAMA J Am Med Assoc.* 2014 Jan 1;311(1):62–73.
40. Hare JM, Fishman JE, Gerstenblith G, et al. Comparison of allogeneic vs autologous bone marrow–derived mesenchymal stem cells delivered by transendocardial injection in patients with ischemic cardiomyopathy: The poseidon randomized trial. *JAMA.* 2012 Dec 12;308(22):2369–79.
41. Toma C, Pittenger MF, Cahill KS, Byrne BJ, Kessler PD. Human Mesenchymal Stem Cells Differentiate to a Cardiomyocyte Phenotype in the Adult Murine Heart. *Circulation.* 2002 Jan 1;105(1):93–8.
42. Shake JG, Gruber PJ, Baumgartner WA, Senechal G, Meyers J, Redmond JM, et al. Mesenchymal stem cell implantation in a swine myocardial infarct model: engraftment and functional effects. *Ann Thorac Surg.* 2002 Jun;73(6):1919–1925; discussion 1926.
43. Silva GV, Litovsky S, Assad JAR, Sousa ALS, Martin BJ, Vela D, et al. Mesenchymal Stem Cells Differentiate into an Endothelial Phenotype, Enhance Vascular Density, and Improve Heart Function in a Canine Chronic Ischemia Model. *Circulation.* 2005 Jan 18;111(2):150–6.
44. Gneocchi M, Zhang Z, Ni A, Dzau VJ. Paracrine mechanisms in adult stem cell signaling and therapy. *Circ Res.* 2008 Nov 21;103(11):1204–19.
45. Gneocchi M, He H, Noiseux N, Liang OD, Zhang L, Morello F, et al. Evidence supporting paracrine hypothesis for Akt-modified mesenchymal stem cell-mediated cardiac protection and functional improvement. *FASEB J.* 2006 Apr 1;20(6):661–9.
46. Gneocchi M, He H, Liang OD, Melo LG, Morello F, Mu H, et al. Paracrine action accounts for marked protection of ischemic heart by Akt-modified mesenchymal stem cells. *Nat Med.* 2005 Apr;11(4):367–8.
47. Takahashi M, Li T-S, Suzuki R, Kobayashi T, Ito H, Ikeda Y, et al. Cytokines produced by bone marrow cells can contribute to functional improvement of the infarcted heart by protecting cardiomyocytes from ischemic injury. *Am J Physiol Heart Circ Physiol.* 2006 Aug;291(2):H886–893.

48. Mirotsov M, Jayawardena TM, Schmeckpeper J, Gneccchi M, Dzau VJ. Paracrine mechanisms of stem cell reparative and regenerative actions in the heart. *J Mol Cell Cardiol.* 2011 Feb;50(2):280–9.
49. Zhang R, Liu Y, Yan K, Chen L, Chen X-R, Li P, et al. Anti-inflammatory and immunomodulatory mechanisms of mesenchymal stem cell transplantation in experimental traumatic brain injury. *J Neuroinflammation.* 2013 Aug 23;10:106.
50. Németh K, Leelahavanichkul A, Yuen PST, Mayer B, Parmelee A, Doi K, et al. Bone marrow stromal cells attenuate sepsis via prostaglandin E(2)-dependent reprogramming of host macrophages to increase their interleukin-10 production. *Nat Med.* 2009 Jan;15(1):42–9.
51. Burchfield JS, Iwasaki M, Koyanagi M, Urbich C, Rosenthal N, Zeiher AM, et al. Interleukin-10 From Transplanted Bone Marrow Mononuclear Cells Contributes to Cardiac Protection After Myocardial Infarction. *Circ Res.* 2008 Jul 18;103(2):203–11.
52. White RL, Nash G, Kavanagh DPJ, Savage COS, Kalia N. Modulating the Adhesion of Haematopoietic Stem Cells with Chemokines to Enhance Their Recruitment to the Ischaemically Injured Murine Kidney. *PLoS ONE.* 2013 Jun 19;8(6):e66489.
53. Kavanagh DPJ, Yemm AI, Alexander JS, Frampton J, Kalia N. Enhancing the adhesion of hematopoietic precursor cell integrins with hydrogen peroxide increases recruitment within murine gut. *Cell Transplant.* 2013;22(8):1485–99.
54. Kavanagh DPJ, Yemm AI, Zhao Y, Frampton J, Kalia N. Mechanisms of Adhesion and Subsequent Actions of a Haematopoietic Stem Cell Line, HPC-7, in the Injured Murine Intestinal Microcirculation In Vivo. *PLOS ONE.* 2013 Mar 12;8(3):e59150.
55. Shi M, Li J, Liao L, Chen B, Li B, Chen L, et al. Regulation of CXCR4 expression in human mesenchymal stem cells by cytokine treatment: role in homing efficiency in NOD/SCID mice. *Haematologica.* 2007 Jul;92(7):897–904.
56. Jones GN, Moschidou D, Lay K, Abdulrazzak H, Vanleene M, Shefelbine SJ, et al. Upregulating CXCR4 in Human Fetal Mesenchymal Stem Cells Enhances Engraftment and Bone Mechanics in a Mouse Model of Osteogenesis Imperfecta. *Stem Cells Transl Med.* 2012 Jan;1(1):70–8.
57. Fan H, Zhao G, Liu L, Liu F, Gong W, Liu X, et al. Pre-treatment with IL-1 β enhances the efficacy of MSC transplantation in DSS-induced colitis. *Cell Mol Immunol.* 2012 Nov;9(6):473–81.
58. Segers VFM, Van Riet I, Andries LJ, Lemmens K, Demolder MJ, De Becker AJML, et al. Mesenchymal stem cell adhesion to cardiac microvascular endothelium: activators and mechanisms. *Am J Physiol - Heart Circ Physiol.* 2006 Apr 1;290(4):H1370–H1377.
59. Stewart M, Hogg N. Regulation of leukocyte integrin function: Affinity vs. avidity. *J Cell Biochem.* 1996;61(4):554–61.

60. Ren G, Zhao X, Zhang L, Zhang J, L'Huillier A, Ling W, et al. Inflammatory cytokine-induced intercellular adhesion molecule-1 and vascular cell adhesion molecule-1 in mesenchymal stem cells are critical for immunosuppression. *J Immunol Baltim Md 1950*. 2010 Mar 1;184(5):2321–8.
61. Honczarenko M, Le Y, Swierkowski M, Ghiran I, Glodek AM, Silberstein LE. Human bone marrow stromal cells express a distinct set of biologically functional chemokine receptors. *Stem Cells Dayt Ohio*. 2006 Apr;24(4):1030–41.
62. Burns JS, Abdallah BM, Guldberg P, Rygaard J, Schrøder HD, Kassem M. Tumorigenic heterogeneity in cancer stem cells evolved from long-term cultures of telomerase-immortalized human mesenchymal stem cells. *Cancer Res*. 2005 Apr 15;65(8):3126–35.
63. Rubio D, Garcia-Castro J, Martín MC, de la Fuente R, Cigudosa JC, Lloyd AC, et al. Spontaneous human adult stem cell transformation. *Cancer Res*. 2005 Apr 15;65(8):3035–9.
64. Hare JM, Traverse JH, Henry TD, Dib N, Strumpf RK, Schulman SP, et al. A randomized, double-blind, placebo-controlled, dose-escalation study of intravenous adult human mesenchymal stem cells (prochymal) after acute myocardial infarction. *J Am Coll Cardiol*. 2009 Dec 8;54(24):2277–86.
65. Ciuculescu F, Giesen M, Deak E, Lang V, Seifried E, Henschler R. Variability in chemokine-induced adhesion of human mesenchymal stromal cells. *Cytotherapy*. 2011 Nov;13(10):1172–9.
66. Xiao Q, Wang S, Tian H, Xin L, Zou Z, Hu Y, et al. TNF- α increases bone marrow mesenchymal stem cell migration to ischemic tissues. *Cell Biochem Biophys*. 2012 Apr;62(3):409–14.
67. Fu X, Han B, Cai S, Lei Y, Sun T, Sheng Z. Migration of bone marrow-derived mesenchymal stem cells induced by tumor necrosis factor- α and its possible role in wound healing. *Wound Repair Regen*. 2009;17(2):185–91.
68. Pontén A, Walsh S, Malan D, Xian X, Schéele S, Tarnawski L, et al. FACS-Based Isolation, Propagation and Characterization of Mouse Embryonic Cardiomyocytes Based on VCAM-1 Surface Marker Expression. *PLoS ONE*. 2013 Dec 30;8(12):e82403.
69. Grieve SM, Lønborg J, Mazhar J, Tan TC, Ho E, Liu C-C, et al. Cardiac magnetic resonance imaging of rapid VCAM-1 up-regulation in myocardial ischemia-reperfusion injury. *Eur Biophys J EBJ*. 2013 Jan;42(1):61–70.

A PRELIMINARY STUDY OF THE MOLECULAR REGULATION OF PLACENTAL
GROWTH FACTOR AND VASCULAR ENDOTHELIAL GROWTH FACTOR IN
MURINE PREADIPOCYTES

by

MARY FRANCES O'LEARY

This project is submitted in partial fulfilment of the requirements for the award of the
degree of MRes

College of Medical and Dental Sciences

University of Birmingham

May 2014

Abstract

Introduction: The vascular endothelial growth factor (VEGF) family may play a role in obesity and the metabolic syndrome. Placental growth factor (PlGF) is physiologically redundant, but pathologically important, making it an attractive anti-obesity target. We principally aimed to establish whether preadipocytes express PlGF and to explore the molecular regulation of PlGF and VEGF in murine preadipocytes.

Methods: Preadipocytes were transfected with FoxO1-expressing adenoviruses and treated with H₂O₂, VEGF and cAMP. Adjunct work included quantification of PlGF secretion from endothelial-specific FoxO1,3,4 knockout livers and optimisation of preadipocyte differentiation to adipocytes. **Results:** Wild-type FoxO1 transfection induced considerable increases in preadipocyte *PlGF* and *VEGF* expression. H₂O₂, VEGF, cAMP and forskolin treatments promoted an increase in preadipocyte *FoxO1*, *VEGF* and *PlGF* expression. Enhanced *PlGF* expression was not accompanied by an increase PlGF secretion. **Conclusion:** This is a preliminary exploration of the molecular regulation of PlGF in preadipocytes. Given the small sample sizes, the results should be interpreted cautiously. The mechanisms underlying our observations must be fully characterised. CREB promotion of *Foxo1* and *PlGF* expression, along with SP-1 promotion of *VEGF* expression are of particular interest.

Acknowledgements

I am grateful to Dr. Peter Hewett for his enthusiastic and engaged supervision of this work. I also thank Dr. Sarah Connor, Dr. Jackson Kirkman-Brown and Dr. Ana Gonzalez for the use of their laboratory space, equipment, reagents and antibodies.

Table of Contents	Page
1. Literature Review / Introduction	1
1.1 Introduction	1
1.2 Vascular Endothelial Growth Factor Family – Structure	1
1.3 Vascular Endothelial Growth Factor Family Receptors	2
1.4 Major Biological Functions of the Vascular Endothelial Growth Factor Family	4
1.4.1 PIGF	4
1.4.2 VEGF	7
1.4.3 VEGF-B	7
1.5 Molecular Regulation of PIGF Expression	8
1.6 The Vascular Endothelial Growth Factor Family in the Metabolic Syndrome	9
1.7 Hypothesis, Objectives and Aims	12
2. Methods	14
2.1 Cell Culture	14
2.1.1 Immortalised Murine Preadipocytes	14
2.1.2 Primary Preadipocytes	14
2.1.3 Preadipocyte Differentiation	15
2.2 Adenovirus Transfection of Cells	16
2.3 Preadipocyte Stimulation	17
2.4 Immunofluorescence	17
2.5 Enzyme-Linked Immunosorbent Assay – Murine PIGF-2	18
2.6 Mouse DNA Extraction	18
2.7 Reverse transcriptase polymerase chain reaction/agarose gel electrophoresis	19

2.8	RNA Extraction	19
2.9	cDNA Synthesis	20
2.10	Quantitative polymerase chain reaction	20
2.11	Liver Slice Culture	22
2.12	Preparation of Murine Aortic Rings	22
2.13	Statistical Analysis	23
3.	Results	24
3.1	Preadipocyte Differentiation	24
3.2	Preadipocyte FoxO1 Adenovirus Transfection	25
3.3	Immunofluorescent Microscopy	29
3.4	Preadipocyte Stimulation	30
3.5	Mouse Genotyping	33
3.6	Liver Slice Culture – PIGF-2 ELISA	35
4.	Discussion	37
4.1	Preadipocyte FoxO1 Adenovirus Transfection	37
4.2	Preadipocyte Stimulation	38
4.3	Preadipocyte Differentiation	40
4.4	Mouse Genotyping	41
4.5	Liver Slice Culture	41
4.6	Conclusion	42
5.	References	44

List of Figures	Page
Figure 1.2. Major cellular effects of PIGF.	5
Figure 3.1. Representative image of immortalised inguinal preadipocyte differentiation at 6 days post-induction.	24
Figure 3.2. FoxO1, VEGF and PIGF gene expression in FoxO1-transfected immortalised murine inguinal preadipocytes.	26
Figure 3.3. PIGF-2 secretion in FoxO1-transfected immortalised murine inguinal preadipocytes.	26
Figure 3.4. FoxO1, VEGF and PIGF gene expression in FoxO1-transfected primary murine preadipocytes.	28
Figure 3.5. Supernatant PIGF-2 concentration in FoxO1-transfected primary murine preadipocytes.	28
Figure 3.6. Representative immunofluorescent microscopy images of control and wild-type FoxO1 transfected immortalised murine inguinal preadipocytes.	29
Figure 3.7. FoxO1, VEGF and PIGF gene expression in treated immortalised murine inguinal preadipocytes.	31
Figure 3.8. PIGF-2 release in treated immortalised murine inguinal preadipocytes.	31
Figure 3.9. FoxO1, VEGF and PIGF gene expression in treated primary murine preadipocytes.	32
Figure 3.10. PIGF-2 release in treated primary murine preadipocytes.	32
Figure 3.11. RT-PCR for the FoxO1 ^{fllox} genotype.	34
Figure 3.12. RT-PCR for the FoxO3 ^{fllox} genotype.	34
Figure 3.13. Effect of endothelial FoxO knockout and precision-cut liver slice stimulation on supernatant PIGF concentration.	

List of Tables	Page
Table 2.1. Cell culture plating details.	15
Table 2.2. Preadipocyte differentiation protocols.	16
Table 2.3. Serum and antibody conditions used for immunofluorescent staining.	18
Table 2.4. Mouse genotyping primer sequences.	19
Table 2.5. cDNA synthesis reagent volumes per reaction.	20
Table 2.6. qPCR reagent volumes per reaction.	21
Table 2.7. Murine qPCR primer sequences.	21

Abbreviations

Abbreviations are defined where they first appear in the text. The human form for forkhead box O1 is denoted by FOXO1. The murine form is denoted by FoxO1.

Gene, mRNA and cDNA symbols are italicised throughout.

1. Literature Review / Introduction

1.1 Introduction

The vascular endothelial growth factors are a family of proteins traditionally associated with angiogenesis and vasculogenesis. However, many other physiological and pathophysiological functions of these proteins have emerged. Biological roles have been suggested for vascular endothelial growth factor (VEGF, also termed VEGF-A), VEGF-B and placental growth factor (PlGF) in the metabolic syndrome and its associated conditions. Notably, inhibition of PlGF and VEGF function has been shown to confer resistance to diet-induced obesity (DIO) (1–5). The physiological redundancy of PlGF makes it a particularly attractive anti-obesity target. Little is known about its molecular regulation, its cellular origins and its adipogenic importance within fat tissue. The work described in this thesis builds upon unpublished work from our lab, which characterised the molecular regulation of PlGF in human umbilical vein endothelial cells (HUVEC). Here we explore the molecular regulation of PlGF in murine preadipocytes. We establish whether such cells can produce PlGF and respond to stimulation with factors including hydrogen peroxide (H₂O₂), VEGF and cyclic AMP (cAMP). Secondary consideration is given to the molecular influences on *VEGF* expression in such cells. We also describe our efforts to optimise the differentiation of an established mouse preadipocyte cell line and primary preadipocytes to adipocytes.

1.2 Vascular Endothelial Growth Factor Family – Structure.

VEGF is the founding member of the VEGF family of proteins. It was first identified as a factor which increased vascular permeability (6–8). Its function as a vascular endothelial cell growth factor was subsequently discovered and named VEGF

proposed. It is a dimeric, disulfide-linked, glycoprotein (9). Several VEGF isoforms of differing amino acid lengths are produced by a single VEGF gene, via alternative mRNA splicing. VEGF₁₆₅ is the predominant human isoform, (VEGF₁₆₄ is the murine equivalent)(10–12). Characterisation of VEGF protein structure allowed identification of a wider VEGF family. The VEGF family now includes VEGF, VEGF-B, VEGF-C, VEGF-D, VEGF-E, VEGF-F and PlGF. All share a core VEGF homology domain (9,11,13). In humans, PlGF exists in 4 isoforms, PlGF-1 (PlGF₁₃₁), PlGF-2 (PlGF₁₅₂), PlGF-3 (PlGF₂₀₃), and PlGF-4 (PlGF₂₂₄) (14). One PlGF isoform has been identified in mice – a 158 amino acid protein with 65% identity to human PlGF-2 (15). Human and murine VEGF-B exist in two isoforms, VEGF-B₁₆₇ and VEGF-B₁₈₆ (16).

1.3 Vascular Endothelial Growth Factor Family Receptors

The VEGF family of receptors are vascular endothelial growth factor receptor 1 (VEGFR-1, also known as fms-like tyrosine kinase; Flt-1), VEGFR-2 (KDR, human; Flk-1, mouse), VEGFR-3, neuropilin-1 (NP-1) and neuropilin-2 (NP-2). Each VEGF family member has its own pattern of receptor interaction (Fig. 1.1). This short review focuses only on those receptors interacting with VEGF, PlGF and VEGF-B.

VEGFR-1 and VEGFR-2 each have seven extracellular immunoglobulin domains, a single transmembrane domain and an intracellular tyrosine kinase domain (17,18). VEGFR-1 also exists in a soluble form (sflt-1) which may antagonise the biological activity of its ligands (16). NP-1 and NP-2 act as co-receptors (9). NP-1 enhances VEGF signalling through VEGFR-2, possibly via pre-existing VEGFR-2/NP-1 complexes (19,20). VEGFR-1 is principally expressed on endothelial cells, however it is also found on osteoblasts, monocytes/macrophages, placental trophoblasts, renal mesangial cells and hematopoietic stem cells (HSCs) (11). VEGFR-2 is also primarily

expressed in endothelial cells, but has also been identified on neuronal cells, osteoblasts, megakaryocytes and HSCs (11).

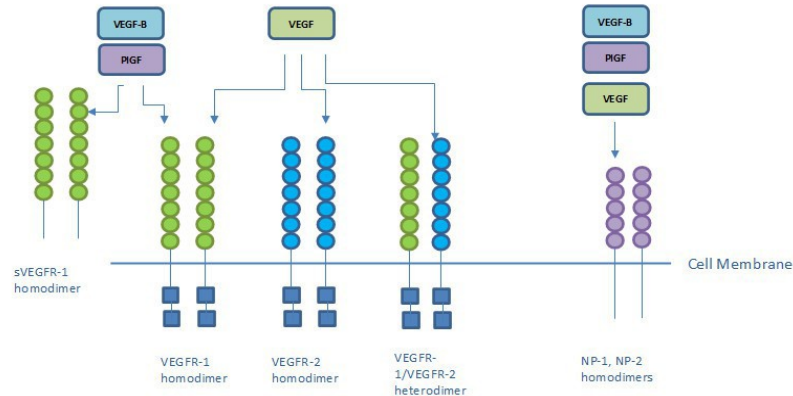


Figure 1.1. Vascular endothelial growth factor receptor interactions. For simplicity, this figure depicts only those interactions between VEGF, VEGF-B, PlGF and their corresponding receptors.

There appears to be a physiological interdependence between the VEGFR-1, sVEGFR-1 and VEGFR-2 receptors. In endothelial cells, VEGFR-2 populations generally predominate, therefore VEGFR-1/VEGFR-2 heterodimers form at the expense of VEGFR-1 homodimers (21). These heterodimers may constitute up to 50% of the total VEGF receptor complexes (22) and their formation favours VEGF signalling over that of VEGF-B or PlGF (Fig. 1.1).

VEGF binds to VEGFR-1 and sVEGFR-1 with greater affinity than to VEGFR-2. Thus, sVEGFR-1 may prevent VEGF binding to VEGFR-2 (16)(23). Although VEGFR-1 activation is not necessary or sufficient for angiogenesis, its activation (e.g. by PlGF) can transphosphorylate VEGFR-2 and therefore potentiate the angiogenic signalling of VEGF via VEGFR-2 (20,24,25). This further illustrates the complicated physiological interdependence of these receptors.

Discussion of intracellular VEGFR-1/VEGFR-2 signal transduction is not possible in this short review, beyond that which is necessary to understand PIGF expression (see Section 1.5). The reader is referred to a recent review on the subject (21).

1.4 Major Biological Functions of the Vascular Endothelial Growth Factor Family

1.4.1 PIGF

Discussion of PIGF's role in the metabolic syndrome and associated conditions will be reserved for Section 1.6.

Like VEGF, PIGF is pro-angiogenic and contributes to the growth, migration and survival of endothelial cells (23,24). PIGF can mobilise HSCs via their VEGFR-1 receptors (25). Bone marrow transplantation from PIGF^{+/+} to PIGF^{-/-} mice restores normal arteriogenesis in hindlimbs with an occluded femoral artery (26). Additionally, PIGF promotes the proliferation and contraction of vascular smooth muscle cells (27). Many other cellular activities are influenced by PIGF (see Fig. 1.2).

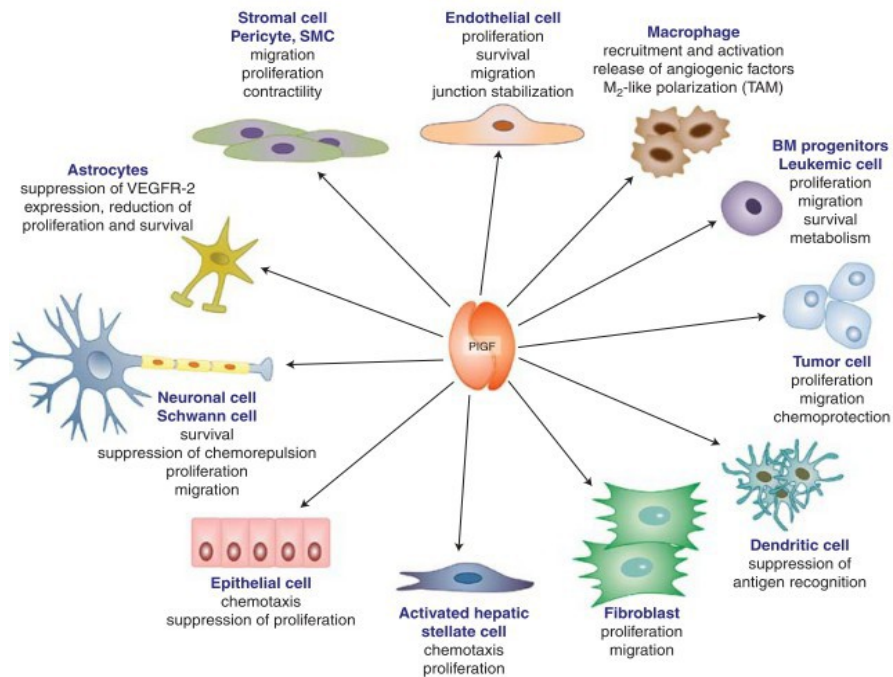


Figure 1.2. Major cellular effects of PlGF. From Dewerchin and Carmeliet. *Cold Spring Harb Perspect Med* 2012;2:a011056.

Despite its widespread cellular influence, PlGF is largely redundant in a physiological sense. VEGF deficient embryos (VEGF^{-/-}) are not viable (see Section 1.4.2) (28).

However the same group have shown the development of PlGF^{-/-} mice to be normal (29). Furthermore, Malik *et al.* have shown that sequestration of VEGF, VEGF-B and PlGF in neonatal and adult mice produces the same effects as when VEGF alone is neutralised (30).

Although PlGF appears to be unnecessary for physiological homeostasis, its deficiency can impair biological responses to pathological challenges. Carmeliet *et al.* have shown that PlGF^{-/-} inhibits angiogenesis in the ischaemic retina (29). Such knockout (KO) also slows the healing of skin wounds and impairs collateral vessel

growth in response to femoral artery occlusion. Transplantation of wild-type (WT) bone-marrow rescues these pathological phenomena (29).

Altering PIGF function has a disease-modifying effect in many pathologies (for a comprehensive review see (31)). Its limited physiological role restricts the side-effects produced by such manipulations. Serum PIGF levels, hepatic PIGF mRNA and hepatic PIGF are higher in patients with liver cirrhosis (32) and PIGF blockade attenuates the progression of CCL4-induced liver cirrhosis in mice (33)(44). PIGF may be proinflammatory in rheumatoid arthritis. The synovium of rheumatoid arthritis patients contains ~5 times the PIGF of the synovium of those with osteoarthritis. (34). In mice with collagen-induced/anti-collagen antibody-induced arthritis, pharmacological PIGF inhibition reduces the severity of disease (34). In some pathologies, enhancing PIGF function may have a therapeutic effect. Post-myocardial infarction (MI) systemic injection of a PIGF-expressing adenovirus to mice promotes cardiac angiogenesis and vessel enlargement and improves left ventricular performance (35).

PIGF mRNA and protein levels often correlate with survival in malignancies (36). There is a good rationale for anti-PIGF therapy in malignancy; angiogenesis is essential for tumour growth and survival. Furthermore, PIGF promotes tumour vessel disorganisation. PIGF blockade reverses this disorganisation in murine hepatocellular carcinoma (51), which may improve tumour oxygenation and chemotherapeutic effectiveness (52). PIGF promotes leukaemia cell migration and thus possibly the clinical migration of malignancies (53). Rolny *et al.* showed that downregulation of PIGF promotes an M1-like tumour-associated macrophage phenotype (52) and thus a shift away from tumorigenic M2-like phenotype (43).

1.4.2 VEGF

VEGF is principally known as a factor involved in angiogenesis and vasculogenesis. It promotes the growth and survival of endothelial cells, in addition to their sprouting and tube formation (16,36,37). VEGF is highly expressed in tissues which are developing new capillaries (38). VEGF deficient embryos (VEGF^{-/-}) are not viable and display defective formation of embryonic and extra-embryonic vasculature (28). Muscle-specific VEGF^{-/-} in adult mice causes a 48% reduction in gastrocnemius capillary density and a 61% reduction in cardiac capillary density (39). Cutaneous overexpression of VEGF induces angiogenesis and a predisposition to the development of a psoriasis-like condition (40). VEGF also upregulates the expression of endothelial nitric oxide (NO) synthase (eNOS) and NO production by endothelial cells, via VEGFR-2 and the protein kinase C (PKC) signalling pathway (41,42). VEGF promotes HSC mobilisation from bone marrow, bone growth and is a monocyte chemoattractant (16); this is consistent with the cellular distribution of VEGFR-1 and VEGFR-2.

1.4.3 VEGF-B

Recent research has shown VEGF-B to have an important role in the regulation of endothelial fatty acid transporter expression and thus fatty acid uptake (43). This will be discussed further in Section 1.7.

The other biological functions of VEGF-B are not well described; however our knowledge of its biology has increased considerably in recent years. It is principally expressed in striated muscle, myocardium and brown fat (16). It appears to inhibit the expression of pro-apoptotic factors, and has shown promise as a neuroprotective agent (44,45). Like PlGF, VEGF-B doesn't appear to be necessary for blood vessel

survival under normal conditions, but may be important for vessel survival under pathological conditions (46). In mice, a cardiomyocyte-specific VEGF-B transgene has been shown to increase the density of the cardiac vasculature. Furthermore, the transgene reduced infarct size following MI and partially protected left ventricular function (47). Recent progress in elucidating the biological actions of VEGF-B is likely to continue in the coming years.

1.5 Molecular Regulation of PIGF Expression

The molecular regulation of PIGF expression is not well characterised. VEGF is known to increase PIGF expression, acting via VEGFR-2, the mitogen activated protein kinase (MAPK) pathway and protein kinase C (PKC) (48,49). Treating human rheumatoid arthritis synovial fibroblasts with PI3k and NF-kB antagonists eliminates a 15-(S)-HETE-mediated increase in PIGF expression (56). An NF-kB binding site has been identified in the PIGF promotor (51). Metal response element-binding transcription factor 1 (MTF-1) binds to the PIGF promotor region and can thus increase *PIGF* expression (52,53). Forkhead/winged helix transcription factor FoxD1 (BF-2) is expressed in stromal cells of the embryonic renal cortex. In these cells, *PIGF* transcription is induced by BF-2 binding to a site in the *PLGF* regulatory region (54). Additionally, two cAMP response elements (CREs) have been identified in the *PIGF* promotor region (55).

Unpublished work from our lab (Samir Sissaoui, PhD thesis) has characterised the transcriptional regulation of PIGF in HUVEC. This work shows that hyperglycaemia and oxidative stress inhibit PI3k/Akt phosphorylation; this promotes FOXO1 nuclear translocation and interaction with the *PIGF* promotor. PIGF release from HUVEC is therefore induced. Conversely, IGF-1 activates the PI3k/Akt pathway –

phosphorylating FOXO1 – causing it to be retained in the cytoplasm and thus preventing *PIGF* transcription.

1.6 The Vascular Endothelial Growth Factor Family in the Metabolic Syndrome

In recent years, possible roles for PIGF, VEGF and VEGF-B in the metabolic syndrome have emerged. The metabolic syndrome is an aggregation of factors which increase the risk of atherosclerotic vascular disease and type 2 diabetes mellitus. The factors which are often included in its definition are dyslipidaemia, hypertension, abnormal glucose homeostasis/insulin resistance and abdominal obesity (56).

There is substantial evidence that PIGF promotes atherosclerotic development. High plasma PIGF levels are associated with an increased long-term risk of coronary heart disease (57) and plasma PIGF levels increase with the number of metabolic syndrome criteria met (58). Khurana *et al.* induced neointimal lesions in hypercholesterolaemic and normocholesterolaemic rabbits, then administered perivascular injections of adenoviruses encoding LacZ or murine PIGF-2. PIGF-2 adenoviral administration significantly increased intimal thickening, macrophage accumulation, endothelial vascular cell adhesion molecule-1 (VCAM-1) expression and adventitial neovascularization in the hypercholesterolaemic rabbits, compared to their LacZ controls. The intima to media ratio was increased in PIGF-transfected normocholesterolaemic rabbits (59). Furthermore, in murine models of atherosclerosis, regular intraperitoneal injection of an anti-PIGF antibody reduces aortic atherosclerotic plaque size and inflammatory cell infiltration into the plaque (60). sVEGFR-1 cannot be used as a sink for PIGF in sVEGFR-1^{-/-} mice. These mice display an increase in atherosclerotic plaque formation and macrophage infiltration

into plaques (61). Given the above evidence and work from our lab demonstrating that PIGF is under the transcriptional control of FOXO1, it is interesting that ablation of all endothelial FOXO transcription factors protects against murine aortic atherosclerosis (62).

A metabolic role for VEGF-B has recently been discovered. VEGF-B^{-/-} mice display impaired uptake of lipids into tissues in which VEGF-B it is usually highly expressed (mitochondria-enriched and fatty acid-metabolising tissues such as muscle, heart, brown adipose tissue) (43). The excess lipids instead accumulate in white adipose tissue. VEGF-B induces fatty acid transport proteins 3 and 4 (FATP3, FATP4) in endothelial cells. *VEGF-B* is co-expressed with mitochondrial genes. It may therefore couple fatty acid transport to metabolic demand for fatty acids (43). Given the role that excessive lipid accumulation is thought to play in skeletal muscle insulin resistance (63), VEGF-B may represent a new clinical target in the metabolic syndrome.

The VEGF family may also be a useful therapeutic target in obesity. It has been known for some time that inhibiting adipose tissue vascular development reduces the size of fat depots (1,2). Some work has suggested that VEGFR-2, but not VEGFR-1 blockade inhibits murine DIO (3) and diet-induced liver steatosis (33). Indeed, inducible repression of VEGF in mice confers resistance to DIO (4). These mice have reduced food efficiency (decreased body weight [BW] gain per unit of caloric intake) and express brown adipocytes in gonadal white adipose tissue (gWAT) depots. Additionally, they display increased expression of brown adipose tissue specific genes, *VEGF-B* and *FATPs* in gWAT. Thus when VEGF is inhibited, WAT acquires the ability to take up fatty acids and metabolise them in an uncoupled fashion, with resulting protection against DIO.

Despite findings that VEGFR-1 blockade does not inhibit murine DIO, evidence for a PIGF role in adipogenesis and obesity exists. In male mice fed a high-fat (HF) diet for 18 weeks, PIGF^{-/-} lowered BW compared to wild-type (WT) controls (5). Additionally, blood vessel density was significantly lower in the PIGF^{-/-} mice compared to controls. Transplantation of PIGF^{-/-} bone marrow to WT mice decreased vessel density, along with a trend towards a decrease in BW and adipose depot size (5). A similar study by the same group, in which HF feeding was restricted to 3 weeks, failed to replicate these results (64). BW, individual fat pad sizes and blood vessel density were unaffected by PIGF^{-/-}. The authors also report that PIGF^{-/-}preadipocytes differentiate normally and that PIGF neutralising antibodies/recombinant PIGF have no effect on 3T3-F442A preadipocyte differentiation into adipocytes (64). A further study from the same group, examined the effect of short-term (< 3 weeks) HF feeding in gravid/non-gravid, PIGF^{-/-}/WT female mice (65). The non-gravid PIGF^{-/-} mice did not differ from their WT controls in terms of BW, individual fat pad sizes and blood vessel density. The pregnant PIGF^{-/-} mice did display reduced adipose tissue blood vessel density and fewer UCP-1 positive adipocytes in white adipose tissue depots (65).

It is unclear whether PIGF plays an important role in adipogenesis; some have found VEGFR-1 blockade to be ineffective at preventing DIO and PIGF^{-/-} protection against DIO has been inconsistent. It is disappointing that the study of long-term HF feeding in PIGF^{-/-} mice (5) has not been replicated. If PIGF plays a role in adipogenesis, it appears likely to be via its promotion of angiogenesis/vasculogenesis, rather than via the direct promotion of preadipocyte differentiation (64). Regardless, adipose tissue production of PIGF may not be restricted to endothelial cells; adipocytes and preadipocytes may contribute to its local production and thus the adipogenic environment. Therefore, an understanding of the molecular regulation of PIGF in

adipocytes and preadipocytes is desirable. The work presented here is a preliminary exploration of such PIGF regulation.

1.7 Hypothesis, Objectives and Aims

As discussed in detail above, PIGF is under the transcriptional control of FOXO1 in HUVEC. The literature also points to other influences on PIGF transcription including VEGF signalling via VEGFR-2 and cAMP activation of cAMP response-element binding protein (CREB). We therefore hypothesised that:

1. PIGF is under the transcriptional control of FOXO1 in preadipocytes and adipocytes.
2. PIGF transcription in preadipocytes and adipocytes is promoted by VEGF and cAMP.
3. Given that VEGF has similar biological functions to PIGF, it is subject to similar transcriptional influences to PIGF in preadipocytes and adipocytes.

Our principal objectives were:

1. To establish whether PIGF is transcribed and released by murine preadipocytes and to gain some insight into the molecular regulation of these events.
2. To establish whether VEGF is transcribed by murine preadipocytes and to gain some insight into the molecular regulation of these events.
3. To optimise the differentiation of an immortalised murine preadipocytes and primary murine preadipocytes into adipocytes.

We aimed:

1. To characterise, in murine preadipocytes, the transcription and cellular release of PIGF in response to oxidative stress, exogenous VEGF/cAMP and FoxO1 adenoviral transfection.
2. To determine, in murine preadipocytes, the transcription of *VEGF* in response to oxidative stress, exogenous VEGF/cAMP and FoxO1 adenoviral transfection.
3. To characterise, in murine preadipocytes, the transcription of *FoxO1* in response to oxidative stress and exogenous VEGF/cAMP.
4. To optimise the differentiation of immortalised murine preadipocytes and primary murine preadipocytes into adipocytes.

Additional work characterising the effect of oxidative stress and insulin treatment on the release of PIGF from liver slice cultures was also undertaken. Preparation of murine aortic rings was carried out in preparation for work yet to be undertaken in our lab.

2. Methods

All reagents used were from Sigma-Aldrich, St. Louis, MO, USA, unless otherwise stated. All cell culture was carried out under sterile conditions in a class II safety cabinet.

2.1 Cell Culture

2.1.1 Immortalised Murine Preadipocytes

Immortalised murine preadipocytes isolated from inguinal fat tissue (IngPA) (see (66)) were cultured in T75 cell culture flasks, each containing 15 mL Dulbecco's Modified Eagle Medium (DMEM), supplemented with 20% fetal bovine serum (FBS), 100 µg/mL penicillin/streptomycin and 2 mM L-glutamine. Cells were fed every 2-3 days and passaged (1:6) before reaching confluence.

2.1.2 Primary Preadipocytes

Primary preadipocytes (PrPA) were isolated from FoxO1,3a,4 floxed mice (FoxO1,3,4^{flox/flox}) on an FVB/n background. The inguinal fat pads were exposed by a ventral midline incision. The fat pads were removed and pooled in a petri dish containing DMEM/F12 (3 mice per pool). The tissue was finely minced between two scalpel blades and incubated in 10 mL of 1 mg/mL type 1 collagenase in DMEM/F12 for 1 hour at 37 °C. The digest was passed through a 1.2 µm filter and the tissue retained by the filter was discarded. DMEM/F12 was added to the filtrate up to a total volume of 30 mL. The tube was centrifuged at 500 g for 15 minutes. The supernatant was discarded and the pellet resuspended in DMEM/F12. Endothelial cell clumps were removed by filtering the solutions through a 40 µm filter. The remaining solution was centrifuged at 500g for 5 minutes. The supernatant was removed and the pellet

resuspended in plating medium (DMEM containing 10 % FBS, 100 µg/mL penicillin/streptomycin, 2 mM L-glutamine). The cells were plated in T25 culture flasks at a density of 2.5×10^4 cells/cm². The medium was replaced at 24 hours and was subsequently replaced every 2-3 days. The cells were passaged (1:4) before they reached confluence (see Table 2.1).

Table 2.1. Cell culture plating details.

Culture Vessel	Trypsin/EDTA volume (mL)	Medium volume (mL)
T-75	1	10-15
T-25	0.5	3-5
6-well	N/A	1-2
24-well	N/A	0.4-0.6

To subculture the cells, the culture media was aspirated and the vessel washed once with sterile phosphate buffered saline (PBS). The PBS was aspirated and the cells enzymatically dissociated using 1x trypsin. 7 mL of serum-containing medium was added to the flask. The contents of the flask were aspirated into a 15 mL falcon tube and centrifuged at 300 g, 21 °C for 10 minutes. The supernatant was removed, the pellet resuspended in fresh medium and split into culture flasks containing 14 mL of prewarmed (37°C) media. The flasks were incubated at 37 °C, 5 % CO₂.

2.1.3 Preadipocyte Differentiation

Differentiation of preadipocytes was performed using several different protocols (Table 2.2).

IngPA and PrPA were grown to confluence on 6-well/24-well culture plates. 24 hours post confluence the medium was changed to induction medium for 24-48 hours (see Table 2.2). The medium was subsequently changed to differentiation medium (see Table 2.2). The differentiation medium was changed every 48 hours.

Table 2.2. Preadipocyte differentiation protocols.

Protocol Number	Differentiation medium	Induction medium	Induction period	Reason for alteration
1	Growth medium ^a + 20 nM Insulin + 1 nM T3	Differentiation medium + 0.125 mM indomethacin + 5 μM dexamethasone + 0.5 mM IBMX	24 hours	N/A
2	As above	As above	48 hours	Poor differentiation at 2 weeks. Some protocols use 48 hour induction.
3	Growth medium + 172nM Insulin	As above	48 hours	Poor differentiation at 2 weeks. Some protocols use increased insulin concentration without T3.

^a Growth medium = DMEM + 20% Fetal Bovine Serum + 100 μg/mL penicillin/streptomycin+ 2 mM L-glutamine. Changes from previous protocol in bold.

2.2 Adenovirus Transfection of Cells

Preadipocytes were grown to confluence on 6-well cell culture plates/chambered cell culture slides in their relevant growth media. The cells were transfected with adenoviral vectors (1×10^9 IFU) encoding wild-type FoxO1 (WT-FoxO1), constitutively active FoxO1 (CA-FoxO1) and dominant-negative FoxO1 (DN-FoxO1). The phosphorylation sites of CA-FoxO1 are mutated, rendering it immune to negative regulation by PI3k/Akt (67), DN-FoxO1, retains its DNA binding activity, but lacks a transactivation domain (68). On 6-well culture plates, 2 μL adenovirus in 1 mL of transfection medium (DMEM, 2 % FBS) was added to each well. 0.5 μL of adenovirus in 300 μL of transfection medium was added to each chamber of cell culture slides. At 24 hours, the transfection medium was changed replaced with growth medium. After a further 24 hours the medium was collected and stored at -80 °C. If destined for

immunofluorescent examination, cells were incubated in a fixative solution (2 % formaldehyde, 2 % glucose, 0.2 % w/v sodium azide in PBS) for 30 minutes, then stored under PBS at 4 °C. For quantitative PCR (qPCR) experiments, cells were lysed with 150 µL/well of cell lysis solution (Norgen Biotek, ON, Canada). The lysates were stored at -80°C.

2.3 Preadipocyte Stimulation

IngPA and PrPA were grown to confluence in their respective growth media on 6-well and 24-well cell culture plates. Wells were treated in duplicate/triplicate with one of the following: H₂O₂ (1 mM, 200 µM), recombinant VEGF₁₆₄ (10 ng/mL), forskolin (10 µM) or cAMP (2.5 mM). At 24 hours the medium was aspirated, retained and stored at -80 °C. Cells on 6-well plates were lysed with 150 µL/well of cell lysis solution (Norgen Biotek). The lysates were pooled by treatment and stored immediately at -80 °C.

2.4 Immunofluorescence

Chambered cell culture slides which had been prepared for immunofluorescence were incubated in 100 % methanol for 10 minutes. The wells were washed twice in PBS and incubated with 5 % blocking serum (250 µL/well, serum was from same species as that in which the secondary antibody was raised) for 20 minutes at room temperature (Table 2.3). The serum was aspirated and the cells incubated for 1 hour at room temperature in 250 µL/well primary antibody diluted in 1 % BSA/PBS. The wells were washed twice in PBS. The slides were incubated at room temperature for 1 hour in secondary antibody diluted in 1.5 % serum (Table 2.3). The wells were washed as before. The plastic chambers were removed and the slides mounted in an aqueous mounting medium containing 4',6-diamidino-2-phenylindole (DAPI). Slides

were stored in the dark at 4 °C and subsequently imaged using a fluorescence microscope.

Table 2.3. Serum and antibody conditions used for immunofluorescent staining.

Experiment	Primary antibody (dilution)	Secondary antibody (dilution)	Blocking serum
1	1° polyclonal rabbit anti-FKHK (FoxO1) (Santa Cruz Biotechnology) (1:50) Rabbit anti-heme-oxygenase-1 (Abcam) (1:400)	Goat anti-rabbit Alexa Fluor 594 (Life Technologies) (1:1000)	Goat
2	1° polyclonal rabbit anti-FKHK (FoxO1) (Santa Cruz Biotechnology) (1:50)	Donkey anti-rabbit FITC (Jackson ImmunoResearch) (1:1000)	Donkey

2.5 Enzyme-Linked Immunosorbent Assay – Murine PIGF-2

A murine PIGF-2 ELISA kit (R&D systems, Minneapolis, MN, USA) was used according to the manufacturer's instructions.

2.6 Mouse DNA Extraction

100 µL of 1x DNA extraction mix (25 mM NaOH, 0.2 mM EDTA) was added to each tissue sample. The sample was incubated at 95 °C for 20 minutes, centrifuged briefly at 13,000 rpm and 100 µL of 40 mM Tris-HCl was then added. The sample was vortexed and transferred to a clean tube. An aliquot of this sample was retained and stored at -20 °C, along with any remaining tissue. 20 µL of 3 M NaCl was added to the remaining sample. 200 µL isopropanol was then added and the sample

centrifuged at 13,000 rpm for 15 minutes at 4 °C. The pellet was washed with 100 µL 70 % EtOH and the sample centrifuged at 13,000 rpm for 5 minutes. The supernatant was again discarded and the tube dried by evaporation. The DNA was resuspended in 50 µL sterile water and stored at -20 °C.

2.7 Reverse transcriptase polymerase chain reaction/agarose gel electrophoresis

PCR was carried out on DNA extracted from murine tissues (section 2.6) using a DNA polymerase kit (MangoTaq™ DNA Polymerase, Bionline, London, UK) containing a reaction buffer suitable for agarose gel electrophoresis. The reaction consisted of 4 µL 5x reaction buffer, 50 mM (2 µL) MgCl₂, 0.4 µL dNTPs, 0.25 µL Taq polymerase, 0.4 µL primer mix (Table 2.4), 3 µL of DNA and PCR-grade H₂O to 20 µL total volume. A DNA-free negative control was prepared during each experiment.

Table 2.4. Mouse genotyping primer sequences.

Name	Primers (5'→3')	Conditions
Universal Cre	Universal Cre 5: ACC TGA AGA TGT TCG CGA TTA TCT Universal Cre 3: ACC GTC AGT ACG TGA GAT ATC TT	95°C 5 min (95°C 30 sec, 58°C 30 sec, 72°C 60 sec) x 35 cycles 72°C 10 min
FoxO1 ^{lox}	oFK1ckA: CGT TAG AGC AGA GAT GTT CTC ACA TT oFK1ckB: CCA GAG TCT TTG TAT CAG GCA AAT AA oFK1ckD: CAA GTC CAT TAA TTC AGC ACA TTG A	95°C 5 min (95°C 30 sec, 58°C 30 sec, 72°C 60 sec) x 35 cycles 72°C 10 min
FoxO3 ^{lox}	oFK2ckAnew: GGT TTT CAT GCA GTC CGA GA oFK2ckBnew: AAG CAG AAC GTA TGC TTT GA oFK2ckDnew: GTG CCA TTC CTT TGG AAA TC	95°C 5 min (95°C 30 sec, 56°C 30 sec, 72°C 60 sec) x 38 cycles 72°C 10 min

A 1-2 % agarose solution in 1xTAE buffer was prepared. 5 µL Midori-green DNA stain (Geneflow, Lichfield, UK) was added per 100 mL of agarose solution. An agarose gel was poured and the PCR products were added to the wells. The gel was run at 100 V for 40 minutes. The DNA bands were visualised by UV illumination at 300 nm.

2.8 RNA Extraction

Total RNA was extracted from cell lysates (Sections 2.2, 2.3) using an RNA extraction kit (Norgen Biotek). The concentration of eluted RNA was measured using the spectrophotometric absorbance of the sample at 260/280 nm. RNA not used immediately for cDNA synthesis was stored at -80 °C.

2.9 cDNA Synthesis

cDNA was synthesised from total RNA using the Bioline Tetro cDNA synthesis kit (Bioline, Taunton, MA, USA). The synthesis was carried out in 20 µL reactions (Table 2.5). Once prepared for cDNA synthesis, samples were incubated in a water bath at 45 °C for 1 hour. The temperature was then raised to 55 °C for 30 minutes and 60 °C for a further 30 minutes. Samples were stored at -20 °C.

Table 2.5. cDNA synthesis reagent volumes per reaction.

Reagent	Volume/reaction (µL)
RNA	Volume equivalent to ~5µg
Primer: Oligo (dT) ₁₈	1
10mM dNTP mix	1
5x buffer	4
RNase inhibitor	1
Tetro reverse transcriptase	1
DEPC-treated water	To 20µL

2.10 Quantitative polymerase chain reaction

SYBR-Green qPCR was carried out using the SensiMix SYBR Kit (Bioline). cDNA was diluted 1:5 in PCR-grade H₂O. 15 µL reactions, prepared in duplicate in strip tubes (Qiagen, Hilden, Germany) were used (Table 2.6). cDNA-free H₂O controls were run, in duplicate, for each primer used (Table 2.7). The samples were run on a Rotor-Gene 6000 PCR machine (Corbett Life Science, Hilden, Germany). The

denaturation step was carried out at 95 °C for 10 minutes. This was followed by 40 cycles of: (1) denaturation at 95 °C for 10 seconds; (2) annealing at 58 °C for 15 seconds; (3) extension at 72 °C for 20 seconds and 75 °C for 5 seconds. Finally, a melt curve was performed by stepwise (1°C) increase of the temperature from 62 °C to 95 °C. The threshold fluorescence was set using a logarithmic view of the curve. It was placed in the linear phase of the reaction, above the background signal. Ct (cycle threshold) values for each sample were defined the cycle number at which the curve crossed the threshold. The relative quantities of RNA were calculated using the Pfaffl method (69). Efficiency of the primers used had previously been determined using dilutions of target cDNA.

Table 2.6. qPCR reagent volumes per reaction.

Reagent	Volume/reaction (µL)
SensiMix 2x SYBR	7.5
Primer mix	0.3
PCR grade H ₂ O	6.2
Sample/ H ₂ O negative control	1

Table 2.7. Murine qPCR primer sequences.

Gene	Sequence
β-actin	5'-GTATGCCTCGGTCGTACCA-3' 5'-CTTCTGCATCCTGTCAGCAA-3'
PIGF	5'-GAAGTGGAAGTGGTGCCTTT-3' 5'-CGACTCAGAAGGACACAGGA-3'
VEGF	5'-GAG TAC CCC GAC GAG ATA GAG T-3' 5'-GGT GAG GTT TGA TCC GCA TGA-3'
FoxO	?
Flt-1	5'-GAG GAG GAT GAG GGT GTC TAT AGG T-3' 5'-GTG ATC AGC TCC AGG TTT GAC TT-3'

All primers designed in-house and synthesised by MWG Eurofins (Ebersberg, Germany).

2.11 Liver Slice Culture

Age and sex matched mice with conditional endothelial-cell specific FoxO knockout (Tie-2-Cre⁺ FoxO1,3a,4 [eFoKO] or floxed FoxO1,3a,4 [FoFlox]) mice. The mice were sacrificed by cervical dislocation in accordance with Home Office rules. Ear samples were retained to confirm genotype. A ventral midline incision was made, the peritoneum opened and the liver detached at the hilum and diaphragm. Each liver was washed in PBS containing 100 µg/mL penicillin/streptomycin, transferred to a 50 mL falcon tube containing DMEM and stored on ice. Liver slices were precision-cut by Dr. Trish Lalor, transferred to 16-well plates and incubated for 7 hours in 500 µL/well Williams E medium at 37 °C, 5 % CO₂. After 7 hours, the old medium was aspirated and replaced. The livers were treated in duplicate, with one of the following: DMEM only, H₂O₂, (100 µM/ 500 µM), insulin (3 µg/mL). The livers were incubated at 37 °C, 5 % CO₂ for 20 hours. The supernatants from each well were stored at -80 °C. One liver slice per treatment condition was snap frozen in liquid nitrogen. The other was weighed and fixed in 3 mL 4% formalin for 1 hour. The formalin was then replaced by 3 mL 10% sucrose/PBS solution for 1 hour, 3 mL 20 % sucrose/PBS solution for 1 hour and finally 3 mL 30 % sucrose/PBS solution for 1 hour. The sections were mounted in OCT compound, frozen in an isopentane bath, transferred to liquid nitrogen and stored at -80 °C.

2.12 Preparation of Murine Aortic Rings

The thoracic and abdominal cavities of eFoKO/FoFlox mice were exposed and the thoracic and abdominal aortas excised (76). The aortic lengths were cleaned of perivascular tissue under microscopic guidance and cut into even (~1 mm), ringed slices.

The slices were stored in DMEM at 4 °C overnight. The DMEM and aortic rings were retained and stored at -80 °C.

2.13 Statistical Analysis

Given the small sample sizes ($N < 3$) for most of our experiments, application of tests of statistical significance was considered inappropriate. Given more time, larger sample sizes would have been employed. The sample size was larger for the liver-slice culture experiment. T-tests were employed to determine the statistical significance of any mean differences (IBM SPSS Statistics 21).

3. Results

3.1 Preadipocyte Differentiation

We had intended to also investigate the expression of VEGFs in adipocytes. Problems were encountered with the number of IngPA and PrPA undergoing differentiation. Clusters lipid-filled cells appeared ~ 7 days post-induction (Fig. 3.1), however these clusters did not develop further, even when the protocol was amended (Section 2.1.3). When left in culture for greater than 2 weeks, the preadipocyte monolayer became too confluent and began to die. Given these problems, we focused our investigations on the expression of VEGFs in preadipocytes.

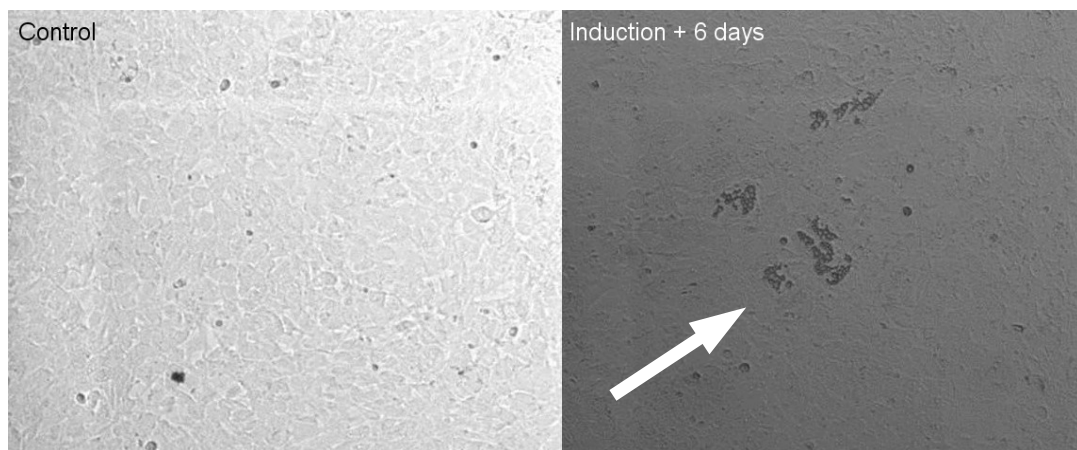


Figure 3.1. Representative image of immortalised inguinal preadipocyte differentiation at 6 days post-induction. Arrow indicates cluster of lipid-filled cells.

3.2 Preadipocyte FoxO1 Adenovirus Transfection

To determine whether FoxO1 can regulate the expression of VEGFs in preadipocytes, IngPA and PrPA were infected with adenoviruses encoding FoxO1. IngPA transfection of an adenovirus encoding WT FoxO1 resulted in a 74 ± 5.5 -fold (mean \pm SEM) increase in *FoxO1* mRNA expression (Fig. 3.2). A 3.7 ± 3.3 -fold increase in *VEGF* expression and a 7.2 ± 6.6 -fold increase in *PIGF* expression were also observed. Transfection of an adenovirus encoding CA FoxO1 induced no obvious alteration in *FoxO1* (1.3 ± 0.6), *VEGF* (2.3 ± 1.7) or *PIGF* (0.8 ± 0.1) expression (Fig. 3.2). An adenovirus encoding DN FoxO1 did not produce dramatic changes in *FOXO1* (3 ± 1.9) and *PIGF* (1.2 ± 0.1) expression, although *VEGF* expression increased 6.3 ± 0.6 -fold (Fig. 3.2). There was no increase in PIGF production compared with uninfected control cells when the corresponding supernatants were examined by ELISA (Figure 3.3).

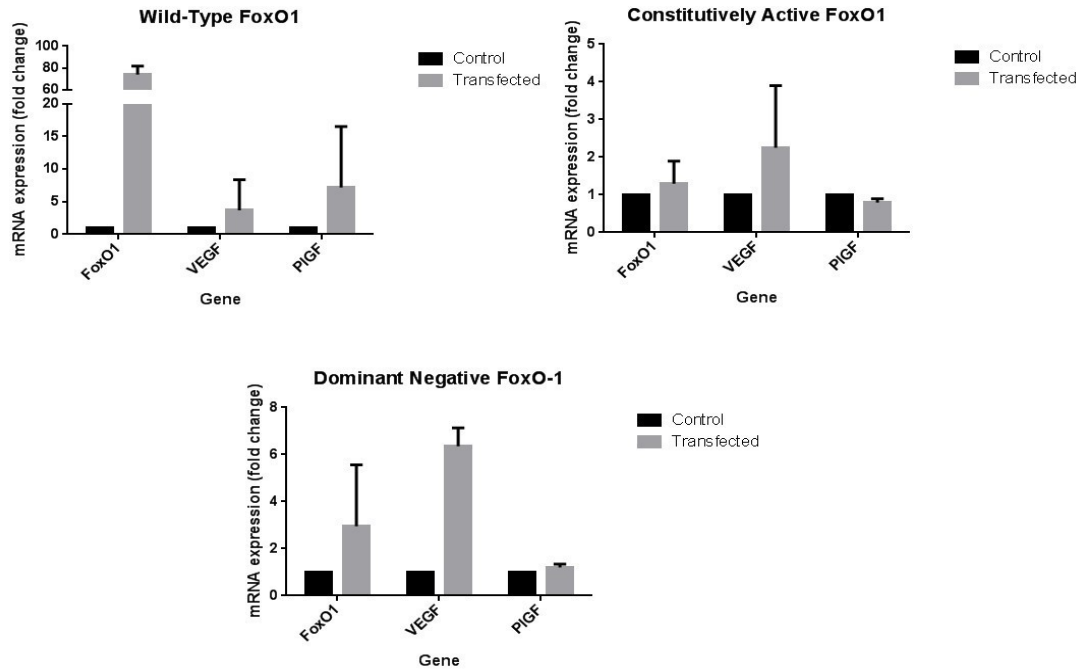


Figure 3.2. FoxO1, VEGF and PIGF gene expression in FoxO1-transfected immortalised murine inguinal preadipocytes. Preadipocytes were incubated with FoxO1 adenoviruses (wild type, dominant negative, constitutively active) for 24 hours. At 48 hours, the cells were lysed. Total RNA was extracted from the lysates, cDNA was synthesised and used in SYBR Green qPCR measurement of FoxO1, VEGF and PIGF mRNA expression. Data expressed as mean \pm SEM. N=2.

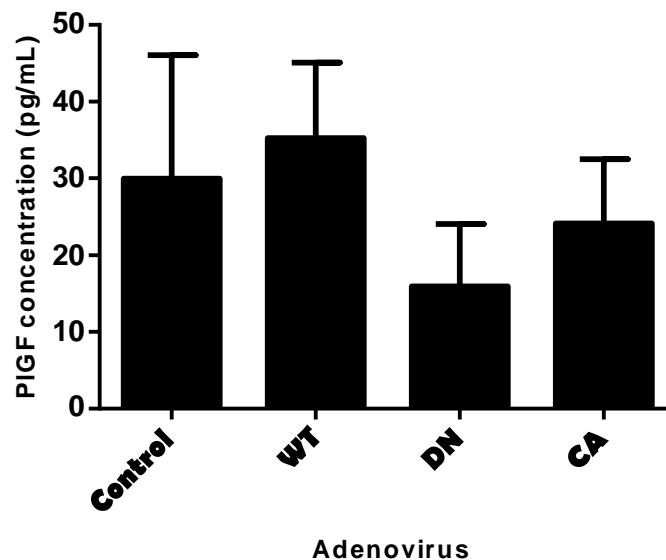


Figure 3.3. PIGF-2 secretion in FoxO1-transfected immortalised murine inguinal preadipocytes. Preadipocytes were incubated with FoxO1 adenoviruses (wild type, dominant negative, constitutively active) for 24 hours. The medium was then changed. After a further 24 hours, PIGF was measured in the medium by ELISA. Data expressed as mean \pm SEM. N=2.

The same FoxO1 adenoviral transfections were carried out in PrPA cells. WT FoxO1 induced increases in *FoxO1* (9.1-fold), *VEGF* (2-fold) and *PIGF* (9.2-fold) expression (Fig. 3.4). There were small changes in *FoxO1*, *VEGF* and *PIGF* expression with CA and DN FoxO1 transfection (Fig. 3.4). The supernatants from transfected cells contained considerably more PIGF-2 (WT = 34.3 pg/mL, CA = 46.3 pg/mL, DN = 31.5 pg/mL) than an untransfected control (4.4 pg/mL) (Fig. 3.5). Given that these results are from a single experiment and the small magnitude of the changes observed, caution should be exercised in their interpretation.

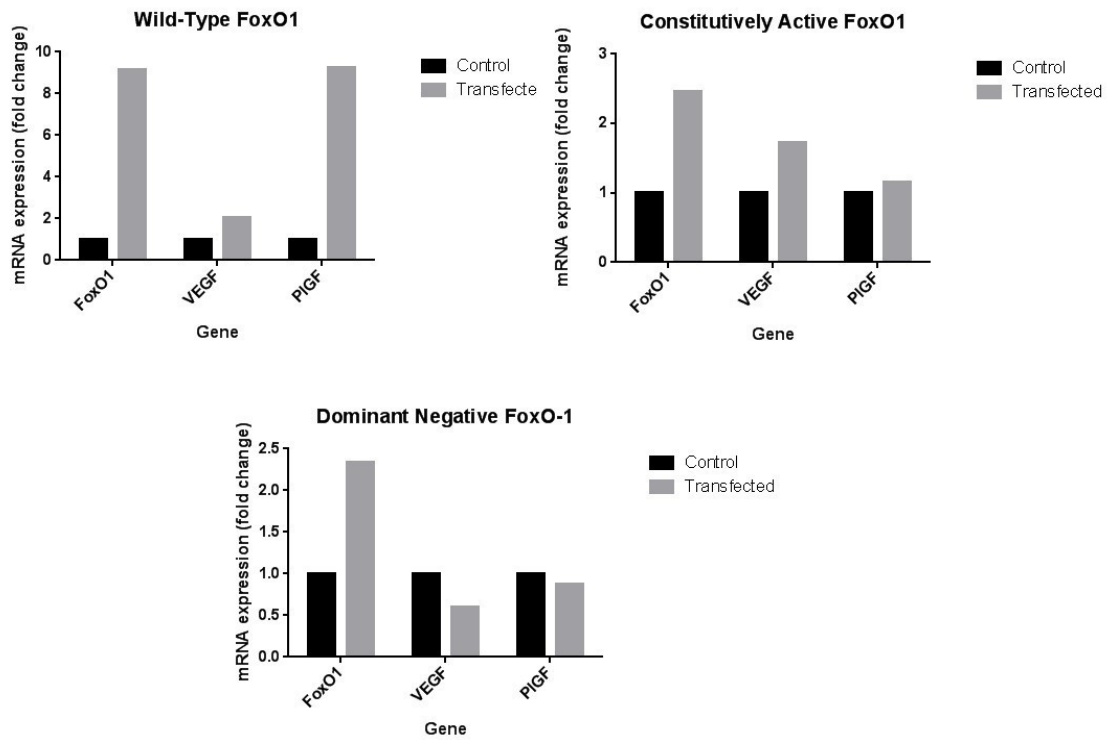


Figure 3.4. FoxO1, VEGF and PIGF gene expression in FoxO1-transfected primary murine preadipocytes. Preadipocytes were incubated with FoxO1 adenoviruses (wild type, dominant negative, constitutively active) for 24 hours. At 48 hours the cells were lysed. Total RNA was extracted from the lysates, cDNA was synthesised and used in SYBR Green qPCR measurement of FoxO1, VEGF and PIGF mRNA expression. N=1.

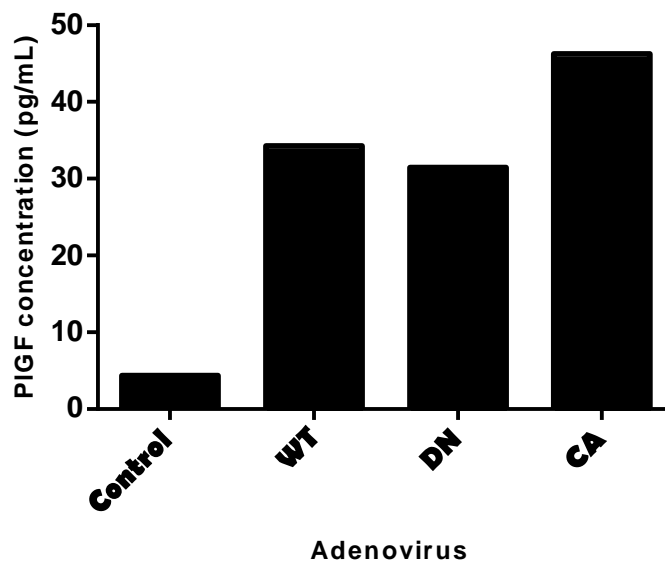


Figure 3.5. Supernatant PIGF-2 concentration in FoxO1-transfected primary murine preadipocytes. Preadipocytes were incubated with FoxO1 adenoviruses (wild type, dominant negative, constitutively active) for 24 hours. The medium was then changed. After a further 24 hours, PIGF was measured in the medium by ELISA. Data expressed as mean \pm SEM. N=1

3.3 Immunofluorescent Microscopy

IngPA were transfected with adenoviruses encoding WT, DN or CA FoxO1. FoxO1 localisation and abundance were visualised by immunofluorescent labelling. Time constraints and limited equipment access restricted our imaging to the control and WT-FoxO1 transfected cells. Considerable background fluorescence can be appreciated on the control image, along with some cytoplasmic FoxO1 expression (Fig. 3.6). Strong cytoplasmic FoxO1 expression is seen in many of the WT-FoxO1 transfected cells (Fig. 3.6).

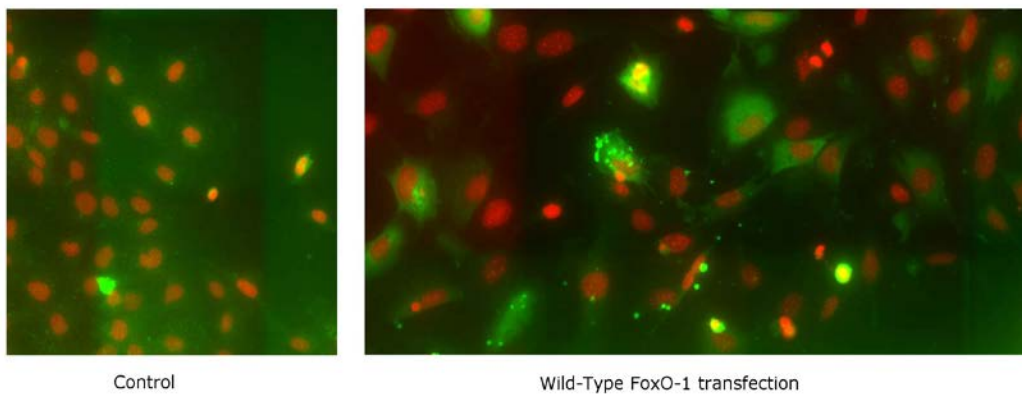


Figure 3.6. Representative immunofluorescent microscopy images of control and wild-type FoxO1 transfected immortalised murine inguinal preadipocytes. Green = FITC-labelled FoxO1, red = DAPI. Magnification = 40x.

3.4 Preadipocyte Stimulation

To assess whether factors which may influence FoxO1 activity can regulate the expression of VEGFs in preadipocytes, such cells were stimulated for 24 hours with H₂O₂, VEGF, cAMP and Forskolin .

Treatment of IngPA with H₂O₂ (1mM), VEGF, cAMP and Forskolin induced considerable increases in *FoxO1*, *VEGF* and *PIGF* expression (Fig. 3.7). However, the PIGF-2 concentration of the corresponding supernatants was unaffected (Fig. 3.8). The same treatments also induced increases in PrPA *FoxO1*, *VEGF* and *PIGF* expression, although the magnitude of these changes was not as great as those seen in the IngPA line (Fig. 3.9). The PrPA supernatants contained less PIGF-2 than their IngPA counterparts (Fig. 3.8, 3.10), and H₂O₂ and VEGF treatments did appear to increase PIGF-2 secretion (Fig. 3.10).

Given the prominent effects of VEGF treatment on gene expression, we confirmed expression of *VEGFR-1* in both IngPA and PrPA.

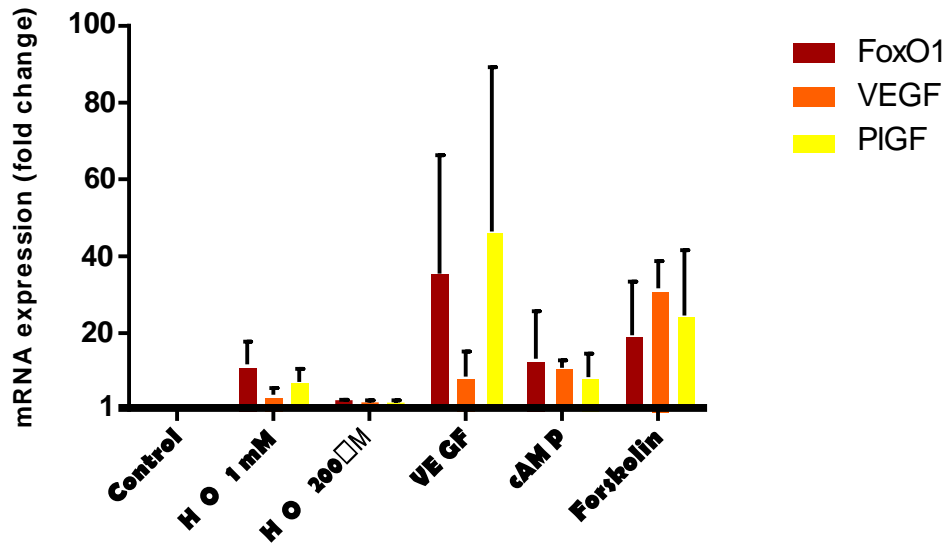


Figure 3.7. FoxO1, VEGF and PIGF gene expression in treated immortalised murine inguinal preadipocytes. Preadipocytes were incubated with one of the following: H₂O₂ (1 mM, 200 μM), recombinant VEGF₁₆₄ (10 ng/mL), forskolin (10 μM) or cAMP (2.5 mM) for 24 hours. The cells were lysed. Total RNA was extracted from the lysates, cDNA was synthesised and used in SYBR Green qPCR measurement of FoxO1, VEGF and PIGF mRNA expression. Data expressed as mean ± SEM. N=2.

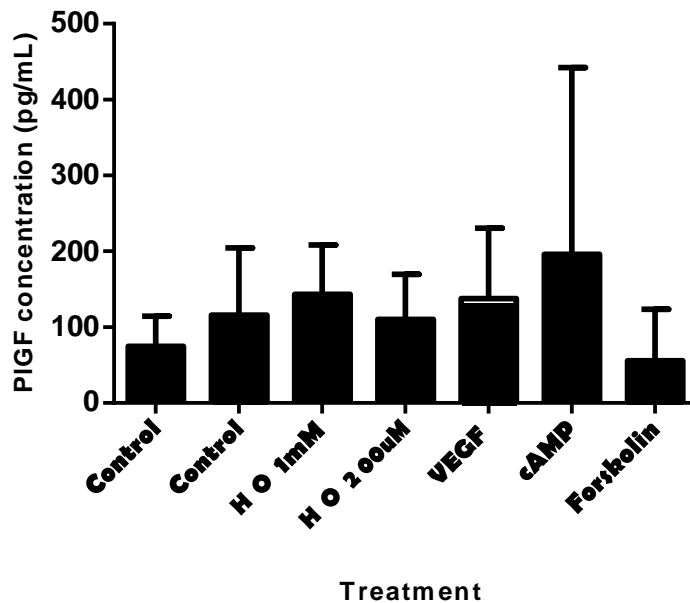


Figure 3.8. PIGF-2 release in treated immortalised murine inguinal preadipocytes. Preadipocytes were incubated with one of the following: H₂O₂ (1 mM, 200 μM), recombinant VEGF₁₆₄ (10 ng/mL), forskolin (10 μM) or cAMP (2.5 mM) for 24 hours. The medium was collected and its PIGF concentration measured by ELISA. Data expressed as mean ± SEM. N=2.

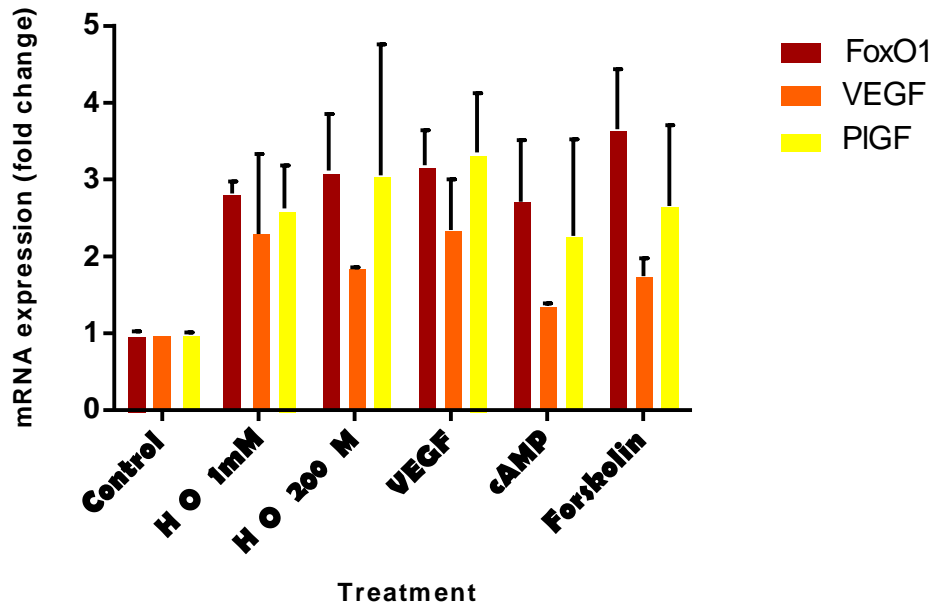


Figure 3.9. FoxO1, VEGF and PIGF gene expression in treated primary murine preadipocytes. Preadipocytes were incubated with one of the following: H₂O₂ (1 mM, 200 μM), recombinant VEGF₁₆₄ (10 ng/mL), forskolin (10 μM) or cAMP (2.5 mM) for 24 hours. The cells were lysed. Total RNA was extracted from the lysates, cDNA was synthesised and used in SYBR Green qPCR measurement of FoxO1, VEGF and PIGF mRNA expression. Data expressed as mean ± SEM. N=2.

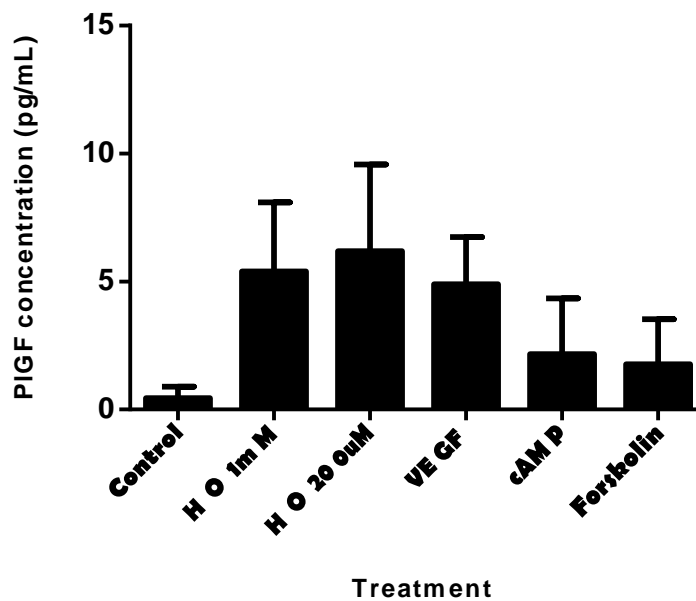


Figure 3.10. PIGF-2 release in treated primary murine preadipocytes. Preadipocytes were incubated with one of the following: H₂O₂ (1 mM, 200 μM), recombinant VEGF₁₆₄ (10 ng/mL), forskolin (10 μM) or cAMP (2.5 mM) for 24 hours. The medium was collected and its PIGF concentration measured by ELISA. Data expressed as mean ± SEM. N=2.

3.5 Mouse Genotyping

eFoKO, FoFloX and WT mice were genotyped by RT-PCR using primers designed to identify the FoxO1^{flox} and FoxO3^{flox} genotypes. The floxed products are evident in all floxed mice (Fig. 3.11, Fig. 3.12). The WT product was identified in the WT mouse samples (Fig. 3.11, Fig. 3.12). The FoxO3 KO products are clearly evident in the aortic samples (Fig. 3.12), but not the ear samples from the eFoKO mice. This was expected, given the endothelial-specific nature of the knockout. The FoxO1 KO is less clear, although some poorly resolved bands may be present in the aortic samples from the eFoKO mice (Fig. 3.11).

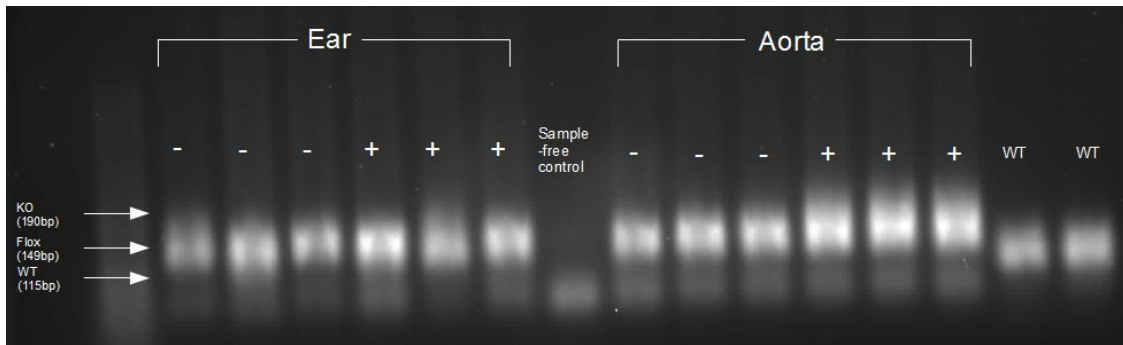


Figure 3.11. RT-PCR for the FoxO1^{flox} genotype. DNA was extracted from murine ear and aortic tissue sample. RT-PCR was carried out using primers designed to identify wild-type, floxed and knockout FoxO1 sequences. The products were run on an agarose gel and visualised by UV illumination at 300nm. - = eFoFloX mice + = eFoKO mice, WT = wild-type mice.

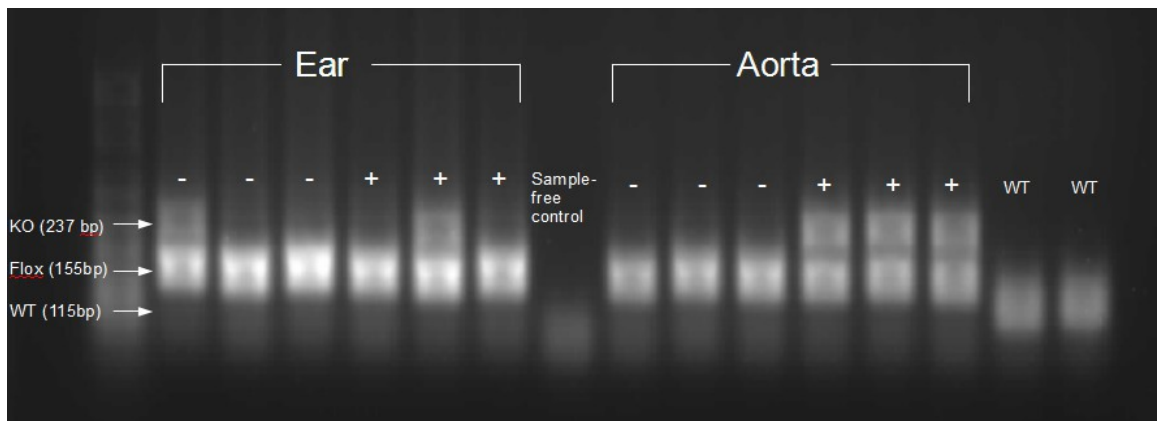


Figure 3.12. RT-PCR for the FoxO3^{flox} genotype. DNA was extracted from murine ear and aortic tissue sample. RT-PCR was carried out using primers designed to identify wild-type, floxed and knockout FoxO3 sequences. The products were run on an agarose gel and visualised by UV illumination at 300nm. - = eFoFloX mice + = eFoKO mice, WT = wild-type mice.

3.6 Liver Slice Culture – PIGF-2 ELISA

The liver is an important site of lipid uptake and steatosis is often associated with the metabolic syndrome/obesity. Precision-cut slices of liver from the FoFlox and eFoKO mice were used to assess whether factors that may influence FoxO1 activity can regulate the liver-slice secretion of PIGF.

No significant difference in supernatant PIGF concentration existed between the untreated FoFlox and eFoKO liver slices (Fig. 3.13). H₂O₂ (500 μM and 100 μM) treatments also produced no effect. However, insulin (3 μg/mL) induced a significant increase in PIGF secretion from the eFoKO liver slices (Fig. 3.13).

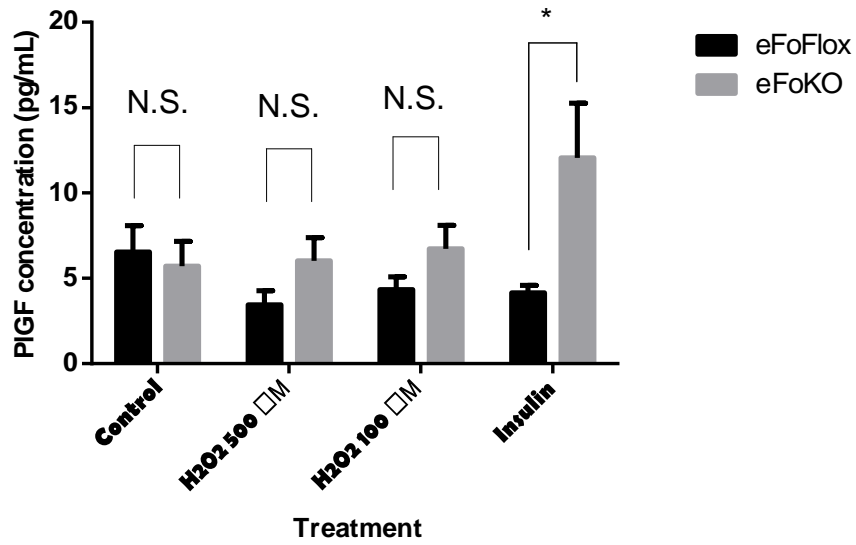


Figure 3.13. Effect of endothelial FoxO knockout and precision-cut liver slice stimulation on supernatant PIGF concentration. Liver slices were precision-cut and maintained in culture for 20 hours with DMEM only (control), H₂O₂ (100μM/ 500μM) or insulin (3μg/mL). The PIGF concentration of each supernatant was measure by ELISA and normalised to the liver slice weight. Data presented as mean ± SEM. * p<0.05 by independent samples T-test, N.S. = non-significant. eFoFloxed = floxed FoxO1,3a,4 mice, n=3; eFoKO = endothelial FoxO1, 3a, 4 knockout, n=3.

4. Discussion

4.1 Preadipocyte FoxO1 Adenovirus Transfection

Previous results from our lab have shown that PIGF is under the transcriptional control of FoxO1 in HUVEC. We used FoxO1 adenoviral vectors to indicate whether this control might be conserved in preadipocytes. WT-FoxO1 transfection was successful, with robust increases in FoxO1 mRNA observed in IngPA and PrPA cells. Additionally, an increase in cellular FoxO1 was observed by immunofluorescent imaging. *PIGF* expression was observed to increase considerably with WT-FoxO1 adenoviral transfection.

No increase in PIGF secretion was observed in the WT-FoxO1 transfected IngPA cells, despite a clear increase in its mRNA expression. An increase of PIGF in the supernatant was seen in all transfected PrPA cells, despite *PIGF* being upregulated in the WT-FoxO1 transfected cells only. Given the small sample size we cannot have confidence in the accuracy of these results. They may reflect the influence of post-transcriptional events on protein abundance and secretion (70). Quantification of cellular PIGF by Western blotting would determine whether the increased *PIGF* mRNA expression is accompanied by an increase in its protein expression.

The *FoxO1* expression data would suggest that infection of the cells with CA-FoxO1 and DN-FoxO1 adenoviruses was unsuccessful, visual confirmation by immunofluorescent imaging was not possible in the time available. However, the DN-FoxO1 adenovirus did induce a ~6-fold increase in IngPA *VEGF* expression. This was not replicated in PrPAs. This may be an anomalous result or artefact of adenoviral infection itself. Adenovirus vectors are capable of inducing cellular immune responses *in vitro*. As a case in point, NF- κ B activation by adenovirus vectors has

been demonstrated (67), furthermore VEGF expression is NF- κ B dependent in human macrophages (72).

Given the time constraints on this work, the amount of virus used was determined by a previously successful multiplicity of infection (MOI) in HUVEC. The viruses used had also been stored for some time and their titres may consequently have decreased. If definitive further work is to be carried out, the titres of such viruses should be checked and the optimal MOI for these cells established.

4.2 Preadipocyte Stimulation

In both IngPA and PrPA, 1mM H₂O₂, VEGF, cAMP and Forskolin induced considerable increases in *FoxO1*, *VEGF* and *PIGF* expression.

That H₂O₂ induces PIGF expression is unsurprising, given that our lab has shown it to inhibit PI3k/Akt phosphorylation, facilitating FOXO1 nuclear translocation and binding to the *PIGF* promotor in HUVEC (unpublished work). A complete characterisation of this signalling pathway is necessary in preadipocytes; alternative explanations such as NF- κ B mediated *PIGF* expression (51) should also be explored. H₂O₂ also induced the upregulation of *Foxo1* expression. Little is known about the regulation of *Foxo1* expression despite our extensive knowledge of FOXO1 molecular biology. Recent work has suggested that *FoxO1* expression is mediated by the transcription factor cAMP response element-binding protein (CREB) and its co-activators (73). This requires upstream PKA phosphorylation of CREB at Ser133, a phenomenon which can be induced by H₂O₂ (74–76), although some have found H₂O₂ to inhibit PKA activation in adipocytes (77) and fibroblasts (78). Negative regulation of the PI3K/Akt pathway by H₂O₂ would be expected to decrease *VEGF* expression, yet we found that its expression increased (79). Many factors promote the transcription of *VEGF*,

including specificity factor 1 (SP-1) (80). SP-1 is cAMP-dependent, and may therefore be subject to induction by H₂O₂ (74–76). These mechanisms warrant further investigation.

Forskolin increases intracellular cAMP levels (81,82). Forskolin and cAMP treatment may have increased *FoxO1* expression via activation of CREB and its co-activators. A resulting increase in Foxo1 protein levels could subsequently have promoted *PIGF* expression. CREB may also directly mediate a cAMP-induced increase in *PIGF* expression. In BeWo choriocarcinoma cells, Depoix *et al.* demonstrated that exogenous forskolin and cAMP upregulate *PIGF* expression and identified two CREs in the *PIGF* promoter region (55). Our results also show that IngPA *VEGF* was induced by cAMP and forskolin. As previously discussed, the VEGF transcription factor SP-1 is cAMP dependent and may therefore have mediated the increase in *VEGF* expression.

VEGF treatment increased the expression of *FoxO1*, *PIGF* and to a lesser extent, *VEGF* itself. VEGF is known to strongly induce *PIGF* gene and protein expression via VEGFR-2 but not VEGFR-1. VEGFR-1 (and VEGFR-3) signalling appear to inhibit *PIGF* expression. The signal is transduced intracellularly via the MAPK and PKC (48,49). Interestingly, unpublished work from our lab has shown that knockdown of endogenous VEGF also stimulates *PIGF* expression in HUVEC, yet inhibition of the VEGFR-2 alone does not promote such an increase (49). It is possible that knockdown of VEGF causes the loss of inhibitory signalling via VEGFR-1 and VEGFR-3 and a subsequent increase in *PIGF* expression. This serves to illustrate the complexity of VEGF-family signalling and the need to characterise such events further if they are ultimately to be exploited for therapeutic purposes.

VEGF has been shown to negatively regulate FOXO1 activity (83), but little is known about its transcriptional influence on *FOXO1/FoxO1*. VEGF signalling through VEGFR-2 promotes Ser133 phosphorylation of CREB in rat neurons and endothelial cells (84), which may in turn induce FoxO1 transcription (73). Such cAMP activity could explain VEGF promoting its own gene expression, via PKA activation of the *VEGF* transcription factor SP-1.

Little difference in supernatant PIGF concentration is evident between the treated IngPA cells and their control. In PrPA cells, H₂O₂ and VEGF appear to have induced an increase in such concentrations. However, the absolute concentrations of PIGF in PrPA supernatants are low (<10 pg/mL) and it is impossible to trust the accuracy of results derived from 2 experiments. Again, quantification of cellular PIGF would illustrate whether the observed increases in *PIGF* mRNA expression are accompanied by an increase in protein expression.

4.3 Preadipocyte Differentiation

Differentiation of IngPA and PrPA was disappointing, despite alterations being made to the protocol. Such protocols have previously been used on mouse embryonic fibroblasts in our lab, with some success. Differentiation was induced at 24 hours post-confluence, in order to ensure the cells had undergone post-confluent mitosis. This growth arrest is necessary for adipogenesis (85). Our cells displayed overlapping growth at 7 days post-confluence and subsequently detached from their growth plate, a phenomenon which has also been described by others (86). Their growth arrest may therefore have been poor. This may explain the disappointing results obtained. Cao *et al.* used serum starvation to halt the growth of subconfluent 3T3-L1 preadipocytes; this facilitated their differentiation (90% adipocyte morphology at 19 days) and prevented their detachment (86). Preadipocyte differentiation is more

successful in cells from younger rats (87). The mice used in our work were relatively old (10 weeks). Younger mice should be used for future isolation of primary preadipocytes.

4.4 Mouse Genotyping

Genotyping of the eFoKO and FoFlox mice used in the preparation of liver slices for culture was largely successful, particularly in the endothelium-rich aortic samples. The resolution of the bands depicted in Fig. 3.11 leave something to be desired. It is possible that some poorly resolved FoxO1 KO bands are present in the aortic samples from the eFoKO mice (Fig. 3.11). The FoxO1 KO bands are only 41 base pairs removed from the flox bands, making their resolution difficult. Previous attempts by our lab to resolve these bands have failed. Further attempts might be made by casting a thinner gel (< 3 mm thick) as this could affect the resolution of these small fragments. Reducing the quantity of DNA in each well, and lowering of the voltage applied may also improve the resolution. Given the small size of the DNA fragments, a polyacrylamide gel may separate them more effectively (88). The genotyping of these mice is complicated by the endothelial-specific nature of their genetic modification. Isolation and culture of endothelial cells (along with other cell types as a control) and their subsequent genotyping – see (89) – might yield better results.

4.5 Liver Slice Culture

Culture of precision-cut liver slices from eFoKO and FoFlox mice was carried out in order to explore the effect of such KO on hepatic PIGF production. Anti-angiogenic treatment attenuates non-alcoholic steatosis (NASH) development, although this appears to be a VEGFR-2 mediated effect (33).

In untreated livers, eFoKO had no effect on PIGF production, perhaps reflecting the relatively small number of endothelial cells compared to other cell types within the liver (90). Surprisingly, the PIGF concentration in supernatant (normalised to liver slice weight) was significantly greater in insulin-treated eFoKO mice compared to that in insulin-treated FoFlox mice. Tsuchiya *et al.* have shown increased endothelial nitric oxide (NO) production in hepatic eFoKO endothelial cells, which causes tyrosine nitration of hepatic insulin receptors (InsRs). This prevents tyrosine-induced InsR phosphorylation. Insulin treatment further promotes endothelial eNOS expression in eFoKO, promoting greater InsR phosphorylation. Consequently, insulin receptor substrate-1 (*Irs1*) and Akt Ser473/Thr308 phosphorylation is impaired, along with FoxO1/3a phosphorylation (90). Insulin-induced impairment of FoxO1/3a phosphorylation would be expected to promote hepatic PIGF production, possibly explaining our results. These findings have important metabolic consequences; eFoKO promotes hepatic insulin resistance and a resulting increase in hepatic PIGF could conceivably promote maladaptive microvascular changes. The findings also illustrate the importance of an integrated approach when assessing the consequences of manipulating cellular physiology.

4.6 Conclusion

This work was intended as a preliminary exploration of the molecular regulation of PIGF in murine preadipocytes, given its emerging importance in the metabolic syndrome and potential contribution to an adipogenic environment. Secondary consideration was given to VEGF. WT-FoxO1 adenoviral transfection was successful and in keeping with previous findings from our lab, induced an increase in *PIGF* expression. DN-FoxO1 and CA-FoxO1 transfections were unsuccessful; approaches to remedying this have been outlined. H₂O₂, VEGF, cAMP and forskolin treatment

induced increases in *FoxO1*, *VEGF* and *PIGF* expression. Mechanisms which may underlie these increases have been discussed. CREB promotion of *Foxo1* and *PIGF* expression, along with SP-1 promotion of *VEGF* expression are of particular interest and should be explored further. Increases in *PIGF* mRNA expression were not generally reflected in supernatant PIGF concentrations. Intracellular PIGF quantification by Western blotting would give some indication as to whether increased mRNA expression is accompanied by enhanced protein expression. Surprisingly, eFoKO increased precision-cut liver slice production of PIGF. We failed to optimise the differentiation of IngPA and PrPA into adipocytes. It had been hoped to generate adipocytes to allow the molecular regulation of PIGF to be explored in these cells. Further optimisation of the differentiation protocol (see Section 4.3) will allow this work to progress. Given the attractiveness of PIGF as an anti-obesity target, further efforts should be made to characterise its adipogenic role and molecular regulation in both the vascular and adipose fractions of adipose tissue.

References

1. Rupnick MA, Panigrahy D, Zhang C-Y, Dallabrida SM, Lowell BB, Langer R, et al. Adipose tissue mass can be regulated through the vasculature. *Proc Natl Acad Sci U S A*. 2002 Aug 6;99(16):10730–5.
2. Kolonin MG, Saha PK, Chan L, Pasqualini R, Arap W. Reversal of obesity by targeted ablation of adipose tissue. *Nat Med*. 2004 Jun;10(6):625–32.
3. Tam J, Duda DG, Perentes JY, Quadri RS, Fukumura D, Jain RK. Blockade of VEGFR2 and not VEGFR1 can limit diet-induced fat tissue expansion: role of local versus bone marrow-derived endothelial cells. *PLoS One*. 2009;4(3):e4974.
4. Lu X, Ji Y, Zhang L, Zhang Y, Zhang S, An Y, et al. Resistance to obesity by repression of VEGF gene expression through induction of brown-like adipocyte differentiation. *Endocrinology*. 2012 Jul;153(7):3123–32.
5. Lijnen HR, Christiaens V, Scroyen I, Voros G, Tjwa M, Carmeliet P, et al. Impaired adipose tissue development in mice with inactivation of placental growth factor function. *Diabetes*. 2006 Oct;55(10):2698–704.
6. Dvorak HF, Orenstein NS, Carvalho AC, Churchill WH, Dvorak AM, Galli SJ, et al. Induction of a Fibrin-Gel Investment: An Early Event in Line 10 Hepatocarcinoma Growth Mediated by Tumor-Secreted Products. *J Immunol*. 1979 Jan 1;122(1):166–74.
7. Senger DR, Galli SJ, Dvorak AM, Perruzzi CA, Harvey VS, Dvorak HF. Tumor cells secrete a vascular permeability factor that promotes accumulation of ascites fluid. *Science*. 1983 Feb 25;219(4587):983–5.
8. Senger DR, Connolly DT, Van de Water L, Feder J, Dvorak HF. Purification and NH₂-terminal amino acid sequence of guinea pig tumor-secreted vascular permeability factor. *Cancer Res*. 1990 Mar 15;50(6):1774–8.
9. Hoeben A, Landuyt B, Highley MS, Wildiers H, Oosterom ATV, Bruijn EAD. Vascular Endothelial Growth Factor and Angiogenesis. *Pharmacol Rev*. 2004 Dec 1;56(4):549–80.
10. Tischer E, Mitchell R, Hartman T, Silva M, Gospodarowicz D, Fiddes JC, et al. The human gene for vascular endothelial growth factor. Multiple protein forms are encoded through alternative exon splicing. *J Biol Chem*. 1991 Jun 25;266(18):11947–54.
11. Neufeld G, Cohen T, Gengrinovitch S, Poltorak Z. Vascular endothelial growth factor (VEGF) and its receptors. *FASEB J*. 1999 Jan 1;13(1):9–22.
12. Ng Y-S, Rohan R, Sunday M e., Demello D e., D'Amore P a. Differential expression of VEGF isoforms in mouse during development and in the adult. *Dev Dyn*. 2001 Feb 1;220(2):112–21.

13. Ortega N, Hutchings H, Plouët J. Signal relays in the VEGF system. *Front Biosci J Virtual Libr.* 1999 Feb 1;4:D141–152.
14. Ribatti D. The discovery of the placental growth factor and its role in angiogenesis: a historical review. *Angiogenesis.* 2008;11(3):215–21.
15. DiPalma T, Tucci M, Russo G, Maglione D, Lago CT, Romano A, et al. The placenta growth factor gene of the mouse. *Mamm Genome Off J Int Mamm Genome Soc.* 1996 Jan;7(1):6–12.
16. Otrrock ZK, Makarem JA, Shamseddine AI. Vascular endothelial growth factor family of ligands and receptors: Review. *Blood Cells Mol Dis.* 2007 May;38(3):258–68.
17. Shibuya M, Yamaguchi S, Yamane A, Ikeda T, Tojo A, Matsushime H, et al. Nucleotide sequence and expression of a novel human receptor-type tyrosine kinase gene (flt) closely related to the fms family. *Oncogene.* 1990 Apr;5(4):519–24.
18. Takahashi H, Shibuya M. The vascular endothelial growth factor (VEGF)/VEGF receptor system and its role under physiological and pathological conditions. *Clin Sci.* 2005 Sep 1;109(3):227.
19. Shraga-Heled N, Kessler O, Prahst C, Kroll J, Augustin H, Neufeld G. Neuropilin-1 and neuropilin-2 enhance VEGF121 stimulated signal transduction by the VEGFR-2 receptor. *FASEB J Off Publ Fed Am Soc Exp Biol.* 2007 Mar;21(3):915–26.
20. Neufeld G, Kessler O, Herzog Y. The interaction of Neuropilin-1 and Neuropilin-2 with tyrosine-kinase receptors for VEGF. *Adv Exp Med Biol.* 2002;515:81–90.
21. Koch S, Claesson-Welsh L. Signal Transduction by Vascular Endothelial Growth Factor Receptors. *Cold Spring Harb Perspect Med* [Internet]. 2012 Jul [cited 2014 Apr 9];2(7). Available from: <http://www.ncbi.nlm.nih.gov/pmc/articles/PMC3385940/>
22. Mac Gabhann F, Popel AS. Dimerization of VEGF receptors and implications for signal transduction: a computational study. *Biophys Chem.* 2007 Jul;128(2-3):125–39.
23. Ziche M, Maglione D, Ribatti D, Morbidelli L, Lago CT, Battisti M, et al. Placenta growth factor-1 is chemotactic, mitogenic, and angiogenic. *Lab Investig J Tech Methods Pathol.* 1997 Apr;76(4):517–31.
24. Yonekura H, Sakurai S, Liu X, Migita H, Wang H, Yamagishi S, et al. Placenta growth factor and vascular endothelial growth factor B and C expression in microvascular endothelial cells and pericytes. Implication in autocrine and paracrine regulation of angiogenesis. *J Biol Chem.* 1999 Dec 3;274(49):35172–8.

25. Hattori K, Heissig B, Wu Y, Dias S, Tejada R, Ferris B, et al. Placental growth factor reconstitutes hematopoiesis by recruiting VEGFR1(+) stem cells from bone-marrow microenvironment. *Nat Med*. 2002 Aug;8(8):841–9.
26. Scholz D, Elsaesser H, Sauer A, Friedrich C, Luttmann A, Carmeliet P, et al. Bone marrow transplantation abolishes inhibition of arteriogenesis in placenta growth factor (PlGF) $-/-$ mice. *J Mol Cell Cardiol*. 2003 Feb;35(2):177–84.
27. Bellik L, Vinci MC, Filippi S, Ledda F, Parenti A. Intracellular pathways triggered by the selective FLT-1-agonist placental growth factor in vascular smooth muscle cells exposed to hypoxia. *Br J Pharmacol*. 2005 Oct;146(4):568–75.
28. Carmeliet P, Ferreira V, Breier G, Pollefeyt S, Kieckens L, Gertsenstein M, et al. Abnormal blood vessel development and lethality in embryos lacking a single VEGF allele. *Nature*. 1996 Apr 4;380(6573):435–9.
29. Carmeliet P, Moons L, Luttmann A, Vincenti V, Compernelle V, De Mol M, et al. Synergism between vascular endothelial growth factor and placental growth factor contributes to angiogenesis and plasma extravasation in pathological conditions. *Nat Med*. 2001 May;7(5):575–83.
30. Malik AK, Baldwin ME, Peale F, Fuh G, Liang W-C, Lowman H, et al. Redundant roles of VEGF-B and PlGF during selective VEGF-A blockade in mice. *Blood*. 2006 Jan 15;107(2):550–7.
31. Dewerchin M, Carmeliet P. PlGF: a multitasking cytokine with disease-restricted activity. *Cold Spring Harb Perspect Med*. 2012;2(8).
32. Van Steenkiste C, Ribera J, Geerts A, Pauta M, Tugues S, Casteleyn C, et al. Inhibition of placental growth factor activity reduces the severity of fibrosis, inflammation, and portal hypertension in cirrhotic mice. *Hepatology*. 2011 May;53(5):1629–40.
33. Coulon S, Legry V, Heindryckx F, Van Steenkiste C, Casteleyn C, Olievier K, et al. Role of vascular endothelial growth factor in the pathophysiology of nonalcoholic steatohepatitis in two rodent models. *Hepatology*. 2013 May;57(5):1793–805.
34. Yoo S-A, Yoon H-J, Kim H-S, Chae C-B, De Falco S, Cho C-S, et al. Role of placenta growth factor and its receptor flt-1 in rheumatoid inflammation: a link between angiogenesis and inflammation. *Arthritis Rheum*. 2009 Feb;60(2):345–54.
35. Roncal C, Buyschaert I, Chorianopoulos E, Georgiadou M, Meilhac O, Demol M, et al. Beneficial effects of prolonged systemic administration of PlGF on late outcome of post-ischaemic myocardial performance. *J Pathol*. 2008 Oct 1;216(2):236–44.
36. Ferrara N, Gerber H-P, LeCouter J. The biology of VEGF and its receptors. *Nat Med*. 2003 Jun;9(6):669–76.

37. Gerber HP, Dixit V, Ferrara N. Vascular endothelial growth factor induces expression of the antiapoptotic proteins Bcl-2 and A1 in vascular endothelial cells. *J Biol Chem*. 1998 May 22;273(21):13313–6.
38. Shweiki D, Itin A, Neufeld G, Gitay-Goren H, Keshet E. Patterns of expression of vascular endothelial growth factor (VEGF) and VEGF receptors in mice suggest a role in hormonally regulated angiogenesis. *J Clin Invest*. 1993 May;91(5):2235–43.
39. Olfert IM, Howlett RA, Tang K, Dalton ND, Gu Y, Peterson KL, et al. Muscle-specific VEGF deficiency greatly reduces exercise endurance in mice. *J Physiol*. 2009 Apr 15;587(8):1755–67.
40. Xia Y-P, Li B, Hylton D, Detmar M, Yancopoulos GD, Rudge JS. Transgenic delivery of VEGF to mouse skin leads to an inflammatory condition resembling human psoriasis. *Blood*. 2003 Jul 1;102(1):161–8.
41. Shen BQ, Lee DY, Zioncheck TF. Vascular endothelial growth factor governs endothelial nitric-oxide synthase expression via a KDR/Fik-1 receptor and a protein kinase C signaling pathway. *J Biol Chem*. 1999 Nov 12;274(46):33057–63.
42. Hood JD, Meininger CJ, Ziche M, Granger HJ. VEGF upregulates eNOS message, protein, and NO production in human endothelial cells. *Am J Physiol*. 1998 Mar;274(3 Pt 2):H1054–1058.
43. Hagberg CE, Falkevall A, Wang X, Larsson E, Huusko J, Nilsson I, et al. Vascular endothelial growth factor B controls endothelial fatty acid uptake. *Nature*. 2010 Apr 8;464(7290):917–21.
44. Li Y, Zhang F, Nagai N, Tang Z, Zhang S, Scotney P, et al. VEGF-B inhibits apoptosis via VEGFR-1-mediated suppression of the expression of BH3-only protein genes in mice and rats. *J Clin Invest*. 2008 Mar;118(3):913–23.
45. Poesen K, Lambrechts D, Van Damme P, Dhondt J, Bender F, Frank N, et al. Novel role for vascular endothelial growth factor (VEGF) receptor-1 and its ligand VEGF-B in motor neuron degeneration. *J Neurosci Off J Soc Neurosci*. 2008 Oct 15;28(42):10451–9.
46. Zhang F, Tang Z, Hou X, Lennartsson J, Li Y, Koch AW, et al. VEGF-B is dispensable for blood vessel growth but critical for their survival, and VEGF-B targeting inhibits pathological angiogenesis. *Proc Natl Acad Sci U S A*. 2009 Apr 14;106(15):6152–7.
47. Kivelä R, Bry M, Robciuc MR, Räsänen M, Taavitsainen M, Silvola JM, et al. VEGF-B-induced vascular growth leads to metabolic reprogramming and ischemia resistance in the heart. *EMBO Mol Med*. 2014 Mar;6(3):307–21.
48. Yao Y-G, Yang HS, Cao Z, Danielsson J, Duh EJ. Upregulation of placental growth factor by vascular endothelial growth factor via a post-transcriptional mechanism. *FEBS Lett*. 2005 Feb 14;579(5):1227–34.

49. Zhao B, Cai J, Boulton M. Expression of placenta growth factor is regulated by both VEGF and hyperglycaemia via VEGFR-2. *Microvasc Res.* 2004 Nov;68(3):239–46.
50. Wu M-Y, Yang R-S, Lin T-H, Tang C-H, Chiu Y-C, Liou H-C, et al. Enhancement of PLGF production by 15-(S)-HETE via PI3K-Akt, NF- κ B and COX-2 pathways in rheumatoid arthritis synovial fibroblast. *Eur J Pharmacol.* 2013 Aug 15;714(1-3):388–96.
51. Cramer M, Nagy I, Murphy BJ, Gassmann M, Hottiger MO, Georgiev O, et al. NF-kappaB contributes to transcription of placenta growth factor and interacts with metal responsive transcription factor-1 in hypoxic human cells. *Biol Chem.* 2005 Sep;386(9):865–72.
52. Nishimoto F, Sakata M, Minekawa R, Okamoto Y, Miyake A, Isobe A, et al. Metal transcription factor-1 is involved in hypoxia-dependent regulation of placenta growth factor in trophoblast-derived cells. *Endocrinology.* 2009 Apr;150(4):1801–8.
53. Green CJ, Lichtlen P, Huynh NT, Yanovsky M, Laderoute KR, Schaffner W, et al. Placenta growth factor gene expression is induced by hypoxia in fibroblasts: a central role for metal transcription factor-1. *Cancer Res.* 2001 Mar 15;61(6):2696–703.
54. Zhang H, Palmer R, Gao X, Kreidberg J, Gerald W, Hsiao L, et al. Transcriptional activation of placental growth factor by the forkhead/winged helix transcription factor FoxD1. *Curr Biol CB.* 2003 Sep 16;13(18):1625–9.
55. Depoix C, Tee MK, Taylor RN. Molecular regulation of human placental growth factor (PIGF) gene expression in placental villi and trophoblast cells is mediated via the protein kinase a pathway. *Reprod Sci Thousand Oaks Calif.* 2011 Mar;18(3):219–28.
56. Kassi E, Pervanidou P, Kaltsas G, Chrousos G. Metabolic syndrome: definitions and controversies. *BMC Med.* 2011 May 5;9(1):48.
57. Cassidy A, Chiuve SE, Manson JE, Rexrode KM, Girman CJ, Rimm EB. Potential role for plasma placental growth factor in predicting coronary heart disease risk in women. *Arterioscler Thromb Vasc Biol.* 2009 Jan;29(1):134–9.
58. Siervo M, Ruggiero D, Sorice R, Nutile T, Aversano M, Stephan BCM, et al. Angiogenesis and biomarkers of cardiovascular risk in adults with metabolic syndrome. *J Intern Med.* 2010 Oct;268(4):338–47.
59. Khurana R, Moons L, Shafi S, Luttun A, Collen D, Martin JF, et al. Placental growth factor promotes atherosclerotic intimal thickening and macrophage accumulation. *Circulation.* 2005 May 31;111(21):2828–36.
60. Roncal C, Buyschaert I, Gerdes N, Georgiadou M, Ovchinnikova O, Fischer C, et al. Short-term delivery of anti-PIGF antibody delays progression of atherosclerotic plaques to vulnerable lesions. *Cardiovasc Res.* 2010 Apr 1;86(1):29–36.

61. Matsui M, Takeda Y, Uemura S, Matsumoto T, Seno A, Onoue K, et al. Suppressed soluble Fms-like tyrosine kinase-1 production aggravates atherosclerosis in chronic kidney disease. *Kidney Int.* 2014 Feb;85(2):393–403.
62. Tsuchiya K, Tanaka J, Shuiqing Y, Welch CL, DePinho RA, Tabas I, et al. FoxOs integrate pleiotropic actions of insulin in vascular endothelium to protect mice from atherosclerosis. *Cell Metab.* 2012 Mar 7;15(3):372–81.
63. Turner N, Cooney GJ, Kraegen EW, Bruce CR. Fatty acid metabolism, energy expenditure and insulin resistance in muscle. *J Endocrinol.* 2014 Feb;220(2):T61–79.
64. Christiaens V, Voros G, Scroyen I, Lijnen HR. On the role of placental growth factor in murine adipogenesis. *Thromb Res.* 2007;120(3):399–405.
65. Hemmeryckx B, van Bree R, Van Hoef B, Vercruyse L, Lijnen HR, Verhaeghe J. Adverse adipose phenotype and hyperinsulinemia in gravid mice deficient in placental growth factor. *Endocrinology.* 2008 May;149(5):2176–83.
66. Kovsan J, Osnis A, Maissel A, Mazor L, Tarnovscki T, Hollander L, et al. Depot-specific adipocyte cell lines reveal differential drug-induced responses of white adipocytes--relevance for partial lipodystrophy. *Am J Physiol Endocrinol Metab.* 2009 Feb;296(2):E315–322.
67. Deng X, Zhang W, O-Sullivan I, Williams JB, Dong Q, Park EA, et al. FoxO1 inhibits sterol regulatory element-binding protein-1c (SREBP-1c) gene expression via transcription factors Sp1 and SREBP-1c. *J Biol Chem.* 2012 Jun 8;287(24):20132–43.
68. Martinez SC, Tanabe K, Cras-Méneur C, Abumrad NA, Bernal-Mizrachi E, Permutt MA. Inhibition of Foxo1 Protects Pancreatic Islet β -Cells Against Fatty Acid and Endoplasmic Reticulum Stress-Induced Apoptosis. *Diabetes.* 2008 Apr 1;57(4):846–59.
69. Pfaffl MW. A new mathematical model for relative quantification in real-time RT-PCR. *Nucleic Acids Res.* 2001 May 1;29(9):e45.
70. Vogel C, Marcotte EM. Insights into the regulation of protein abundance from proteomic and transcriptomic analyses. *Nat Rev Genet.* 2012 Apr;13(4):227–32.
71. Borgland SL, Bowen GP, Wong NC, Libermann TA, Muruve DA. Adenovirus vector-induced expression of the C-X-C chemokine IP-10 is mediated through capsid-dependent activation of NF-kappaB. *J Virol.* 2000 May;74(9):3941–7.
72. Kiriakidis S, Andreakos E, Monaco C, Foxwell B, Feldmann M, Paleolog E. VEGF expression in human macrophages is NF-kappaB-dependent: studies using adenoviruses expressing the endogenous NF-kappaB inhibitor I κ B α and a kinase-defective form of the I κ B kinase 2. *J Cell Sci.* 2003 Feb 15;116(Pt 4):665–74.

73. Wondisford AR, Xiong L, Chang E, Meng S, Meyers DJ, Li M, et al. Control of Foxo1 Gene Expression by Co-activator P300. *J Biol Chem*. 2014 Feb 14;289(7):4326–33.
74. Ozgen N, Guo J, Gertsberg Z, Danilo P, Rosen MR, Steinberg SF. Reactive Oxygen Species Decrease cAMP Response Element Binding Protein Expression in Cardiomyocytes via a Protein Kinase D1-Dependent Mechanism That Does Not Require Ser133 Phosphorylation. *Mol Pharmacol*. 2009 Oct;76(4):896–902.
75. Ichiki T, Tokunou T, Fukuyama K, Iino N, Masuda S, Takeshita A. Cyclic AMP Response Element–Binding Protein Mediates Reactive Oxygen Species–Induced c-fos Expression. *Hypertension*. 2003 Aug 1;42(2):177–83.
76. Barlow CA, Kitiphongspattana K, Siddiqui N, Roe MW, Mossman BT, Lounsbury KM. Protein kinase A-mediated CREB phosphorylation is an oxidant-induced survival pathway in alveolar type II cells. *Apoptosis Int J Program Cell Death*. 2008 May;13(5):681–92.
77. De Piña MZ, Vázquez-Meza H, Pardo JP, Rendón JL, Villalobos-Molina R, Riveros-Rosas H, et al. Signaling the signal, cyclic AMP-dependent protein kinase inhibition by insulin-formed H₂O₂ and reactivation by thioredoxin. *J Biol Chem*. 2008 May 2;283(18):12373–86.
78. Raynaud F, Evain-Brion D, Gerbaud P, Marciano D, Gorin I, Liapi C, et al. Oxidative modulation of cyclic AMP-dependent protein kinase in human fibroblasts: possible role in psoriasis. *Free Radic Biol Med*. 1997;22(4):623–32.
79. Pore N, Liu S, Shu H-K, Li B, Haas-Kogan D, Stokoe D, et al. Sp1 Is Involved in Akt-mediated Induction of VEGF Expression through an HIF-1-independent Mechanism. *Mol Biol Cell*. 2004 Nov;15(11):4841–53.
80. Pagès G, Pouysségur J. Transcriptional regulation of the Vascular Endothelial Growth Factor gene—a concert of activating factors. *Cardiovasc Res*. 2005 Feb 15;65(3):564–73.
81. Shoback DM, Brown EM. Forskolin increases cellular cyclic adenosine monophosphate content and parathyroid hormone release in dispersed bovine parathyroid cells. *Metabolism*. 1984 Jun;33(6):509–14.
82. Takeda J, Adachi K, Halprin KM, Itami S, Levine V, Woodyard C. Forskolin Activates Adenylate Cyclase Activity and Inhibits Mitosis in In Vitro in Pig Epidermis. *J Invest Dermatol*. 1983 Sep;81(3):236–40.
83. Potente M, Urbich C, Sasaki K, Hofmann WK, Heeschen C, Aicher A, et al. Involvement of Foxo transcription factors in angiogenesis and postnatal neovascularization. *J Clin Invest*. 2005 Sep 1;115(9):2382–92.
84. Lee H-T, Chang Y-C, Tu Y-F, Huang C-C. VEGF-A/VEGFR-2 signaling leading to cAMP response element-binding protein phosphorylation is a shared pathway underlying the protective effect of preconditioning on neurons and endothelial cells. *J Neurosci Off J Soc Neurosci*. 2009 Apr 8;29(14):4356–68.

85. Moreno-Navarrete JM, Fernández-Real JM. Adipocyte Differentiation. In: Symonds ME, editor. Adipose Tissue Biology [Internet]. Springer New York; 2012 [cited 2014 May 4]. p. 17–38. Available from: http://link.springer.com/chapter/10.1007/978-1-4614-0965-6_2
86. Zhenhui Cao. Growth arrest induction of 3T3-L1 preadipocytes by serum starvation and their differentiation by the hormonal adipogenic cocktail. J Cell Anim Biol [Internet]. 2012 Mar 15 [cited 2014 Apr 30];6(5). Available from: <http://www.academicjournals.org/journal/JCAB/article-abstract/AF1A87113746>
87. Djian P, Roncari AK, Hollenberg CH. Influence of anatomic site and age on the replication and differentiation of rat adipocyte precursors in culture. J Clin Invest. 1983 Oct;72(4):1200–8.
88. Ven S, Rani A. Discriminatory Power of Agarose Gel Electrophoresis in DNA Fragments Analysis. In: Magdeldin S, editor. Gel Electrophoresis - Principles and Basics [Internet]. InTech; 2012 [cited 2014 May 4]. Available from: <http://www.intechopen.com/books/howtoreference/gel-electrophoresis-principles-and-basics/discriminatory-power-of-agarose-gel-electrophoresis-in-dna-fragment-analysis>
89. Liao Y, Day KH, Damon DN, Duling BR. Endothelial cell-specific knockout of connexin 43 causes hypotension and bradycardia in mice. Proc Natl Acad Sci U S A. 2001 Aug 14;98(17):9989–94.
90. Tsuchiya K, Accili D. Liver sinusoidal endothelial cells link hyperinsulinemia to hepatic insulin resistance. Diabetes. 2013 May;62(5):1478–89.